

Copyright Warning & Restrictions

The copyright law of the United States (Title 17, United States Code) governs the making of photocopies or other reproductions of copyrighted material.

Under certain conditions specified in the law, libraries and archives are authorized to furnish a photocopy or other reproduction. One of these specified conditions is that the photocopy or reproduction is not to be “used for any purpose other than private study, scholarship, or research.” If a user makes a request for, or later uses, a photocopy or reproduction for purposes in excess of “fair use” that user may be liable for copyright infringement,

This institution reserves the right to refuse to accept a copying order if, in its judgment, fulfillment of the order would involve violation of copyright law.

Please Note: The author retains the copyright while the New Jersey Institute of Technology reserves the right to distribute this thesis or dissertation

Printing note: If you do not wish to print this page, then select “Pages from: first page # to: last page #” on the print dialog screen

The Van Houten library has removed some of the personal information and all signatures from the approval page and biographical sketches of theses and dissertations in order to protect the identity of NJIT graduates and faculty.

ABSTRACT

ANALYSIS OF A COMPOSITE DIELECTRIC-FERRITE LOADED RESONATOR USING THE TRANSMISSION LINE MODEL WITH APPLICATION TO A TUNABLE DUAL MODE BANDPASS FILTER

**by
Charlotte Blair**

A magnetically tuned filter is presented in this dissertation. Filter tuning of a dielectric ceramic resonator is accomplished using by using two oppositely biased ferrites. Specifically, a change in the applied magnetic field is used to alter the permeability of the ferrite so as to achieve maximum tuning range. Through electromagnetic (EM) simulations and laboratory experiments, tuning of the filter passband by 20 MHz is demonstrated.

This investigation focuses on the design of a bandpass resonator using a combination of dielectric-ferrite material layers. An initial simplification of the geometry of the structure is used as the basis for a program developed to give a fast frequency analysis using the Transmission Line Method (TLM).

The TLM analysis is compared to a full wave EM simulation as well as results from the Experimental Model to insure compliance and validation. A suggestion is included to improve and modify the initial Experimental Model using the applied bias to optimize the frequency shift and bandwidth performance.

**ANALYSIS OF A COMPOSITE DIELECTRIC-FERRITE LOADED
RESONATOR USING THE TRANSMISSION LINE MODEL WITH
APPLICATION TO A TUNABLE DUAL MODE BANDPASS FILTER**

by
Charlotte Blair

**A Dissertation
Submitted to the Faculty of
New Jersey Institute of Technology
in Partial Fulfillment of the Requirements for the Degree of
Doctor of Philosophy in Electrical Engineering
Department of Electrical and Computer Engineering**

January 2012

Copyright © 2012 by Charlotte Blair
ALL RIGHTS RESERVED

APPROVAL PAGE

**ANALYSIS OF A COMPOSITE DIELECTRIC-FERRITE LOADED
RESONATOR USING THE TRANSMISSION LINE MODEL WITH
APPLICATION TO A TUNABLE DUAL MODE BANDPASS FILTER**

Charlotte Blair

Dr. Edip Niver, Dissertation Advisor Date
Professor of Electrical and Computer Engineering, NJIT

Dr. Richard V. Snyder, Dissertation Advisor Date
Adjunct Professor of Electrical and Computer Engineering, NJIT

Dr. Gerald Whitman, Committee Member Date
Professor of Electrical and Computer Engineering, NJIT

Dr. Haim Grebel, Committee Member Date
Professor of Electrical and Computer Engineering, NJIT

Dr. Simone Bastioli, Committee Member Date
RS Microwave, Butler, NJ

BIOGRAPHICAL SKETCH

Author: Charlotte Blair
Degree: Doctor of Philosophy
Date: January 2012

Undergraduate and Graduate Education:

- Doctor of Philosophy in Electrical Engineering,
New Jersey Institute of Technology, Newark, NJ, 2011
- Master of Science in Electrical Engineering,
New Jersey Institute of Technology, Newark, NJ, 1988
- Bachelor of Science in Electrical Engineering,
Rutgers University – College of Engineering, Newark, NJ, 1984

Major: Electrical Engineering

Presentations and Publications:

- C. Blair, "Magnetically Tunable Dual Mode Dielectric-Ferrite Resonator Bandpass Filter," *IEEE Microwave and Wireless Components Letters*, tbd 2012.
- R.V. Snyder, C. Alvarez, "Metal dielectric composite resonator, " USA Patent 6,476,693, November 5, 2002.
- R.V. Snyder, C. Alvarez, "Filters using a new type of resonator: the partially-metallized dielectric slug," presented at the IEEE MTT, Anaheim, Ca, 1999.

This dissertation is dedicated to my husband, Bill and to my daughters, Danielle and Victoria for all the years of patience, love and support.

ACKNOWLEDGMENT

There are so many people to whom I owe my gratitude for helping me along the way. Dr. Richard Snyder has been instrumental in guiding my research. He has had a major influence from both an academic and industrial perspective. I also owe special thanks to Dr. Edip Niver who also served as my MSEE advisor. He was always there to provide encouragement. And to Dr. Haim Grebel where no words can express my gratitude for his support and guidance and the belief I could complete this great achievement. Dr. Gerald Whitman for his academic insight and Dr. Simone Bastioli for his input and comments on circuit equivalents and EM tools. I thank all the members of my committee for their time and interest and for serving on my committee.

Special Thanks to Cleo Alexander of Agilent Technologies for providing me with the Agilent EESOFTE Suite of tools which include the EMPro full 3D EM solver used in this dissertation.

This dissertation was done on a part time basis while working and raising a family. It would have been an impossibility to complete this arduous task without the support of my husband, my daughters and Daisy. To my husband, Bill who without much complaint allowed me to pursue my dream a great big thank you and all my love. To my daughters, Danielle and Victoria, I hope my persistence in completing my dissertation will be an example to you that with hard work and dedication almost anything can be accomplished. Thank you to Daisy, my late night companion who would lay beside me until the early hours of the morning for nothing but a few treats and a shout out to Shawn.

Without these people, my life dream would have gone unfulfilled.

TABLE OF CONTENTS

Chapter	Page
1 INTRODUCTION	1
1.1 Problem Statement	1
1.2 Previous Work and Background	4
1.3 Dissertation Overview	8
1.4 Contributions and Summary	15
2 FERRITE ANALYSIS.....	16
2.1 Overview	16
2.2 General Ferrite Properties	17
2.2.1 Ferrite Permeability.....	19
2.2.2 Resonance Frequency and Line Width.....	21
2.2.3 Saturation Magnetization.....	26
2.3 Properties of G113 Ferrite as Used in Investigation.....	28
2.4 Summary of Microwave Ferrite Use in a Bandpass Filter Application.....	34
3 TRANSMISSION LINE ANALYSIS	36
3.1 Overview	36

TABLE OF CONTENTS
(Continued)

Chapter	Page
3.2 Transmission Line Method for a Multilayer Structure.....	37
3.2.1 Two-Layer Waveguide.....	39
3.2.2 Three-Layer Waveguide.....	40
3.3 Simple Five-Layer Model - Single Mode TLM Analysis.....	48
3.3.1 EM Simulated Simple Five-Layer Model Single Pole Filter.....	53
3.4 Dual Mode and Coupling Analysis.....	53
3.4.1 Experimental Model.....	54
3.4.2 TLM Program Simple Five-Layer Model Dual Mode Bandpass Filter.	56
3.4.3 EM Simulated Simple Five-Layer Model Dual Mode Bandpass Filter.	64
3.4.4 Next Higher Order Mode.....	66
3.4.5 Ferrite Materials for Simple Five-Layer Dual Mode Bandpass Filter Model	68
3.4.6 Summary of Dual Mode Bandpass Filter Analysis	72
4 TLM/SIMPLE FIVE-LAYER MODEL ANALYSIS APPLIED TO A NEW DESIGN REQUIREMENT	74
4.1 TLM Program New Dual Mode Bandpass Filter Application	74
4.2 EMPro Simulated Analysis New Dual Mode Bandpass Filter Application...	79
4.3 Summary of New Dual Mode Bandpass Filter Application	81
5 CONCLUSION.....	83

TABLE OF CONTENTS
(Continued)

Chapter	Page
5.1 Summary of Work	83
5.2 Future Work	85
APPENDIX A MATLAB Source code	87
A.1 Ferrite Analysis	87
A.2 Transmission Line Method – Impedance Calculation	96
APPENDIX B Details for TLM Based Figure 3.29.....	118
REFERENCES	124

LIST OF TABLES

Table		Page
2.1	Trans-Tech G113 Datasheet [13].....	18
2.2	Trans-Tech G510 Datasheet [14].....	18
2.3	Trans-Tech TTVG1950 Datasheet [15].....	19
2.4	Tabulated Parameters from TLM program used to generate Figure 3.15.....	33
3.1	Permittivity Values for Five-Layer Model.....	42
3.2	Permeability Values for Five-Layer Model.....	42
3.3	Frequency Shift of f_1 , f_2 and Center Frequency f_0 with 200 Oe Applied Bias.....	62
4.1	Specifications of New Filter Structure.....	72

LIST OF FIGURES

Figure	Page
1.1 A dual mode bandpass filter electronically tunable with ferrite tiles.....	2
1.2 Conceptual picture of previous work in [10].....	6
1.3 Conceptual picture of previous work in [11].....	6
1.4 Flowchart of Dissertation Progress.....	8
1.5 Experimental Model as developed and measured at RS Microwave, Butler, NJ...	9
1.6 Simple Five-Layer Model used as an initial approximation to the Experimental Model.....	10
1.7 Definition of “same” and “opposite” bias”.....	11
1.8 Photograph of the experimental setup.....	12
2.1 Snapshots of ferrite magnetization with electron spin as bias H_0 increases [19].	17
2.2 Numerical solution of permeability and susceptibility in Polder tensor as a function of frequency for a ferrite medium with $M_s=1800$ Oe and an applied bias of 3750 Oe [1, Figure 10.8]	20
2.3 Variation of permeability and susceptibility in Polder tensor as a function of applied bias for a ferrite medium with $M_s=3000$ Oe and resonant frequency = 2800 MHz [7, Figure 4-3].....	21
2.4 Definition of ferrite line width.....	22
2.5 The real part of the dispersive components of the susceptibility tensor. These values are computed for a RF frequency of 2800 MHz and a saturation magnetization of $4\pi M_s=3000$ gauss [7, Figure 4-3].....	23
2.6 The imaginary part of the dispersive components of the susceptibility tensor. These values are computed for a resonance frequency of 2800 MHz and a saturation magnetization of $4\pi M_s=3000$ gauss [7, Figure 4-3].....	24

**LIST OF FIGURES
(Continued)**

Figure	Page
2.7 The real part of the dissipative components of the susceptibility tensor. These values are computed for a resonance frequency of 2800 MHz and a saturation magnetization of $4\pi M_s=3000$ gauss [7, Figure 4-3].....	24
2.8 The imaginary part of the dissipative components of the susceptibility tensor. These values are computed for a resonance frequency of 2800 MHz and a saturation magnetization of $4\pi M_s=3000$ gauss [7, Figure 4-3].....	25
2.9 Expanded view of magnitude of Figure 3.8.....	25
2.10 Resonant frequency as a function of applied EAVSMF bias.....	26
2.11 Saturation Frequency as a function of Saturation Magnetization.....	27
2.12 Susceptibility and Relative Permeability as a function of applied bias for G113 and an operating frequency of 2800 MHz.....	29
2.13 Susceptibility as a function of frequency for G113 and applied bias=400 Oe.....	30
2.14 Susceptibility as a function of frequency for G113 and applied bias=500 Oe.....	31
2.15 Magnitude of Susceptibility as a function of frequency for G113 and applied bias=500 Oe with line width indicated.....	32
2.16 Susceptibility as a Function of Frequency for G113 and applied bias=1050 Oe..	34
3.1 Transmission Line Model of a Two-Layer Dielectric Waveguide.....	39
3.2 MATLAB Results for Two-Layer Model used to validate TLM method for dielectrics only.....	40
3.3 Three-Layer Model used to validate TLM method for dielectrics only.....	40
3.4 MATLAB TLM result for a Three-Layer Model.....	41

LIST OF FIGURES
(Continued)

Figure	Page
3.5 Simple Five-Layer Model used as an initial approximation to the Experimental Model.	43
3.6 Relationship of physical and material characteristics of Simple Five-Layer Model layers with Transmission Line Equivalent	43
3.7 Bisected diagram of Simple Five-Layer Model.....	44
3.8 Plot of transcendental equations for Simple Five-Layer Model with no applied bias. Lowest order mode is located at curve intersection.....	48
3.9 The equivalent transmission line model of Simple Five-Layer Model.	49
3.10 Equivalent circuit of Five-Layer Model - Single Pole Filter.....	50
3.11 TLM Program – S Parameter curves for Simple Five-Layer Model single pole with “opposite “ bias.....	52
3.12 AGILENT Single Mode filter structure	53
3.13 Tunable dual mode bandpass filter.....	55
3.14 Circuit model of dual mode filter	56
3.15 Equivalent circuit for corner cut coupling used to design a dual mode filter.....	57
3.16 Equivalent circuit for dual mode bandpass filter including corner cut coupling.....	58
3.17 Fractional bandwidth as a function of the ratio of equivalent resonant L and C of Experimental Model at zero bias.....	60
3.18 Equivalent circuit with values calculated from TLM Program for dual mode bandpass filter including corner cut coupling.....	60
3.19 TLM Program S Parameter results for dual mode five-layer filter model with various applied “same” bias	61

LIST OF FIGURES
(Continued)

Figure	Page
3.20 TLM Program S Parameter results for dual mode five-layer filter model with various applied “opposite” bias	62
3.21 TLM Program S Parameter results comparing zero biased G113 ferrite with 200 Oe external bias applied in “same” and “opposite” directions	63
3.22 Experimental S Parameter results for dual mode five-layer filter model with “opposite” bias	64
3.23 EM simulated single mode experimental filter structure.....	65
3.24 EM simulated dual mode experimental filter structure.....	65
3.25 EM Simulated shift of lowest order mode frequency with cavity chamfer of a sample dual Mode bandpass filter.....	66
3.26 TLM results for 950 Oe “opposite” bias showing crossover for next higher mode.....	67
3.27 Experimental results for 950 Oe “opposite” bias showing next higher mode.....	68
3.28 EM simulated results for 950 Oe “opposite” bias dual mode bandpass filter showing next higher mode	68
3.29 TLM calculated S Parameter curves for a dual mode bandpass filter using G510 ferrite with “opposite” external bias.....	69
3.30 TLM calculated S Parameter curves for a dual mode bandpass filter using TTVG1950 ferrite with “opposite” external bias.....	70
3.31 Calculated relative permeability of G113, G510 and TTVG1950 with 500 Oe applied bias.....	71
3.32 Calculated relative permeability of G113, G510 and TTVG1950 with 900 Oe applied bias.....	71

LIST OF FIGURES
(Continued)

Figure	Page
3.33 Comparison of EM simulated dual mode experimental bandpass filter and TLM Simple Five-Layer Model dual mode bandpass filter at different applied bias.....	72
3.34 Comparison of shift in center frequency of EM simulated model, experimental bandpass filter and TLM Simple Five-Layer Model dual mode bandpass filter with “opposite” applied bias.....	73
4.1 TLM design curve for square cross-section dielectric resonator size vs. center frequency in Simple Five-Layer Model.....	75
4.2 TLM Program – Input dielectric resonator side dimension in inches.....	75
4.3 TLM Program – Single Pole Bandpass Filter with G113 ferrite and .4 in. dielectric layer with zero applied bias.....	76
4.4 TLM Program – Single Pole Bandpass Filter with G113 ferrite and .425 in.....	76
4.5 Conceptual view of New Dual Mode Bandpass filter structure with G113 ferrite and .425 in. dielectric puck.....	77
4.6 TLM Program – New Dual Mode Bandpass Filter with G113 ferrite and .425 in. dielectric layer with zero O_e applied bias.....	78
4.7 TLM Program – New Dual Mode BandPass Filter with G113 ferrite and .4 in. dielectric layer with “opposite” applied bias.....	78
4.8 EMPro Design Curve – corner cut vs. lowest order mode frequency shift.....	79
4.9 EMPro Simulation – S Parameter curves for New Bandpass - Single Pole Filter with zero applied bias (O_e)	80
4.10 EMPro Simulated S Parameter Results for New Dual Mode Filter structure with zero applied bias and .1 inch corner cut	80
4.11 EMPro simulated S Parameter Results for New Dual Mode Filter Structure with zero applied bias and 400 O_e “opposite” applied bias.....	81
4.12 Comparison of EM simulated and TLM results of New Structure’s center frequency shift with “opposite” applied bias.....	82

LIST OF FIGURES
(Continued)

Figure	Page
B.1 Screenshot of line curves for transcendental impedance equations with zero applied bias plotted against frequency.....	116
B.2 Screenshot of required user input for first crossover point for zero bias.....	116
B.3 Screenshot of line curves for transcendental impedance equations with an applied bias plotted against frequency.....	117
B.4 Screenshot of required user input for first crossover point for an applied bias.....	117
B.5 Screenshot of line curves of the propagation constants of the composite structure.....	118
B.6 Screenshot of required user input for the crossover point for propagation curves.....	118
B.7 Calculated S11 and S21 plots of dual mode bandpass filter with zero and applied bias.....	119
B.8 Screenshot of user selected ferrite material.....	119
B.9 Tabulated TLM data for G113, G510 and TTVG-1950.....	120

LIST OF SYMBOLS

B	Magnetic flux density	Tesla
β	Propagation constant	
©	Copyright	
∇	Del operator	
$\nabla \cdot A$	Divergence of A	
$\nabla \times A$	Curl of A	
ΔH	Ferrite line width	Oe
D	Electric flux density	C/m ²
external applied bias	A fixed applied voltage value	Oe
∂	Partial Differential	
δ	Deviation model	
\int	Integral	
E	Electric field intensity	V/m
ϵ	Permittivity	$\epsilon = \epsilon_r \epsilon_0$ F/m
ϵ_0	Permittivity of free space	$8.854 \cdot 10^{-12}$ F/m
ϵ_r	Relative permittivity	
γ	Gyrotropic Ratio	$1.76 \cdot 10^7$ rad/sec Oe
g	Landé factor	g
GHz	Unit of frequency	10^9 Hertz

LIST OF SYMBOLS
(Continued)

H	Magnetic field intensity	A/m , Oe
j	Imaginary unit	
M	Magnetization vector	
μ	Permeability	$\mu = \mu_r \mu_0$ H/m
μ_0	Permeability of free space	$4\pi * 10^{-7}$ H/m
μ_r	Relative permittivity	
Oe	Oersted - unit of measure of H field	$1 \text{ Oe} = \frac{1000}{4\pi} \text{ A/m}$
π	pi	3.415
RF	Radio Frequency	30kHz-300 GHz
S_{ij}	Scattering parameter	
TE	Transverse Electric	
TM	Transverse Magnetic	
χ	Susceptibility	
ω	Angular frequency	rad/s
ω_0	Larmor frequency	rad/s

LIST OF DEFINITIONS

EM	Electromagnetic
EAVSMF	Externally applied, variable static magnetic field
Opposite Bias	Top ferrite layer with same applied bias magnitude with an opposite direction as compared to bottom ferrite layers
Same bias	Top ferrite layer with same applied bias magnitude with same direction as compared to bottom ferrite layers
TLM	Transmission Line Method
Zero biased ferrite	A zero biased ferrite is approximated as a dielectric with the permittivity value of the ferrite and a permeability value of free space $\mu_r=1$.

CHAPTER 1

INTRODUCTION

1.1 Problem Statement

For many years tunable bandpass filters have been of high interest to the wireless communications industry. Tuning by electronic means vs. manual manipulation of the center frequency, f_0 would enable wireless providers to quickly adjust to different channel configurations as specified by the various wireless standards.

A bandpass filter is composed of individual resonators electrically coupled together in a predisposed arrangement with the coupling achieved by various coupling mechanisms. The characteristics of the resonators dictate the performance of the filter system. The characteristics of the coupling dictate the shape of the filter response. Dielectric material is commonly used to shrink the physical size of a resonator while retaining high Q. Such a dielectric structure can be made to exhibit dual mode performance by applying specific perturbations to the physical structure. The perturbation provides a coupling means between two orthogonal modes within the cavity. Thus, a compact, efficient building block for more complex filter structures can be achieved.

One of the major specifications for the resonator is its center frequency. Tunability of the center frequency of such a filter is of particular interest especially where the tuning can be accomplished by some electronic means vs. manual manipulation.

An objective of this paper is to present a different approach to tuning the filter's center frequency by introducing a biased ferrite material into a resonator cavity. Figure 1.1 shows a diagram of the proposed electronically tunable dual mode bandpass filter structure. An analysis and experimental data are presented in this thesis.

In addition, a supplementary objective of this dissertation is to develop an efficient method to predict the tuning of the center frequency of a dielectric resonator with the use of ferrite materials. The main area of concern is the shift of the center frequency, f_0 with an externally applied, variable static magnetic field (EAVSMF). The externally applied magnetic field bias is applied above and below the cavity housing closest to the thin ferrite layers. The symbol “–“ defines a boundary which is the interface between media with different constitutive parameters. A Transmission Line Model (TLM) is developed and the results are compared to those achieved experimentally and simulated with commercially available electromagnetic (EM) tools.

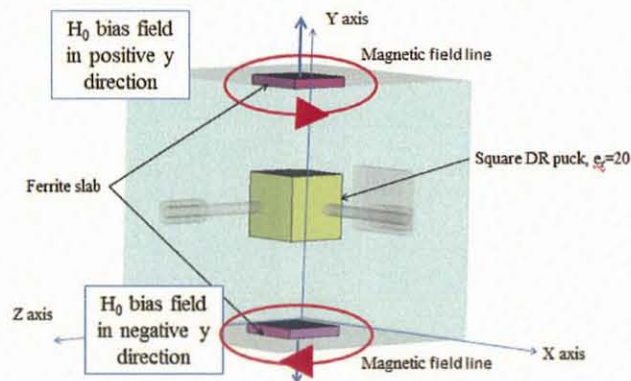


Figure 1.1 A dual mode bandpass filter electronically tunable with ferrite tiles.

This thesis presents an analysis of a square cross-section dielectric resonator centered between two thin ferrite square tile shapes. The square cross-section shaped dielectric resonator and ferrite tiles are enclosed in a square cross-section metal cavity. A simplified five-layer dielectric-ferrite cavity model is used as a representation of the experimental model. Instead of a rigorous solution of Maxwell's equations, the program based on the dispersion equations at resonance is developed and applied to the simplified five-layer model to predict the frequency response of the dielectric-ferrite structure under

the different bias conditions. In order to develop the dispersion equations, Marcuvitz's transverse resonance method (TRM) [16] is applied where the frequency of the lowest order dominant mode is determined from the resonance condition. This approach provides a fast solution to the initial design of the bandpass filter. Results of the TLM analysis are compared with the experimental model.

An initial study of the exact analysis of a dielectric-ferrite interface considering permittivity and permeability components along the major coordinate axis is considered. This initial step is done to gain some insight into the dielectric magnetic interactions at the dielectric-ferrite interface and how these impact the bandpass filter characteristics with respect to center frequency and passband width. An exact analysis will be considered as an analysis using Maxwell's equations for all the field components of the electric (E) and magnetic (H) fields. An exact analysis of the E and H fields across some frequency band would require excessive computational effort and time which will only increase as the structure's complexity increases. This dissertation will present a technique to avoid the time consuming exact analysis.

The insight gained from the initial study of a dielectric-ferrite boundary is applied to a simplified five-layer structure where each layer represents a material interface of a dielectric resonator in a closed metal cavity. This simplified model is referred to as the Simple Five-Layer Model and represents a one pole bandpass filter. This Simple Five-Layer Model is analyzed using the well-known Transmission Line Method (TLM). This work is further extended to analyze a dual mode bandpass filter. An experimental dual mode bandpass filter is used to validate the dissertation analysis along with an EM simulation validation.

1.2 Previous Work and Background

Many EM textbooks or reference books Pozar [1], Harrington [2], Balanis [3], Collin [4], Kong [5], Sodha and Srivastava [6] address the dielectric-dielectric boundary condition. Very few references, such as Pozar [1], Lax and Button [7] and Sodha and Srivastava [6] address the dielectric-ferrite boundary condition. However, the ferrites analyzed in these textbooks are typically saturated and example applications include use of ferrite resonance.

In the published literature, one can find more detail on the exact analysis of partially loaded cavities where the layers are of different dielectric materials enclosed in a metal cavity, [1]–[7]. The metal cavity adds an additional metal-dielectric boundary condition at the extreme ends. There are few published papers on the exact analysis of a partially loaded cavity using both dielectric and ferrite materials [8]–[11]. These materials can be a metal-dielectric-ferrite based structure or a metal-ferrite-dielectric structure. This dissertation considers the later. The previously published applications for this hybrid partially loaded cavity are typically used as electronic structures for antenna applications or photonic structures and not as a filter structure [9],[12].

There are even fewer published papers using ferrite materials as a tuning mechanism [10], [11]. Tuning a dielectric filter's electrical properties by adjusting the material properties of the dielectric is widely used and established whereas the new approach of tuning the filter by adjusting the impedance of the filter network through the ferrite bias to tweak the performance of the bandpass filter is relatively new.

When considering dielectrics, the material's permittivity property, ϵ needs to be defined. When considering ferrites, the material's permittivity, ϵ , and permeability, μ ,

need to be defined. Most dielectrics and ferrites can be described with an isotropic permittivity value. Isotropic permittivity is defined where the permittivity value in all directions and at a specific frequency is equal. For example $\epsilon_x = \epsilon_y = \epsilon_z$ where ϵ_x is a material's permittivity value along the x axis. If these values are the same for all frequencies then the value is a scalar. In contrast, a ferrite's permeability value depends on the magnitude and direction of the applied bias. Therefore, permeability is a tensor.

The boundary conditions of a dielectric-dielectric interface as well as a dielectric-ferrite interface can be determined using Maxwell's integral equations. Typically, the approach is to section the whole structure into smaller subsections and then at each boundary of each subsection satisfy Maxwell's equations - a set of four simultaneous equations. The solution of Maxwell's equations will give detailed information relating E- and H fields along the boundary for each subsection within the structure. This process is used in EM software tools. As the number of subsections increases the number of simultaneous equations that will need to be solved also increases. This makes the solution computationally large.

For filter applications, the critical characteristics of interest are the center frequency and the shape of the frequency response of the structure and not the E and H pattern exclusively. The exact analysis of the E and H fields are also not necessary in a first pass design. In the initial design phase, the structure's center frequency needs to be calculated quickly with efficient methods such as the process developed in this investigation. In the final design phase an exhaustive EM simulation can be performed to validate the design and is used to validate the developed procedure of this dissertation.

Also, note that in the previously published literature of microwave components using both dielectric and ferrite materials many individuals, including Lax and Button [7], J. Krupka [10]-[11] and R.J. Mongia [9], have theoretical and measured data but the rigorous exact analysis has not been published.

Frequency and bandwidth tuning of filters with ferrite materials have been shown in previous work by J. Krupka [10], [11]. In the 1989 published paper [10], a cylindrical ferrite rod is centered in a cylindrical dielectric ring resonator. A single ferrite element is used. Figure 1.2 illustrates a conceptual picture of the structure used. In the 2006 published paper [11], two circumferential ferrite pieces are placed axially on a coaxial cylindrical dielectric ring resonator and illustrated in Figure 1.3. These approaches are single mode TEM applications of the dielectric resonator. The tuning mechanism here is the result of the interaction of both the RF signal and the ferrite resonance.

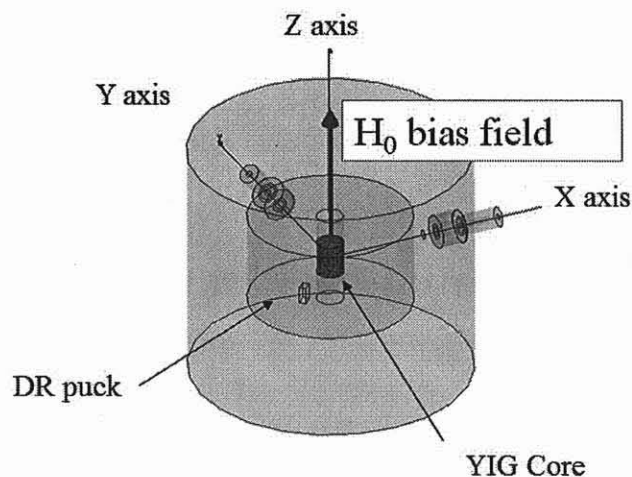


Figure 1.2 Conceptual picture of previous work in [10].

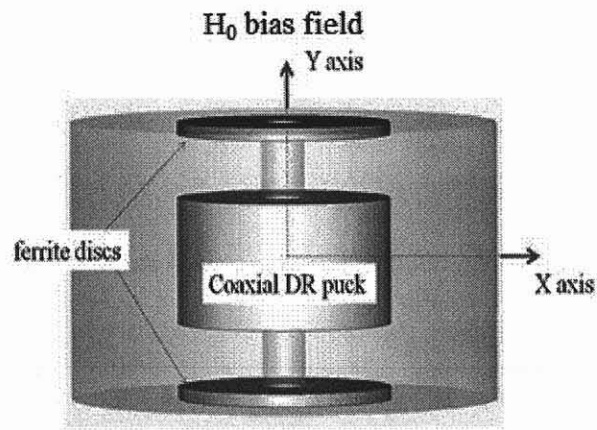


Figure 1.3 Conceptual picture of previous work in [11].

In these past investigations, the ferrite material was used to implement a change of ferrite resonance. Here, the analysis does not depend on the ferrite's resonance or the material's constitutive parameters (ϵ , μ) properties alone but depends on the change of the composite constitutive parameters of the overall structure as a function of applied magnetic field bias and frequency. Previous research typically uses symmetrical static magnetic field biases of the ferrites and claims that the permeability properties of the ferrite account for the shift in frequency. The applied bias for this dissertation is not constrained to have equivalent top and bottom bias values or direction. Previous publications of microwave components use dielectric and ferrite materials that are cylindrical in shape. This dissertation uses a square cross section dielectric resonator with two ferrite square shaped tiles. The previous approaches are single mode TEM applications of the dielectric resonator whereas this investigation involves a dual mode dielectric resonator using the TE/TM mode. In this investigation tuning does not require interaction with ferrite resonance and indeed avoids the ferrite resonance.

1.3 Dissertation Overview

This dissertation describes the analysis of a hybrid partially loaded cavity with dielectric and ferrite materials in a bandpass filter application. Chapter 2 provides enough basic ferrite theory to understand filter tuning mechanism investigated in this dissertation. Chapter 3 continues with the TLM analysis of a single and dual mode bandpass filter. Chapter 4 presents the validation of the TLM method with experimental and EM data and experimental measurements. Finally, Chapter 5 summarizes the major contributions of this work and has suggestions for future investigations. The chapters reflect the phases of the investigation.

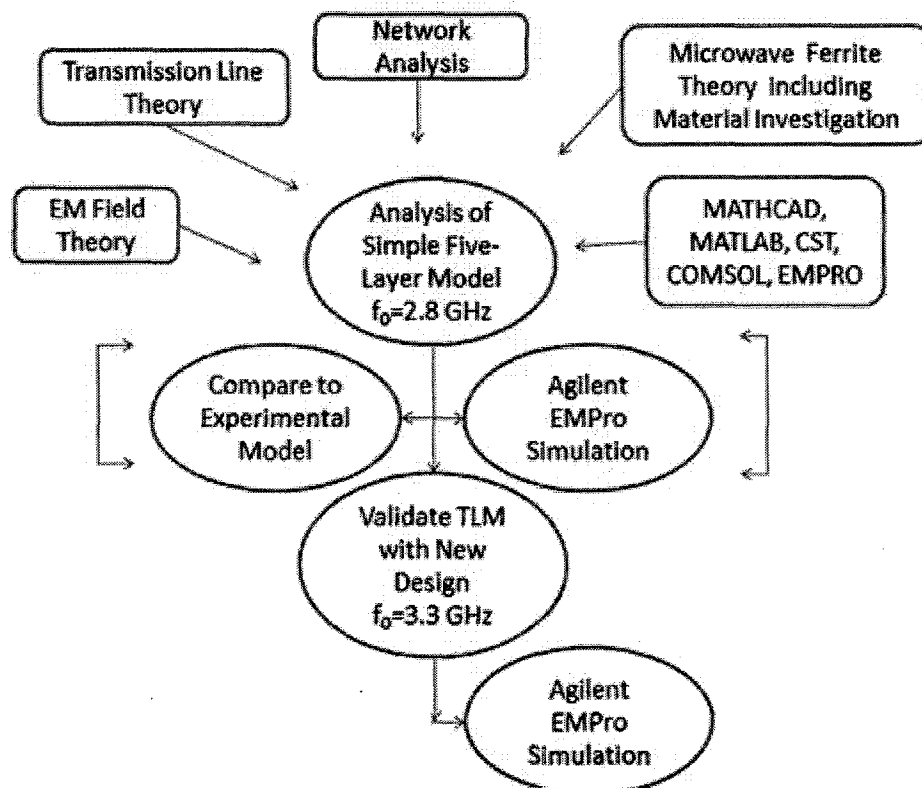


Figure 1.4 Flowchart of dissertation progress.

The Simple Five-Layer Model detailed in Chapter 2 is used to approximate the experimental model. The experimental one pole bandpass model is shown in Figure 1.5.

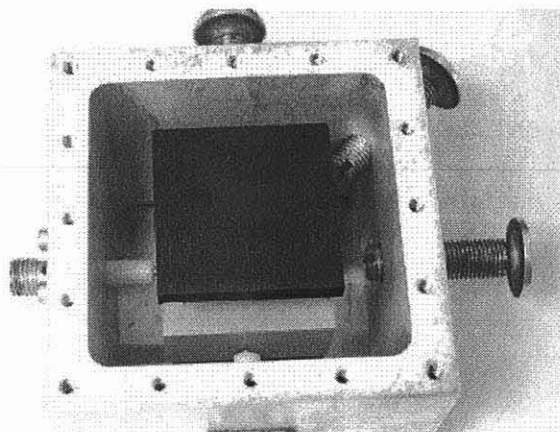


Figure 1.5 Experimental model as developed and measured at RS Microwave, Butler, NJ.

The outside dimensions of the five layer model cavity are the same as the outside dimension of the experimental model cavity. The top and bottom layers of the model represent the ferrite square shaped tiles and have the same thickness and electrical characteristics as the experimental model. The center layer represents the dielectric resonator with the same dielectric properties and height as the experimental model. The relative permittivity of the center layer representing the dielectric resonator is much higher as compared to the air layers about it. Since most of the RF signal is contained within this region the Simple Five-Layer Model is a close approximation of the experimental model. The layers between the dielectric and ferrite in the dissertation analysis model are air filled. In the experimental model within these air layers are mechanical supporting structures for the dielectric. These support are made from a material with a relative permittivity value close to but larger than air, $\epsilon_r > 1$. Each layer

extends the full depth and breadth of the cavity, essentially filling the cavity. The Simple Five-Layer Model is shown in Figure 1.6.

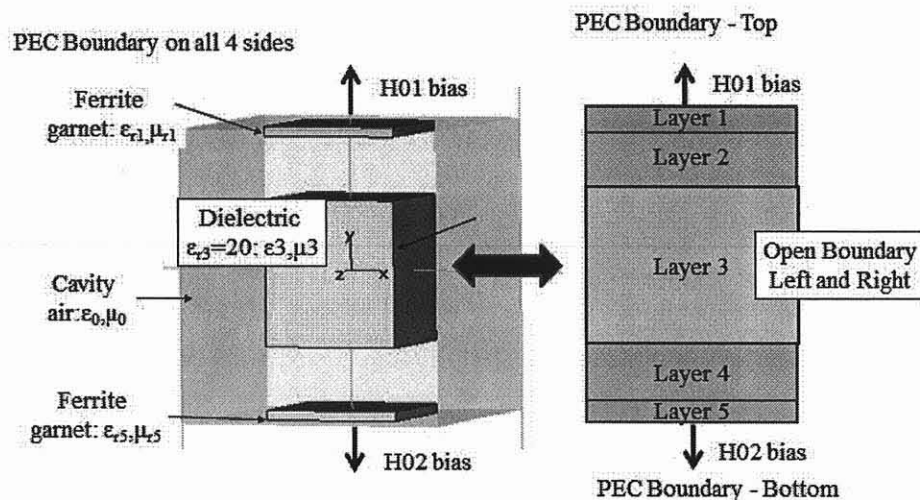


Figure 1.6 Simple Five-Layer Model used as an initial approximation to the experimental model.

The Simple Five-Layer Model approximates the bandpass filter designed with a square cross-section dielectric resonator centered in a square cross section metal cavity. A square cross-section dielectric resonator can support two orthogonal and degenerate eigenmodes. These modes can be coupled to form a resonant pair, and thus form a dual mode resonator. Such resonators can be used to implement a bandpass function and, in this case, will be shown to achieve adjustable center frequencies.

It is assumed that the fields primarily reside in the dielectric. The PEC cavity walls are sufficiently far away from the dielectric resonator to have minimal influence on the results. The thin as compared to wavelength ferrite layers are placed near the top and bottom wall of the cavity with a dielectric air layer between the ferrite and dielectric. The electrically thin layers of ferrite used in the investigation modify the structure's effective permeability value and do not greatly affect the RF signal nor the losses or power

capabilities of the structure. An EAVSMF bias is applied to the ferrite layers normal to the ferrite surface. This is referred to as normal magnetization of the ferrite as opposed to parallel magnetization when the bias is along the ferrite interface. The H field contribution from the external applied bias is parallel to the direction of the bias. The ferrite is assumed to be premagnetized with a bias below the ferrite saturation level and the RF signal is not at the ferrite resonance frequency. Premagnetization is assumed so hysteresis effects are neglected. Hysteresis can be pursued in a future investigation.

The proposed tuning of the bandpass filter is the tuning of the external applied magnetic field bias normal to the ferrite layers. The center frequency, f_0 of the bandpass filter is directly impacted as the structure's composite permeability and permittivity values changes. This dissertation analyzes the effect of EAVSMF on f_0 to the ferrite layers in several modes of operation:

- Zero bias mode when with no bias is applied to the two ferrite layers; [a zero biased ferrite is approximated as a dielectric with the permittivity value of the ferrite and a relative permeability value of free space $\mu_r=1$.];
- “Same” bias mode when the applied biases to the ferrite layers have the same magnitude and polarity;
- “Opposite” bias mode when the applied biases have the same magnitude but different polarity.

Figure 1.7 conceptually depicts “opposite” and “same” applied bias.

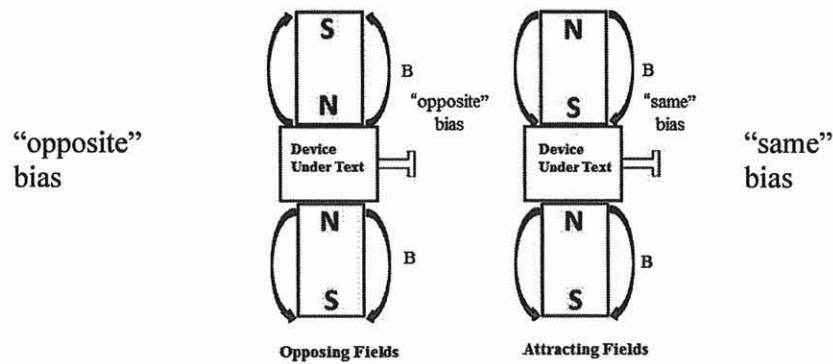


Figure 1.7 Definition of “opposite” and “same” bias.

Figure 1.8 is a photograph of the experimental setup showing the two opposing pole electromagnets that supply “opposite” bias to the ferrite tiles. Typical operating conditions for the electromagnets used in the experiment to bias the ferrite are 6 V.DC, 1.9 A for an average 450 G or 24 V. DC, 7.5 A for an average 1950 G. In tunable filter application using ferroelectric material rather than ferrite material applied voltages in the 100V range is necessary.



Electromagnets in a configuration to supply external “opposite” EAVSMF bias to ferrite.

Figure 1.8 Photograph of the experimental setup.

The one dimensional TLM analysis, as developed in Chapter 3, begins by finding the propagation constant in the y direction for each distinct layer and then is combined to obtain the propagation constant for the composite. A small coupling coefficient is used to split the single pole degenerate modes of the square cross-section to produce a dual mode filter. Practical ways to split the degenerate modes can be achieved by a small corner cut or mitered edge of the dielectric resonator or some other tuner mechanism. The actual implementation of the mode splitting is not considered in this dissertation. The two modes are tuned by varying the ferrite bias.

The TLM developed in this dissertation is shown to provide a means to approximate the resonant frequency change vs. external applied DC bias of the ferrite tiles. The applied magnetic field bias applied along the y direction causes a change in the ferrite's electron alignment which is reflected as a change in the ferrite's permeability value. Each material layer of our simplified model possesses a single transmission line representation. Both an air-dielectric and a ferrite-dielectric interface exist in this Simple Five-Layer Model. Interaction/shaping of the RF signal occurs predominantly in the center dielectric, which represents a dielectric resonator of high permittivity value and can propagate along the layer interfaces or normal to the interface. The propagation constant of the composite structure must include both the permittivity and permeability of the media because of the inclusion of the ferrite layers. The frequency shift of the lowest order mode, when magnetizing the ferrite tiles, is the novel result of this dissertation.

Both experimental and software validation are important. Both Ansys HFSS and AGILENT EM PRO EM simulators are used as the software validation tools. This dissertation uses the TLM as mentioned in Pozar [1], Balanis [3] and others. This

investigation extends the developed TLM for multilayer dielectrics to a mix of dielectrics and ferrites. A major motivation for using this approach to look at this multilayer dielectric-ferrite model is the speed in calculating the center frequency. Once the lowest order dominant hybrid mode of the composite is found, an effective permittivity and permeability can be calculated. This lowest order dominant mode is not purely a Transverse Electric (TE) or Transverse Magnetic (TM) mode as classically defined. To indicate this deviation a δ symbol is added to the mode number. The lowest order mode is then either a $TE_{10\delta}$ or $TM_{10\delta}$.

This investigation does not intend to trivialize the complexity of designing a tunable bandpass filter with the use of ferrite and dielectrics. This is indeed a difficult task. The difficulties encountered include the input and output port couplings and the geometries of the cavity, dielectric and ferrite parts. The material properties of the system such as the dielectric permittivity and ferrite permeability are also frequency, orientation and bias dependent. These material properties affect the calculation of the resonant frequency and should be investigated in a future continuation of this dissertation.

There are many numerical and iterative methods available that use full 3D EM simulators based on solving Maxwell's equations. These 3D EM simulators solve the geometry model at the cost of heavy computing power. The proposed TLM method is quicker than the full 3D EM tools to determine the resonant frequency of the composite structure and to provide an insight to the behavior of the filter's lowest order mode as the ferrite bias changes.

1.4 Contributions and Summary

In summary the emphasis of this dissertation is to provide an efficient design tool to predict the amount of frequency shift of a dielectric-ferrite structure using TLM of the lowest order mode. This simple structure can be used as the basis for more complex structures to be developed.

The contributions of this dissertation are below:

- Previous works investigated a z directed bias in the direction of propagation and along the surface interfaces. This dissertation uses a formal analysis of Polder's permeability tensor with a y directed bias normal to propagation direction and to the surface interfaces.
- Previously published works using microwave ferrites with circulators and isolators are biased at or above saturation levels and takes advantage of the ferrite resonance property. This dissertation uses an applied external bias that avoids both the ferrite resonance and saturation levels..
- A transmission line method for a square cross section shaped structure includes both permittivity and permeability of the materials is developed.
- A passive circuit equivalent for a composite dielectric-ferrite single mode and dual mode bandpass filter with "same" and "opposite" bias as defined above is developed.
- The TLM approach of tuning a composite dielectric- ferrite system with applied bias is used to efficiently design a tunable bandpass filter.

CHAPTER 2

FERRITE ANALYSIS

2.1 Overview

This dissertation involves the use of ferrite material to magnetically tune a dual mode bandpass filter. This requires a few basic ferrite concepts which are review. A more detailed review of ferrite theory can be found in Lax and Button [7].

In the experimental model, the ferrite tiles are located at the the top and bottom metal covers of the cavity. The standard thickness of ferrite tiles provided by Trans-Tech, a ferrite vendor, is in multiples of 1/16'. Therefore, tiles of thickness 1/16" are used for the top and bottom layers, L_5 and L_1 , respectively. This thickness is much less than a wavelength at the frequency of operation. Therefore the ferrite is assumed to be linear and isotropic with negligible gyrotropic effects.

The previous filter ferrite application referred to in Chapter 1 by Krupka [10], [11] bias the ferrites to their resonance level. In this dissertation application, the ferrites are partially magnetized and are not biased to resonance or saturation levels. Partial magnetization with "opposite" bias mode direction is the unique and never before published concept for a filter application. A bias range of +/-100 to +/-500 Oe is used

. The RF frequency is 2800 MHz. Previously published literature biases the ferrite parallel to the interface as this provides more magnetic effects to the RF signal [10], [11]. In this investigation the RF signal propagates parallel to the layer interfaces and the EAVSMF bias is normal to the layer interfaces. In this configuration the ferrite acts more like a dielectric.

2.2 General Ferrite Properties

It is important to understand the ferrite properties on a macroscopic level so that intelligible results can be extrapolated. An applied bias in a ferrimagnetic material changes the electron alignment. Figure 3.1 shows how the free electrons in the ferrite align with the external magnetic field bias, H_0 as it increases. The right most figure below depicts when the applied bias H_0 reaches saturation level defined as M_{sat} . The left and middle figures depict the proposed use.

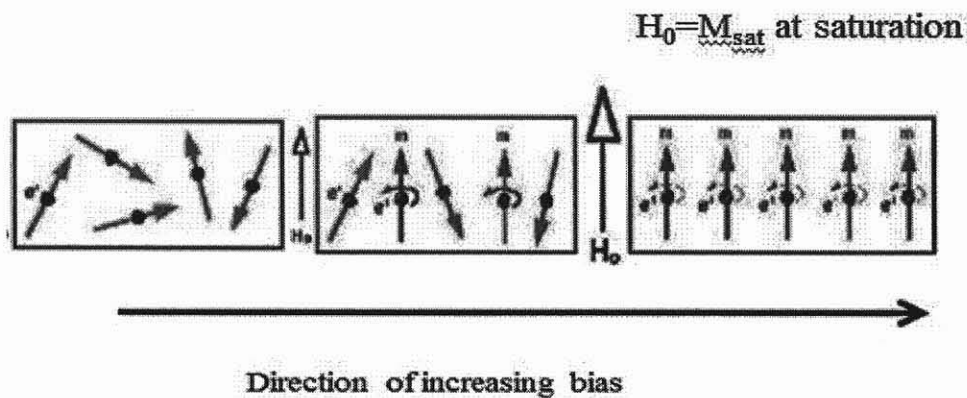


Figure 2.1 Snapshots of ferrite magnetization with electron spin as bias H_0 increases [19].

Ferrites from Trans-Tech that are considered for this investigation include G113 [13], G510 [14] and TTVG-1950 [15]. These ferrites are classified as having high saturation values and narrow line widths. G113 ferrite material is used in the experimental model. G510 ferrite material is considered since it is also a narrow line width ferrite material which has a saturation level less than G113. TTVG1950 ferrite material is also considered since it is also a narrow line width material with a saturation level higher than G113. The datasheets as provided on the Trans-Tech website are copied below.

Table 2.1 Trans-Tech G113 Datasheet [13]

Parameter	Value
Line Width δH Oe @ -3dB	≤ 25
Dielectric Constant	$15.0 \pm 5\%$
Saturation Magnetization $4\pi M_s$	$1780 \pm 5\%$
Landé g-Factor g-eff	1.97
Dielectric Loss Tangent	$<.0002$
Curie Temperature $T_c(^{\circ}C)$	280
Spin Wave Line Width δH_k Oe	1.4
Remanent Induction B_r (Gauss)	1277
Coercive Force H_c (Oe)	45%
Initial Permeability μ_0	134

Table 2.2 Trans-Tech G510 Datasheet [14]

Parameter	Value
Saturation Magnetization $4\pi M_s$	$550 \pm 5\%$
Landé g-Factor g-eff	2
Line Width δH Oe @ -3dB	≤ 48
Dielectric Constant	$14.3 \pm 5\%$
Dielectric Loss Tangent	$<.0002$
Curie Temperature $T_c(^{\circ}C)$	155
Spin Wave Line Width δH_k Oe	1.3
Remanent Induction B_r (Gauss)	398
Coercive Force H_c (Oe)	55%
Initial Permeability μ_0	37

Table 2.3 Trans-Tech TTVG-1950 Datasheet [15]

Parameter	Value
Landé g-Factor g-eff	2
Line Width δH oe @ -3dB	≤ 15
Dielectric Constant	$15.0 \pm 5\%$
Saturation Magnetization $4\pi M_s$	$1950 \pm 5\%$
Dielectric Loss Tangent	$<.0002$
Curie Temperature T_c (°C)	235
Spin Wave Line Width δH_k oe	2.0
Remanent Induction B_r (Gauss)	-
Coercive Force H_c (Oe)	-
Initial Permeability μ_0	-

2.2.1 Ferrite Permeability

For magnetic materials, permeability is a tensor and typically nonreciprocal. For this investigation the magnetic bias is in the y direction perpendicular to the layer surfaces.

The permeability tensor as detailed in Lax and Button [7] is provided below

$$\begin{pmatrix} \mu_{xx} & \mu_{xy} & \mu_{xz} \\ \mu_{yx} & \mu_{yy} & \mu_{yz} \\ \mu_{zx} & \mu_{zy} & \mu_{zz} \end{pmatrix} \longleftrightarrow \begin{pmatrix} \mu_{xx} & 0 & \mu_{xz} \\ 0 & \mu_{yy} & 0 \\ \mu_{zx} & 0 & \mu_{zz} \end{pmatrix} \quad (2.1)$$

In the derivation of the permeability tensor the RF signal is perpendicular to the internal DC magnetic field of the electrons. It is also assumed that the RF magnetization is also much less than the electron magnetization. Damping is also neglected. It is assumed that a steady state of magnetization has been reached, that is the ferrite is

saturated. More detail about ferrite theory is provided in [5],[7],[17]-[19],[21]. The equations below are valid for regions close to the ferrite resonance but not at resonance.

These regions are depicted in Figure 2.15.

The off diagonal components $\mu_{xz} = -\mu_{zx} = \kappa$ are dependent on the ferrite material's saturation value, M_{sat} , the external applied bias, H_0 , and the operating frequency, ω as shown below

$$\mu = \mu_0(1 + \chi_{zx}) = \mu_0(1 + \chi_{xz}) = \mu_0 \left(1 + \frac{\omega_0 \omega_m}{\omega_0^2 - \omega^2} \right) = \mu_0 \mu_r \quad (2.2)$$

$$\kappa = -j\mu_0 \chi_{zx} = j\mu_0 \chi_{xz} = \mu_0 \frac{\omega \omega_m}{\omega_0^2 - \omega^2} \quad (2.3)$$

where

$$\chi_{xx} = \chi_{zz} = \frac{\omega_0 \omega_m}{\omega_0^2 - \omega^2} \quad (2.4)$$

$$\chi_{zx} = -\chi_{xz} = j \frac{\omega \omega_m}{\omega_0^2 - \omega^2} \quad (2.5)$$

$$\omega_0 = \mu_0 \gamma H_0 \quad (2.6)$$

$$\omega_m = \mu_0 \gamma M_{\text{sat}} = 2\pi f_m = 2\pi \cdot 2.8 \cdot 10^6 M_{\text{sat}} \quad (2.7)$$

$$\gamma = 2.8 \text{ MHz/Oe} \quad (2.8)$$

As shown in Equation 2.2, the permeability tensor has a singularity at $\omega_0 = \omega$. This is known as the ferromagnetic or gyromagnetic resonance frequency. As shown in Pozar [1, Figure 10.8] the resonant frequency of a ferrite medium with a saturation magnetization of 1800 Oe and an applied bias of 3570 Oe is 10 GHz. Figure 2.3 is the result from the MATLAB program ferriteCurves.m in Appendix A

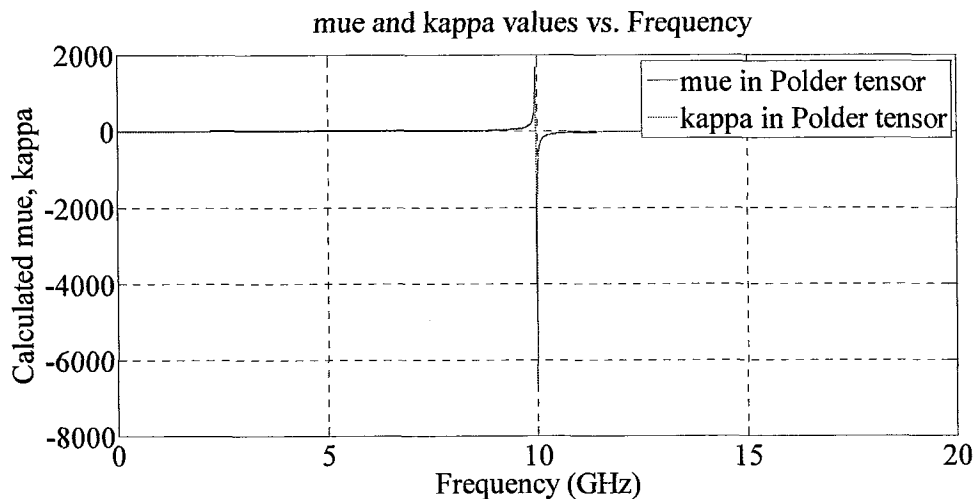


Figure 2.2 Numerical solution of permeability and susceptibility in Polder tensor as a function of frequency for a ferrite medium with $M_s=1800$ Oe and an applied bias of 3750 Oe [1, Figure 10.8].

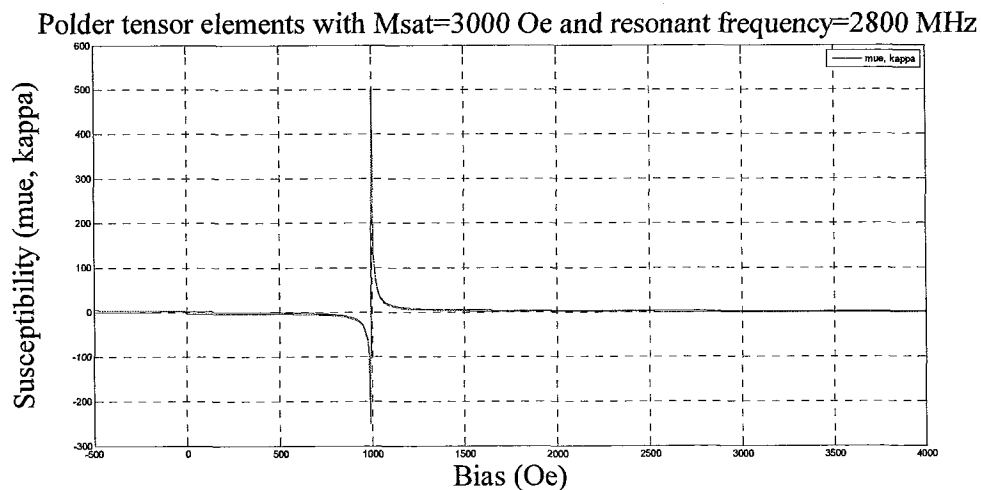


Figure 2.3 Variation of permeability and susceptibility in Polder tensor as a function of applied bias for a ferrite medium with $M_s=3000$ Oe and resonant frequency=2800 MHz [7, Figure 4.3].

2.2.2 Resonance Frequency and Line Width

Figure 2.3 is the numerical solution to Equations 2.2 and 2.3 defining permeability and susceptibility elements in the Polder equation. Loss is neglected here so a sharp discontinuity is seen at the resonant frequency – a singularity in the denominator of these

equations. In practical applications there are losses. More detail concerning these losses can be found in Landau and Lifshitz [21].

The losses are defined by the coefficient α in the Landau-Lifshitz equation and used to define the ferrite line width ΔH . Line width is defined as the frequency bandwidth where the susceptibility (permeability) curve falls 3 dB below the peak of the susceptibility (permeability) curve.

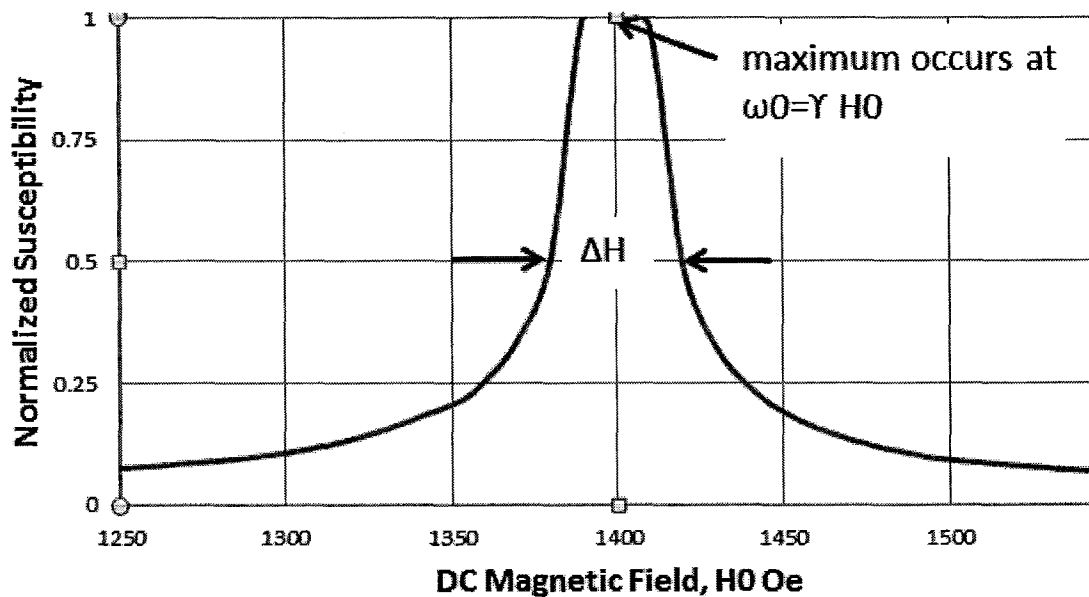


Figure 2.4 Definition of ferrite line width.

According to Lax and Button [7, Sec.4.2], there is a very simple method to convert the lossless form of the susceptibility to one with loss. The rule is to replace ω_0 with $\omega_0 + \frac{j}{T}$ where T defines the relaxation time of the ferrite moment. The expression for T follows [7, eq.(4.35)] repeated below

$$\Delta\omega = \frac{2}{T} = \gamma \cdot \Delta H \quad (2.9)$$

where ΔH is the line width of the ferrite material.

Modifying Equations 3.4 and 3.5 to include loss

$$X_{xx} = \frac{(\omega_0 + \frac{j}{T})\omega_m}{(\omega_0 + \frac{j}{T})^2 - \omega^2} \quad (2.10)$$

$$X_{xy} = \frac{\omega \cdot \omega_m}{(\omega_0 + \frac{j}{T})^2 - \omega^2} \quad (2.11)$$

Using the sample ferrite materials in [7, Figure 4.3] and the ferriteCurve.m MATLAB program, the Figures 2.5 to 2.9 are generated. These curves match the reference curves stated.

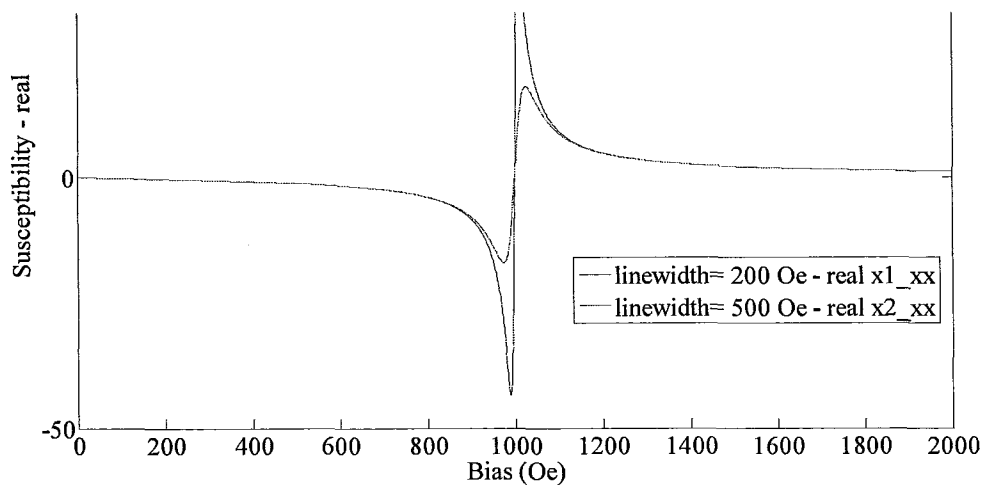


Figure 2.5 The real part of the dispersive components of the susceptibility tensor for G113 ferrite. These values are computed for a RF frequency of 2800 MHz and a saturation magnetization of $4\pi M_s = 3000$ gauss [7, Figure 4.3].

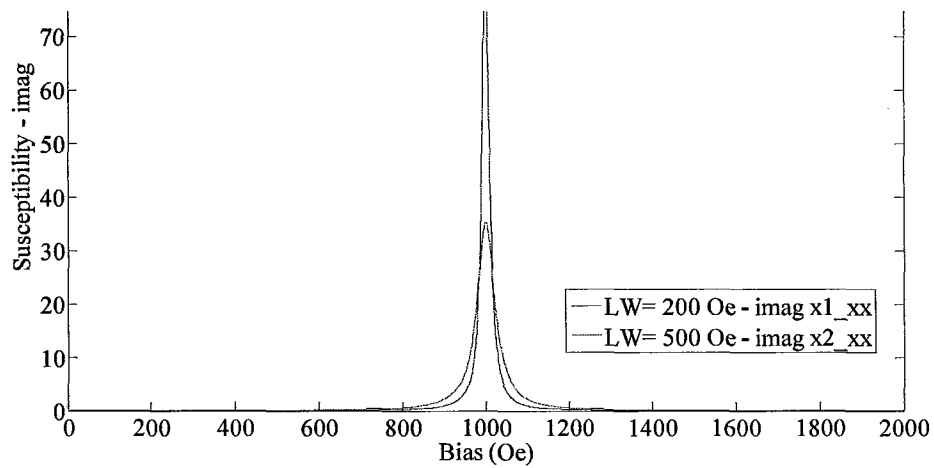


Figure 2.6 The imaginary part of the dispersive components of the susceptibility tensor for G113 ferrite. These values are computed for a resonance frequency of 2800 MHz and a saturation magnetization of $4\pi M_s=3000$ gauss [7, Figure 4.3].

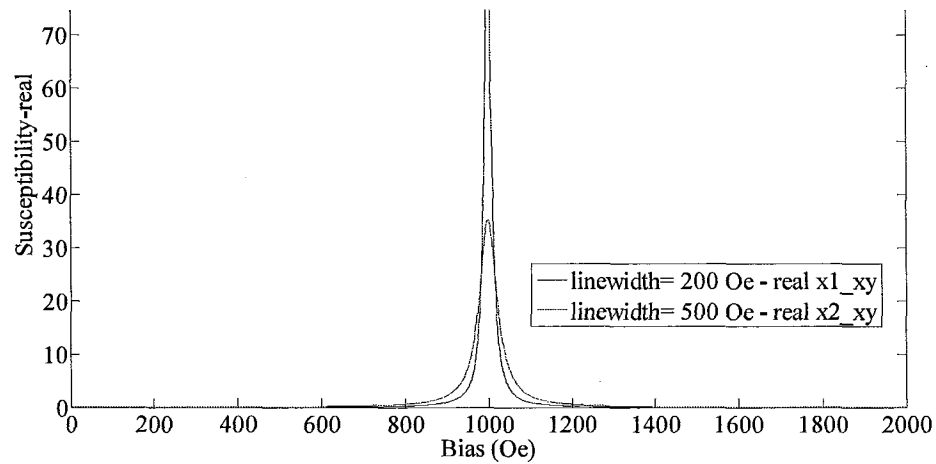


Figure 2.7 The real part of the dissipative components of the susceptibility tensor. These values are computed for a resonance frequency of 2800 MHz and a saturation magnetization of $4\pi M_s=3000$ gauss [7, Figure 4.3].

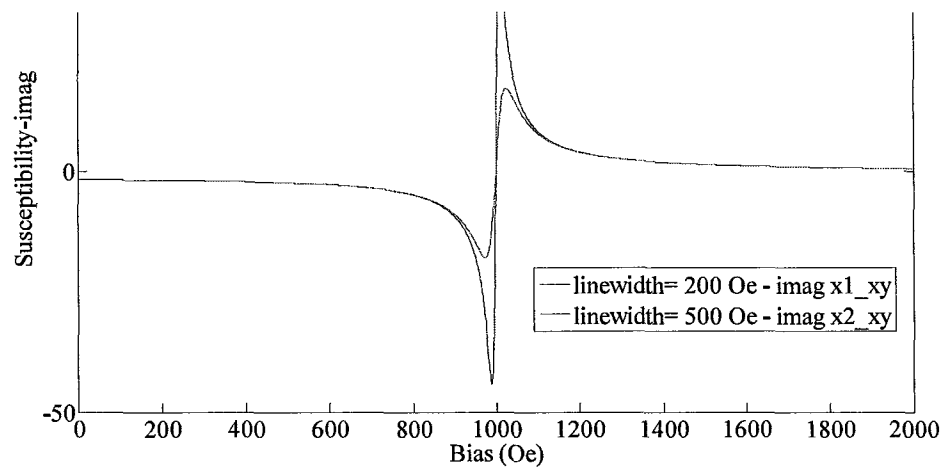


Figure 2.8 The imaginary part of the dissipative components of the susceptibility tensor for G113 ferrite. These values are computed for a resonance frequency of 2800 MHz and a saturation magnetization of $4\pi M_s=3000$ gauss [7, Figure 4.3].

Figures 2.5 to 2.8, following [7, Figure 4.3], clearly shows the effects of line width on the ferrite properties. Figure 2.9 is an expanded view of absolute value of Figure 2.8.

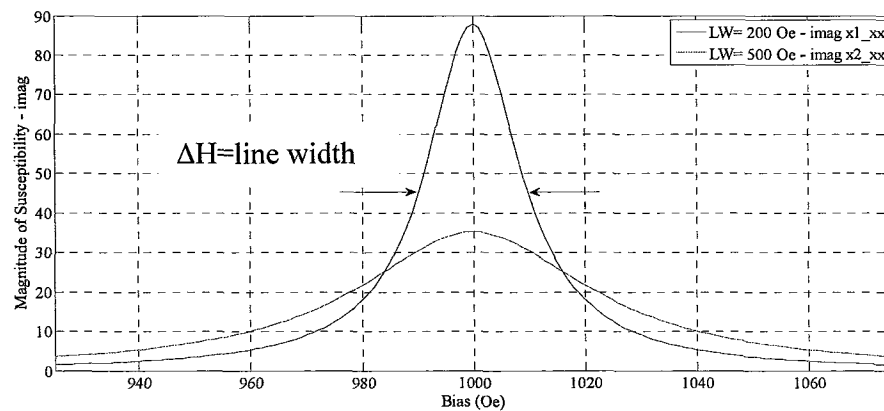


Figure 2.9 Expanded view of magnitude of Figure 2.8.

Figure 2.9 illustrates the effect of line width on a ferrite's susceptibility curve. As the line width is increased the base of the curve expands as the peak is dampened. The sharp change in the ferrite's permeability property is needed in order to cause a large change in the ferrite impedance. A narrow line width ferrite material is indicative of this

sharp change in impedance. It is shown in this dissertation that a narrow line width ferrite is necessary to implement a larger tuning range for a bandpass filter application. Most ferrite materials have a Landé factor of 2 [7, Sec. 2.2]. A Landé factor $\gamma = 2$ is used in the above calculations and throughout this dissertation. The MATLAB program, ferriteCurve.m is used to generate Figure 2.10. The red line in Figure 2.10 indicates the RF frequency. To avoid operation near the resonant frequency of the ferrite, the applied bias should be above or below 1000 Oe.

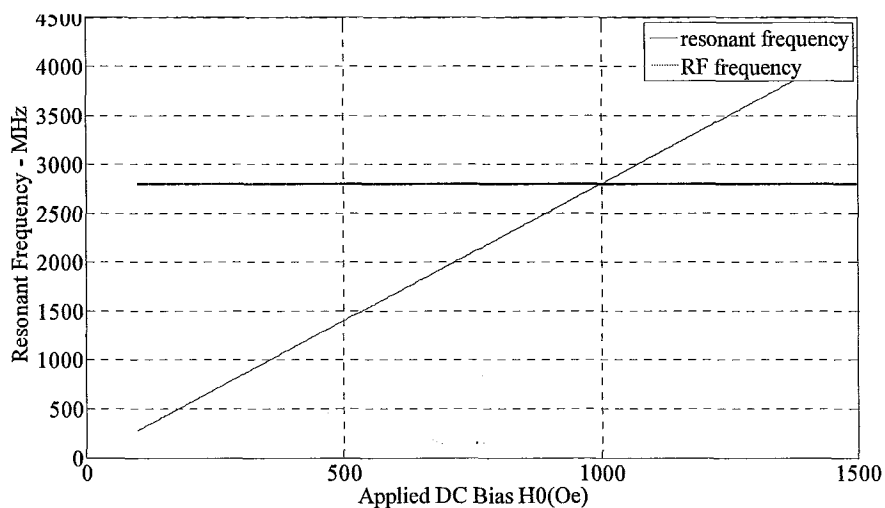


Figure 2.10 Resonant frequency as a function of EAVSMF bias.

2.2.3 Saturation Magnetization

Saturation is defined as the point when the magnetic moment of the ferrite aligns with the applied bias field. Saturation frequency is defined in Equation 2.7 following [7, eq.(4.15)].

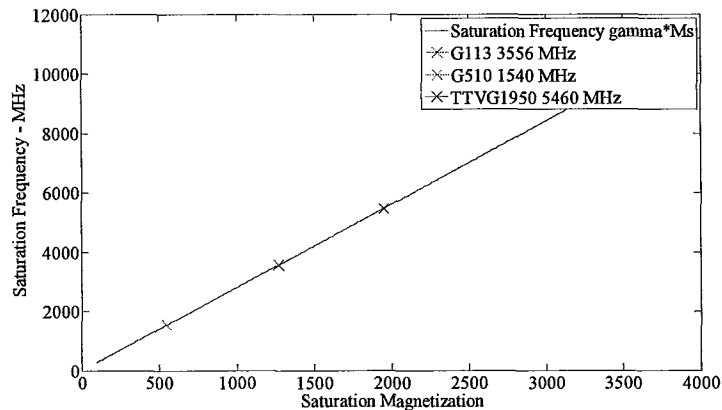


Figure 2.11 Saturation Frequency as a function of Saturation Magnetization.

A negative sign in ω_0 and ω_m indicates a change in direction of the biasing field. When the direction of the applied bias is changed, then both H_0 and M_{sat} will change signs. This includes a change of sign for ω_0 and ω_m . A change in the direction of bias is equivalent to changing the direction of electron rotation. The bias direction change will not affect the value of μ and κ but will affect the sign of κ but not μ .

This investigation does not consider effects of intrinsic ferrite loss mechanisms of the material: due to porosity, surface roughness and impurities or due to the magnetic anisotropy due to magnetic bias on ferrite resonance. There is less loss when operating a ferrite below the ferrite resonance frequency than operating it in the above. It is important that filters have minimal insertion loss, therefore in practical filter applications the ferrite should be biased below the resonant frequency.. Ferrite loss effects as mentioned above when used in filter applications should be considered in a future investigation.

The intrinsic ferrite loss mechanism is enhanced in this filter application because the applied magnetic field is lower than H_{int} needed for resonance of 1000 Oe as calculated above. In previous ferrite loss studies, the ferrite is biased to saturation, that is,

above H_{int} . H_{int} is the amount of applied bias needed to align the ferrite dipoles in the direction of the biasing field. Ferrite anisotropy being defined as the spins of the electrons not aligned in the direction of the applied bias. Issues contributing to ferrite anisotropy include but are not limited to thickness, length and shape of the ferrite tiles, in conjunction with the value and direction of the EAVSMF bias.

The impact of the above mentioned losses to the permeability tensor should be investigated in a pending dissertation.

2.3 Properties of G113 Ferrite as Used in Investigation

For this specific structure, the real part of the susceptibility/permeability dominates the imaginary part of susceptibility/permeability and the real and imaginary parts of susceptibility therefore only curves of the real part of the susceptibility/permeability are shown. Susceptibility/permeability factor is a complex number.

Figure 2.12 is a plot of both the real part of the susceptibility and the relative permeability factor with a RF signal frequency of 2800 MHz of the G113 material used in the ferrite tiles of the experimental model as a function of applied bias. The G113 ferrite material will resonate with the RF signal when an external bias of 1000 Oe is applied. For this investigation this resonant frequency must be avoided therefore the external bias must not equal 1000 Oe. Figure 2.12 can be divided into three distinct regions. Region 1 is defined as the biases below resonance. Region 2 is defined at resonance. Region 3 is defined at biases above resonance. These regions are denoted in Figure 3.12.

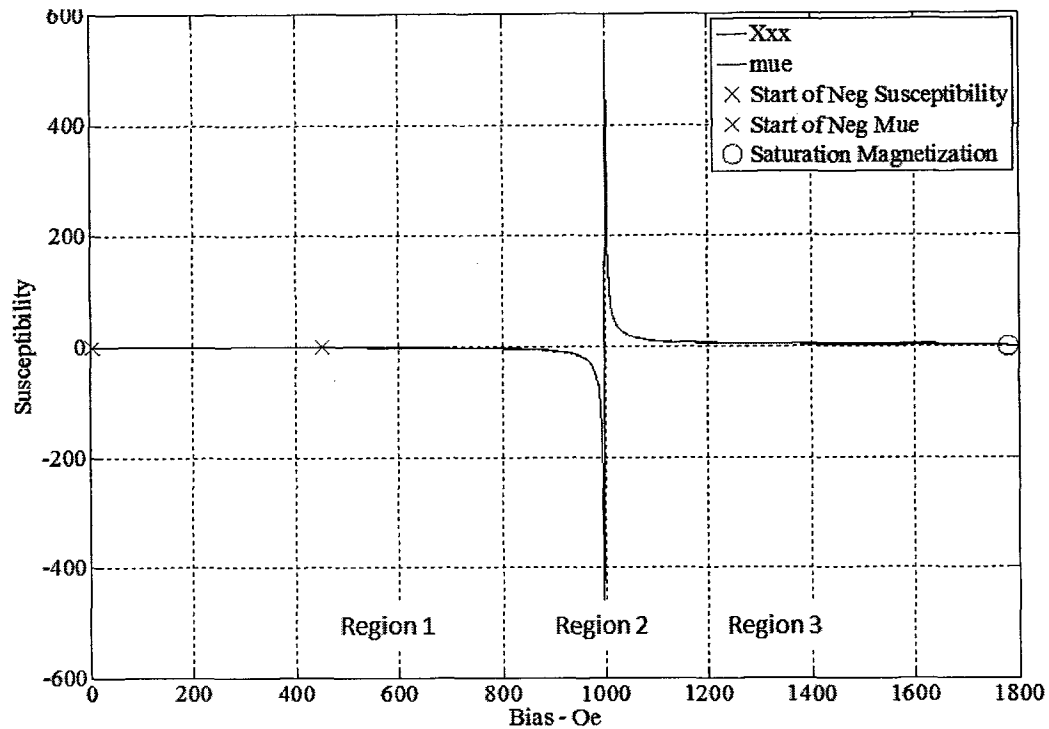


Figure 2.12 Susceptibility and Relative Permeability as a function of applied bias for G113 ferrite and an operating frequency of 2800 MHz.

In Region 1 at biases less than 1000 Oe, both the permeability and the susceptibility may have values less than 1. This initial gradual decline in susceptibility at resonance is detailed in [7] and is a result of the scattering of the electrons in the ferrite lattice. A negative relative permeability value yields an imaginary propagation constant or evanescent region [22].

In Region 2 the ferrite permeability has its steepest slope when operated close to the ferrite resonance.

In Region 3 at bias greater than 1000 Oe the susceptibility/relative permeability factor is greater than 1. Region 3 contains the saturation magnetization where the ferrite has reached its saturation level. For a tuning application magnetic bias must always be lower than the saturation magnetization of the ferrite. As the bias approaches the

saturation level the change in permeability vs. bias is greatly reduced and therefore impractical for tuning applications.

Figures 2.13 and 2.14 are the susceptibility curves of G113 as a function of the RF signal frequency at 2800 MHz and biases of 400 Oe and 500 Oe. These biases are those used in the initial experimental model validating this dissertation.

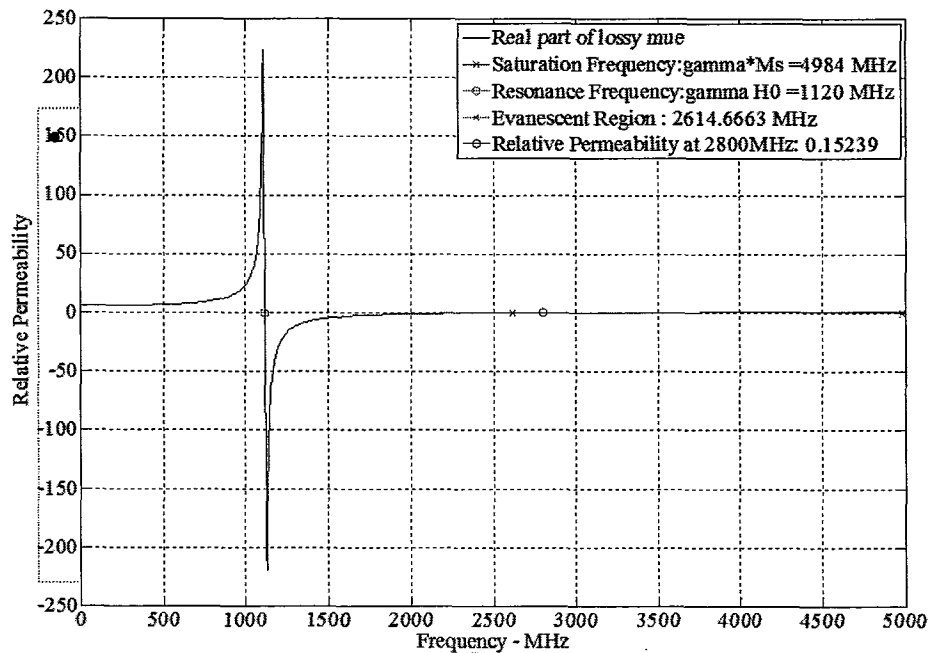


Figure 2.13 Susceptibility as a function of frequency for G113 and applied bias=400 Oe.

In Figure 2.13 the resonant frequency of the G113 material with an applied bias of 400 Oe and at the operating frequency of 2800 MHz is 1120 MHz.

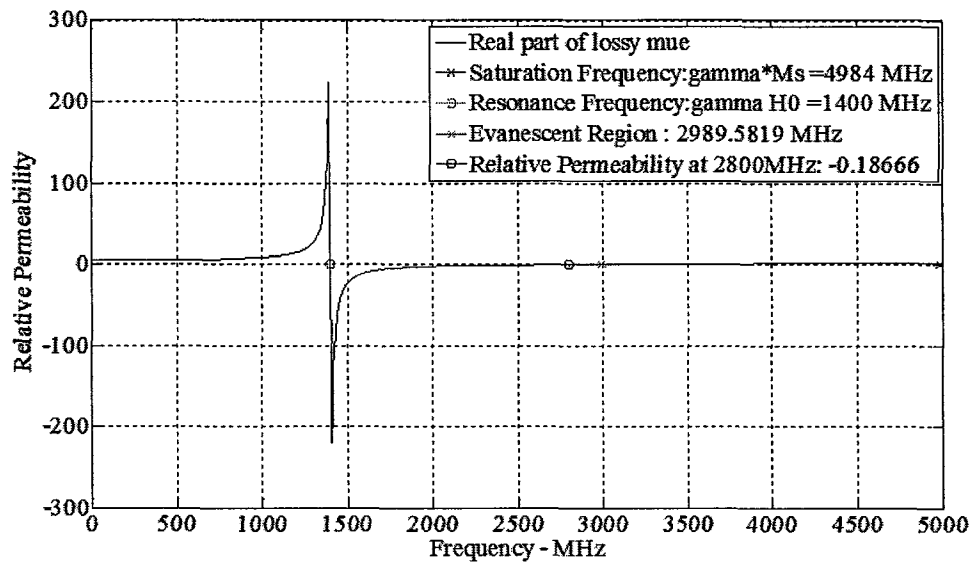


Figure 2.14 Susceptibility as a function of frequency for G113 ferrite and applied bias=500 Oe.

The resonant frequency of the G113 material with an applied bias of 500 OE and at the operating frequency of 2800 MHz is 1400 MHz. Figures 2.13 and 2.14 clearly show that varying the bias will also vary the resonant frequency. These plots show that as bias is increased, the frequency range between the saturation frequency and the resonance frequency is reduced. In Figure 2.12 the frequency range for an applied bias of 400 Oe is 3864 MHz.

$$f_{m_G113} - f_{0_G113} \quad (2.12)$$

$$4984 - 1120 = 3864 \quad (2.13)$$

The frequency range for an applied bias of 500 Oe is 3584 MHz.

$$4984 - 1400 = 3584 \quad (2.14)$$

A more detailed look at the susceptibility/relative permeability tensor is necessary to further define the optimal tuning range of the bandpass filter. The susceptibility term is

a function of bias, frequency and saturation value. An additional figure of merit used to characterize losses in a ferrite is line width, ΔH . Specifically, line width is the 3 dB bandwidth about the ferrite resonant frequency. This range of bias/frequencies needs to be avoided as well. Figure 2.15 is the magnitude of susceptibility curve as shown in Figure 2.14 with the line width indicated.

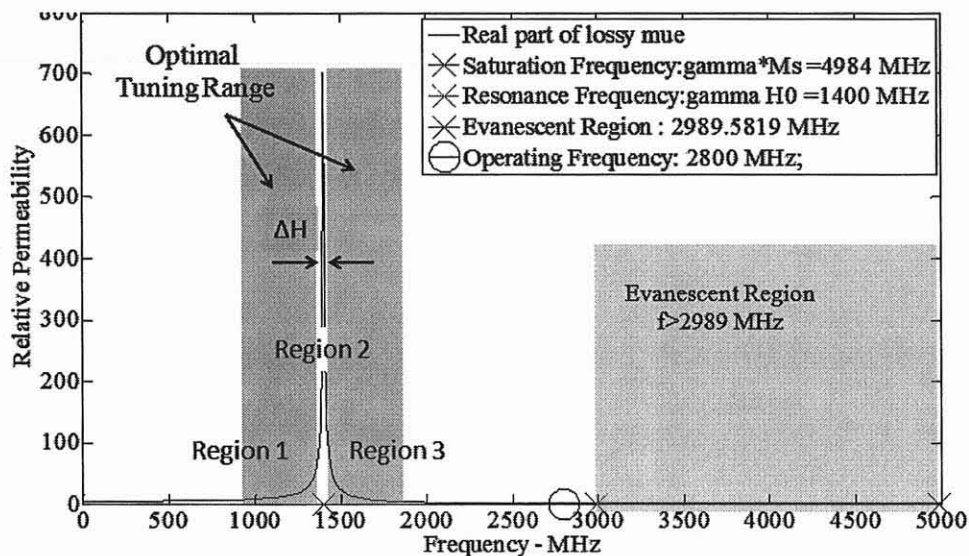


Figure 2.15 Magnitude of susceptibility as a function of frequency for G113 and applied bias=500 Oe and line width =15 Oe.

In general, the operating range of permeability vs. bias should be above or below the ferrite resonant frequency and outside the line width region. The same definition of regions used in the curve of permeability vs. bias will be used in the curve of permeability vs. frequency. The relationship between bias and frequency is the Landé factor. Region 1 is defined as frequencies below the resonant frequency, $f < f_0$. Region 2 is defined at resonance including the ferrite line width interval. This region needs to be avoided for tuning applications. Region 3 is defined above the resonant frequency, $f > f_0$. Region 3 includes the saturation frequency. Just before saturation the relative permeability can be negative, evanescent. For example using G113 material with

$4\pi M_{\text{sat}}=1780$ G, an applied bias of 400 Oe and a signal frequency of 2800 MHz, yields a precession frequency, f_0 of 1120 MHz and a saturation frequency, f_m of 4984 MHz. The susceptibility term is less than 1 yielding a negative permeability value for μ when

$$(f_0 \cdot f_m) > (f_0^2 - f^2) \quad (2.15)$$

Rewriting this equation, Region 3 is defined when

$$f^2 > (f_0^2 + f_0 \cdot f_m) \quad (2.16)$$

Table 2.4 details the computed values used in the TLM program to generate Figure 2.15 for G113 ferrite material with an applied bias of 500 Oe and a signal frequency of 2800 MHz.

Table 2.4 Tabulated Parameters from TLM Program Used To Generate Figure 2.15

Landé Factor	γ	2.8 MHz/Oe
Applied bias	H0	500 Oe
Saturation Magnetization	$4\pi M_{\text{sat}}$	1780 G
Resonant frequency, f_0	$f_0=\gamma H_0$	1400 MHz
Saturation frequency	$f_m=\gamma M_{\text{sat}}$	4984 MHz
Frequency when $\mu_r < 0$	$\sqrt{(f_0^2 + f_0 \cdot f_m)}$	2989 MHz

An applied bias greater than 500 Oe is needed to be in the optimal tuning range for a filter centered at 2800 MHz. The bias must be above what is needed to resonant the ferrite above the operating frequency plus the ferrite line width. A bias of 1050 Oe is selected and results in a resonant frequency of 2940 MHz as shown in Figure 2.16.

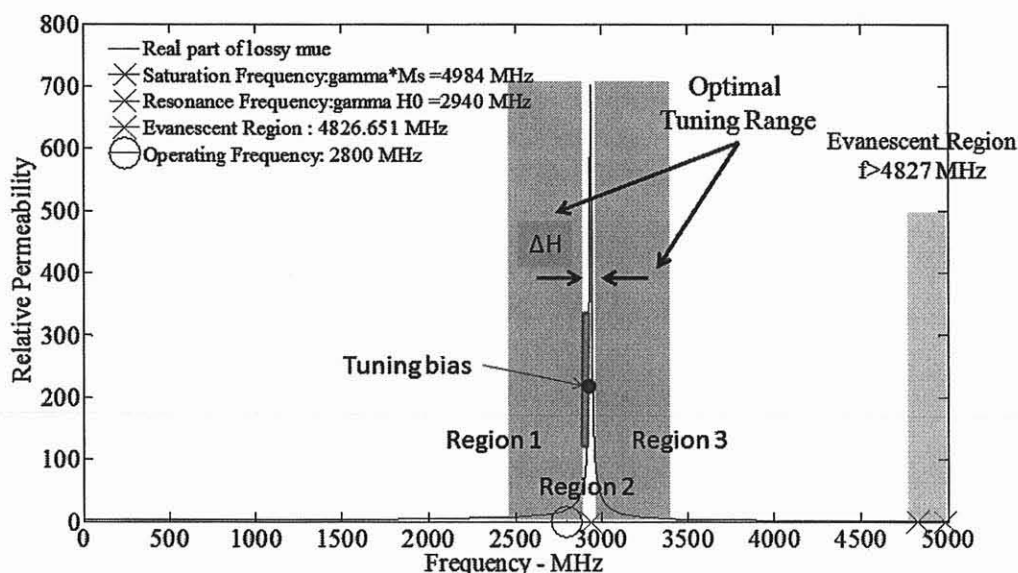


Figure 3216 Susceptibility as a function of frequency for G113 ferrite and applied bias=1050 Oe and line width = 15 Oe.

In the proposed tuning configuration, use of the ferrite material in both the saturation and resonance regions must be avoided. The operating range of permeability vs. bias should be above or below the ferrite resonant frequency and outside the line width region. Operation close to resonance region will guarantee the largest permeability change vs. bias thus maximizing tuning range. To avoid ferrite saturation and evanescent mode operation the ideal tuning range is just past the knee of the curve in the linear region just below the ferrite resonance and its line width region. Some selected tuning bias point and tuning range is indicated in Figure 2.16 to show this operating point.

2.4 Summary of Microwave Ferrite Use in a Bandpass Filter Application

There has been little research in using ferrites below saturation levels in microwave systems. The dielectric properties of the ferrite are used to tune the filter's resonant frequency when the ferrite is below saturation.

This application dictates that the RF signal must not interact with the applied field. This means the RF frequency must be away from the resonant frequency but close to take advantage of the change in permeability values. The tuning of the bandpass filter is heavily dependent on the impedance change of the ferrite with bias. The larger the change the larger the tuning range. This implies the use of a ferrite material with narrow line width.

In this dissertation the electromagnetic field in the XZ direction is propagating perpendicular to the EAVSMF in the Y direction. It has been shown that propagation of RF field in this set up is unaffected by the magnetic medium and propagates as it would in a dielectric. If the RF signal propagates in the same direction as the biasing field, then the magnetic properties of the ferrite will need to be considered. This will be left as future research.

To summarize

- The EAVSMF bias should be below the saturation bias.
- Optimal tuning occurs when the applied bias induces a frequency near but not at the Larmor resonance frequency.
- The use of narrow line width to take advantage of large permeability change and low loss.
- The use of ferrite materials makes application favorable to high power applications.

CHAPTER 3

TRANSMISSION LINE ANALYSIS

3.1 Overview

In the one dimensional TLM approach, the impedance equations are defined for the dielectric and ferrite layers of the Simple Five-Layer Model in the y direction normal to the interface of the layers. The impedance equations are found by following the classical method when analyzing a waveguide. In this analysis the resonant frequency is found from solving the dispersion equation developed by the TLM impedance equations and not solving Maxwell's equations as in a full wave analysis. The dielectric materials used are assumed to be isotropic. Isotropy implies that the permittivity and permeability of the material along the major axes are equal, $\epsilon_x = \epsilon_y = \epsilon_z$ and $\mu_x = \mu_y = \mu_z$. The TLM approach assumes a lossless and non-dispersive case.

Each layer of the Simple Five-Layer Model will be considered as one transmission line media. Input/output port discontinuities are not taken into account. Each layer is considered as a homogenous medium. In a waveguide with both dielectric and ferrite layers both TE and TM modes exist in each layer as well as a hybrid mode. At the interface the continuity condition for either TE or TM or some combination of both needs to be satisfied. Only the lowest order dominant mode is needed for this analysis.

TLM is fundamentally a set of network equations that describe the energy that is transmitted and reflected through the transmission line media. Traditionally TLM is used with Transverse Electric Magnetic (TEM) modes where the E and H fields do not propagate in the same direction as the signal. In recent years TLM is now used in full 3D EM tools to simulate both conductors and dielectrics in both passive and active devices.

In this analysis the 3D structure is discretized into small sections and each section is described as a 1D section of transmission line. Furthermore, the dielectric resonator is square in cross-section generating degenerate modes. A degenerate mode is one where two or more modes propagate at the same frequency. The use of ferrite material causes a deviation from true TE or TM propagation. The symbol δ will be used to indicate a deviation hence the modes in the square cross-section cavity with ferrite are $TE\delta$ and $TM\delta$. For each mode in this symmetrically square cross-section cavity, the equivalent voltage will be defined to be proportional to the $TE\delta$ field and the equivalent current will be defined to be proportional to the $TM\delta$ field.

3.2 Transmission Line Method for a Multilayer Structure

According to Maxwell's equations, the tangential components of the electric and magnetic fields at the interface must be continuous, and therefore the voltage and current are also continuous. The important point is that the input impedance of each section is equal at the interface. The lowest frequency solution where the interface impedances are equal defines the lowest order dominant mode frequency. Using this frequency, the effective permittivity and permeability for the composite structure is calculated. The effective values include the relative layer thickness to the total inside transverse direction dimension of the cavity.

Within the multilayer dielectric/ferrite model, there are two distinct boundary interfaces: dielectric-dielectric or dielectric-ferrite. Layer interfaces are in the Y direction and propagation is in the Z direction. Therefore, $E(x,y)$ and $H(x,y)$ represent the transverse direction. There is no variation in the X direction for each layer. There is no X

dependence. Due to material property differences the propagation constant of each layer with the propagation constant γ is defined as

$$\gamma = \alpha + j\beta$$

where α is the attenuation constant and β is the phase constant. The ferrite layer thickness is small as compared to wavelength and to the dielectric layer. A lossless case is assumed and therefore $\alpha=0$. Therefore

$$\gamma^2 = -\beta^2 = \omega^2 \mu \epsilon \quad (3.1)$$

$$\gamma = j\beta = j\omega\sqrt{\mu\epsilon} \quad (3.2)$$

thus the propagation constant is imaginary.

Calculation of the resonance condition from the composite material stackup is required. At the interface, the input impedance Z_{in} looking at the terminal ends of the composite is equal.

$$Z_{in} = Z_0 \cdot \frac{Z_L \cos(\beta l) + Z_0 \sin(\beta l)}{Z_0 \cos(\beta l) + Z_L \sin(\beta l)} \quad (3.3)$$

The line impedance Z_0 of each layer is directly proportional to the material constants of the layer. When the bias changes direction, β changes direction. The TLM program includes this effect by including the sign of the relative permeability with β , the propagation constant for that specific layer in Equation 3.1.

To calculate the resonant frequency, it was found that many root finding algorithms do not converge when multiple modes are present. There can be numerous

solutions to Z_{in} . Therefore, a graphical approach is used to determine the frequency where the impedance equations were equal.

3.2.1 Two-Layer Cavity

Figure 3.1 depicts a multilayer dielectric cavity with two isotropic dielectric layers. This is analyzed using the proposed TLM method.

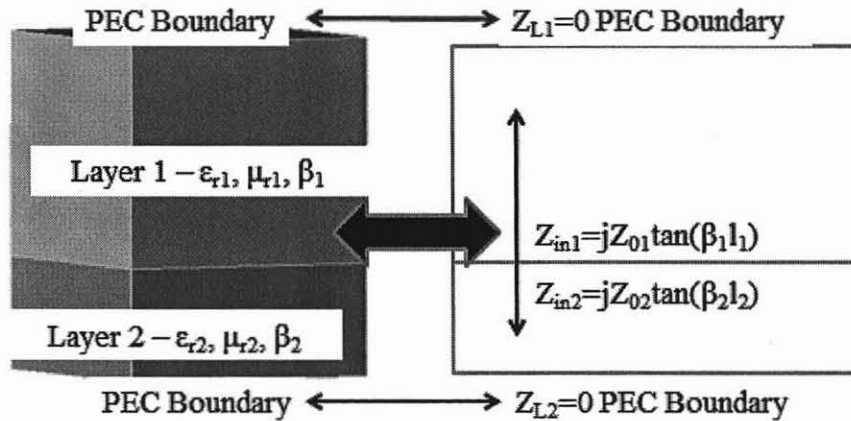


Figure 3.1 Transmission Line Model of a two-layer dielectric cavity.

Applying Equation 3.1 to the two-layer example, the input impedance equation is

$$Z_{01} \tan(\beta_{y1} L_1) + Z_{02} \tan(\beta_{y2} (b-L_1)) = 0 \quad (3.4)$$

where b is the total height in the y direction and L_1 is the height of layer 1 in the y direction

$$Z_{TE} = \frac{j\omega\mu}{\beta} \quad (3.5)$$

and the characteristic impedance of a propagating TM mode is

$$Z_{TM} = \frac{\beta}{j\omega\epsilon} \quad (3.6)$$

The results of the TLM program are validated with an example problem, Example 8.8, in Constantine Balanis' book [3, pp.403]. The MATLAB TLM program result is 12.65 GHz and the Balanis solution is 12.62 GHz. The difference is within 1%.

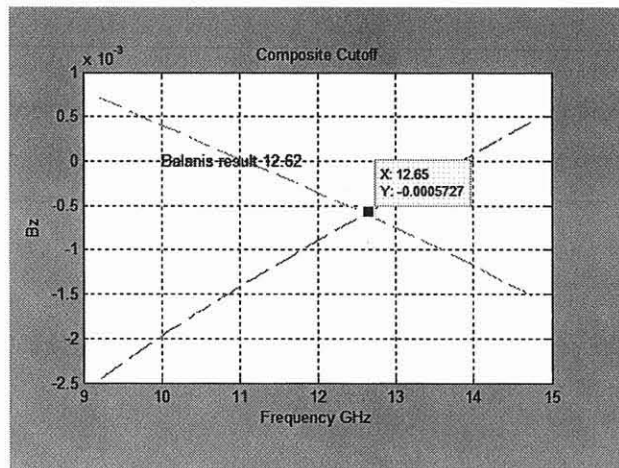


Figure 3.2 MATLAB results for two-layer model used to validate TLM method for dielectrics only.

3.2.2 Three-Layer Cavity

Similarly, a problem from Harrington [2] Problem 4.19, a three dielectric layer model is used.

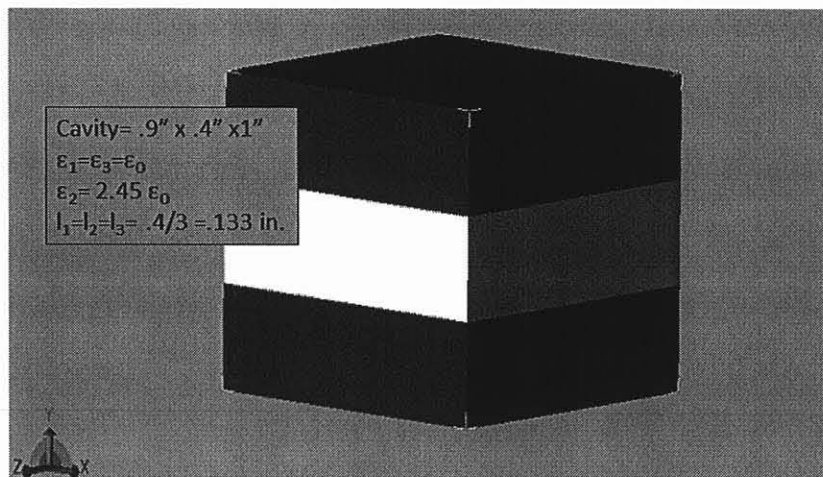


Figure 3.3 Three-layer model used to validate TLM method for dielectrics only.

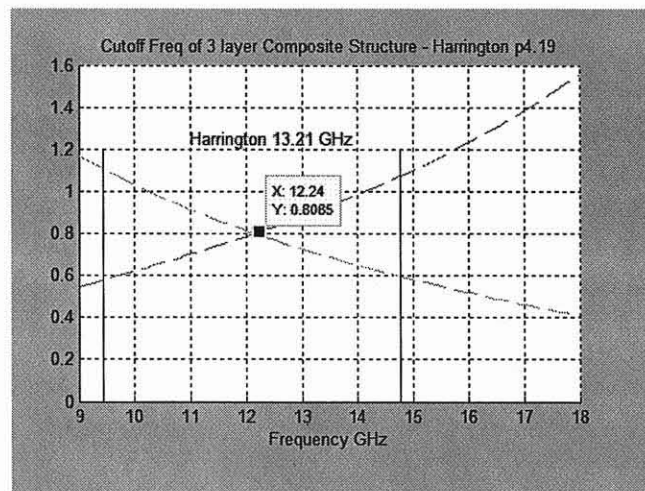


Figure 3.4 MATLAB TLM result for a three-layer model.

The MATLAB TLM program result is 12.24 GHz vs. the Harrington solution is 13.21 GHz, an 8% difference.

As an approximation to the experimental model, a five-layer waveguide configuration is used and referred to as the Simple Five-Layer Model. The filter housing is a metallic cavity. The cavity ends are defined as PEC, short circuits. In the Simple Five Layer-Model, layer 1 is the top ferrite layer and layer 5 is the bottom ferrite layer.

Sandwiched in between is the dielectric resonator surrounded by air. The air layers are representative of the supporting structures of the ferrites and dielectric. Figure 4.5 shows the Simple Five-Layer Model layer stackup. Top layer 1, L_1 and bottom layer 5, L_5 are ferrite materials. Layers two, L_2 three, L_3 and four, L_4 are made up of dielectric material. L_2 and L_4 are air and L_3 is a high dielectric constant ceramic. The relative permittivity is denoted as $\epsilon_{r\#}$ where $\#$ is the layer number and relative permeability $\mu_{r\#}$ again $\#$ stands for the layer number. These values are defined in Tables 3.1 and 3.2.

Table 3.1 Permittivity Values for Simple Five-Layer Model

Layer	Relative Permittivity Variable	Value
Layer 1 G113 ferrite	ϵ_{r1}	15
Layer 2 air	ϵ_{r2}	1
Layer 3 dielectric	ϵ_{r3}	20
Layer 4 air	ϵ_{r4}	1
Layer 5 G113 ferrite	ϵ_{r5}	15

Table 3.2 Permeability Values for Simple Five-Layer Model

Layer	Relative Permeability Variable	Value
Layer 1 G113 ferrite	μ_{r1}	1 at bias at 0 Oe applied bias 0.15238 at 400 Oe applied bias
Layer 2 air	μ_{r2}	1
Layer 3 dielectric	μ_{r3}	1
Layer 4 air	μ_{r4}	1
Layer 5 G113 ferrite	μ_{r5}	1 at bias at 0 Oe applied bias 0.15238 at 400 Oe applied bias

The relative permeability values calculated at an applied bias at 0 Oe and 400 Oe are shown. Relative permeability values are calculated using the equations in Chapter 2.

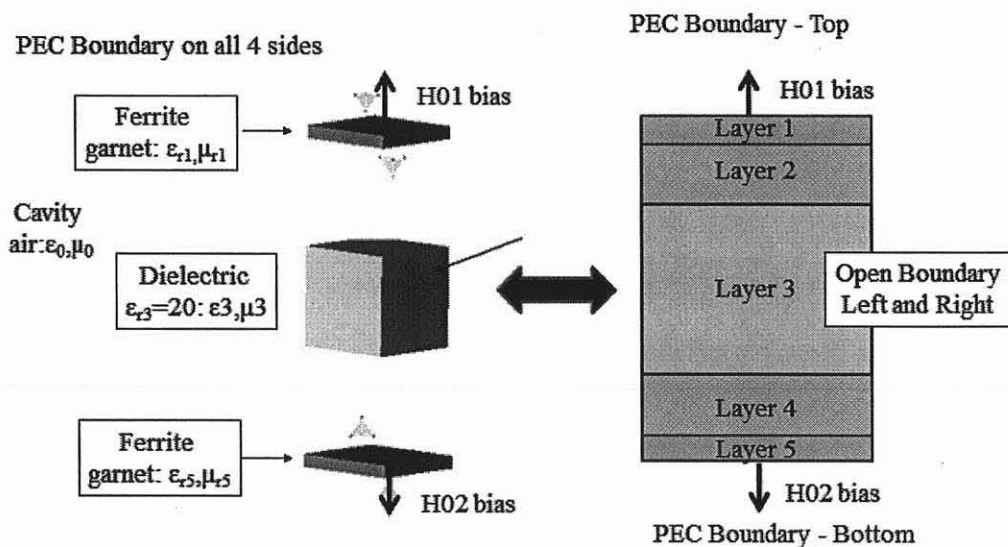


Figure 3.5 Simple Five-Layer Model used as an initial approximation to the experimental model.

Figure 3.6 indicates the relationship between the physical model and the equivalent TLM model.

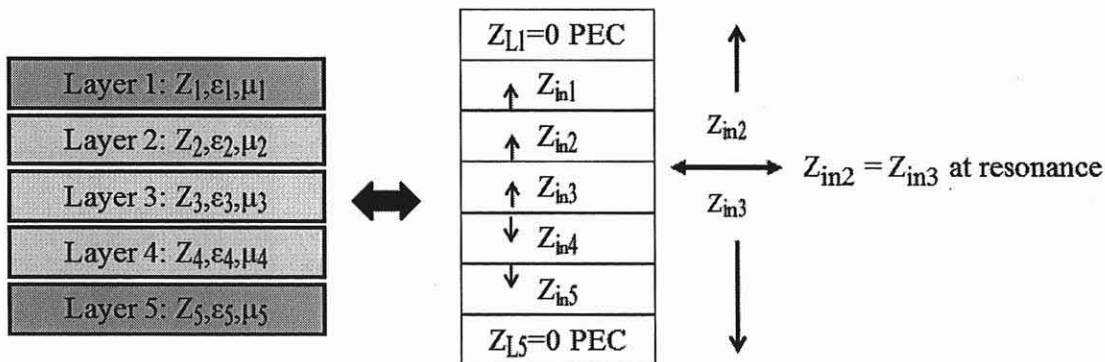


Figure 3.6 Relationship of physical and material characteristics of Simple Five-Layer Model layers with Transmission Line Equivalent.

The simplified model is bisected into two sections at one of the dielectric-air interfaces, the input impedances at the interface looking in opposite directions are equal at resonance. The bisected simplified model is shown in Figure 3.7. The interface is defined where the impedance match is performed. The interface is between layer 2 and 3

which is the air-dielectric interface. Following the TRM procedure as defined in Marcuvitz [16] the impedances looking towards either end of the waveguide at this interface are equal at resonance. All the fields are assumed to be in layer 3 so locating the interface here is a good choice.

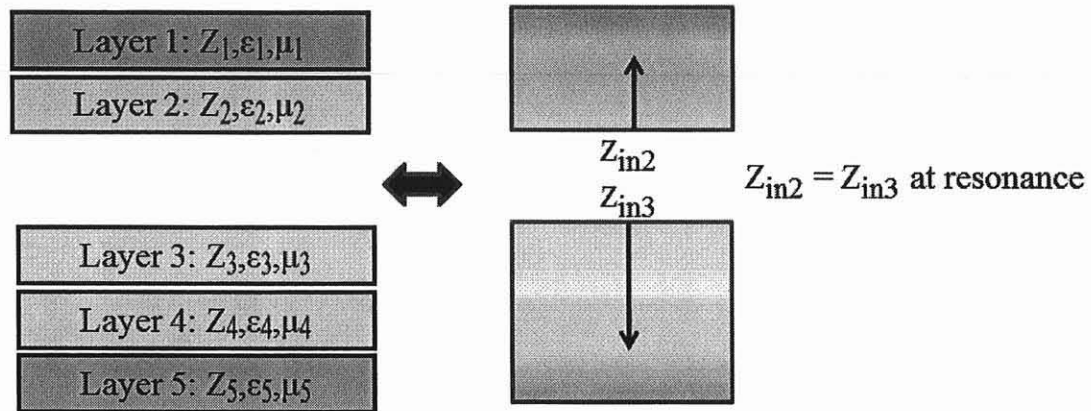


Figure 3.7 Bisected diagram of Simple Five-Layer Model.

The TLM program considers each layer of the Simple Five-Layer Model as a section of transmission line as in Equation 3.1. The metal ends are modeled as a short circuit, a PEC boundary condition. The TLM program separates the Five-Layer Model into two sections, Z_{in2} for layers 1 and 2 and Z_{in3} for layers 3, 4 and 5.

The defining equations for Z_{in2} section starting with layer1 looking towards the shorted end are as follows

$$Z_{in1} = Z_{01} \cdot \frac{Z_{L1} \cdot \cos(\beta_1 \cdot l_1) + Z_{01} \cdot \sin(\beta_1 \cdot l_1)}{Z_{01} \cdot \cos(\beta_1 \cdot l_1) + Z_{L1} \cdot \sin(\beta_1 \cdot l_1)} \quad (3.7)$$

with an input impedance defined as

$$Z_{in1} = j \cdot Z_{01} \cdot \tan(\beta_1 \cdot l_1) \quad (3.8)$$

The line impedance of layer 1 is the impedance of a TE mode as defined in Equation 3.2.

$$Z_{01} = \frac{\omega \mu_{r1} \mu_0}{\beta_1} \quad (3.9)$$

The propagation constant for layer 1 is

$$\beta_1^2 = \omega^2 \mu_{r1} \mu_0 \epsilon_{r1} \epsilon_0 \quad (3.10)$$

The load impedance for layer 2 is Z_{in} of layer 1. The input impedance looking from layer 2 towards the shorted end next to layer 1 is

$$Z_{in2} = Z_{02} \cdot \frac{Z_{L2} \cos(\beta_2 l_2) + Z_{02} \sin(\beta_2 l_2)}{Z_{02} \cos(\beta_2 l_2) + Z_{L2} \sin(\beta_2 l_2)} \quad (3.11)$$

$$Z_{in2} = Z_{02} \cdot \frac{Z_{in1} \cos(\beta_2 l_2) + Z_{02} \sin(\beta_2 l_2)}{Z_{02} \cos(\beta_2 l_2) + Z_{in1} \sin(\beta_2 l_2)} \quad (3.12)$$

The line impedance of layer 2 is again the impedance of a TE mode as defined in Equation 3.2.

$$Z_{02} = \frac{\omega \mu_{r2} \mu_0}{\beta_2} \quad (3.13)$$

The propagation constant for layer 2 is

$$\beta_2^2 = \omega^2 \mu_{r2} \mu_0 \epsilon_{r2} \epsilon_0 \quad (3.14)$$

Equation 3.12 is the input impedance of the variable named Z_{in2} of TLM program line 488.

Proceeding with the above methodology Z_{in3} looking towards the shorted end next to layer 5 is defined. The load impedance of layer 5 is a shorted end as with layer 1.

$$Z_{in5} = jZ_{05} \tan(\beta_5 l_5) \quad (3.15)$$

The load impedance of layer 4 is Z_{in5} . The input impedance of layer 4 looking towards the shorted end of layer 5 is

$$Z_{in4} = Z_{04} \frac{Z_{L4} \cos(\beta_4 l_4) + Z_{04} \sin(\beta_4 l_4)}{Z_{04} \cos(\beta_4 l_4) + Z_{L4} \sin(\beta_4 l_4)} \quad (3.16)$$

$$Z_{in4} = Z_{04} \frac{Z_{in5} \cos(\beta_4 l_4) + Z_{04} \sin(\beta_4 l_4)}{Z_{04} \cos(\beta_4 l_4) + Z_{in5} \sin(\beta_4 l_4)} \quad (3.17)$$

The line impedance of layer 4 is again the impedance of a TE mode as defined in Equation 3.2.

$$Z_{04} = \frac{\omega \mu_{r4} \mu_0}{\beta_4} \quad (3.18)$$

The propagation constant for layer 4 is

$$\beta_4^2 = \omega^2 \mu_{r4} \mu_0 \epsilon_{r4} \epsilon_0 \quad (3.19)$$

The load impedance for layer 3 is the input impedance to layer 4. The input impedance of layer 3 looking towards the shorted end next to layer 5 is

$$Z_{in3} = Z_{03} \cdot \frac{Z_{L3} \cos(\beta_3 l_3) + Z_{03} \sin(\beta_3 l_3)}{Z_{03} \cos(\beta_3 l_3) + Z_{L3} \sin(\beta_3 l_3)} \quad (3.20)$$

$$Z_{in3} = Z_{03} \cdot \frac{Z_{in4} \cos(\beta_3 l_3) + Z_{03} \sin(\beta_3 l_3)}{Z_{03} \cos(\beta_3 l_3) + Z_{in4} \sin(\beta_3 l_3)} \quad (3.21)$$

The line impedance of layer 3 is again the impedance of a TE mode as defined in Equation 3.2.

$$Z_{03} = \frac{\omega \mu_{r3} \mu_0}{\beta_3} \quad (3.22)$$

The propagation constant for layer 3 is

$$\beta_3^2 = \omega^2 \mu_{r3} \mu_0 \epsilon_{r3} \epsilon_0 \quad (3.23)$$

Equation 3.21 is the input impedance of the variable named Z_{in3} of TLM program line 500. The impedances at the interface must be equal. There are an infinite number of possible solutions due to the cosine-sine dependency so an initial value near RF signal frequency is used. The lowest frequency from line 488 and line 500 in the TLM program is considered the lowest order mode. The equation equating Z_{in2} and Z_{in3} is a transcendental equation. The lowest frequency where the transcendental equation equals zero is the lowest order frequency. The resulting dispersion equation for the Simple Five-Layer Model with no external bias is plotted against frequency in the Figure 3.7. The first zero crossing indicated by red circle is considered the lowest order mode.

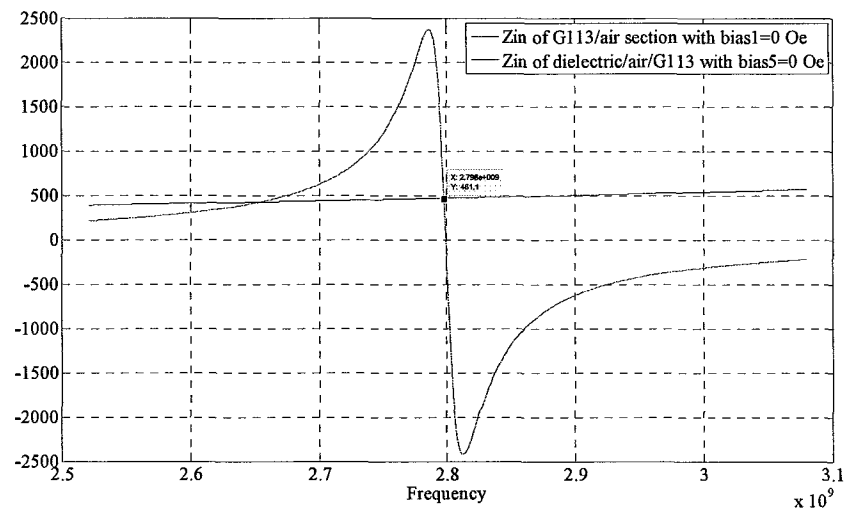


Figure 3.8 Plot of transcendental equation for Simple Five-Layer Model with no applied bias. Lowest order mode is located at curve intersection.

3.3 Simple Five-Layer Model - Single Mode TLM Analysis

To calculate the center frequency of the composite dielectric-ferrite structure each layer is considered as a section of transmission line as detailed in Marcuvitz [16]. The simplified Five-Layer Model is shown in Figure 3.6. The equivalent transmission line model of this simplified geometry is shown in Figure 3.9.

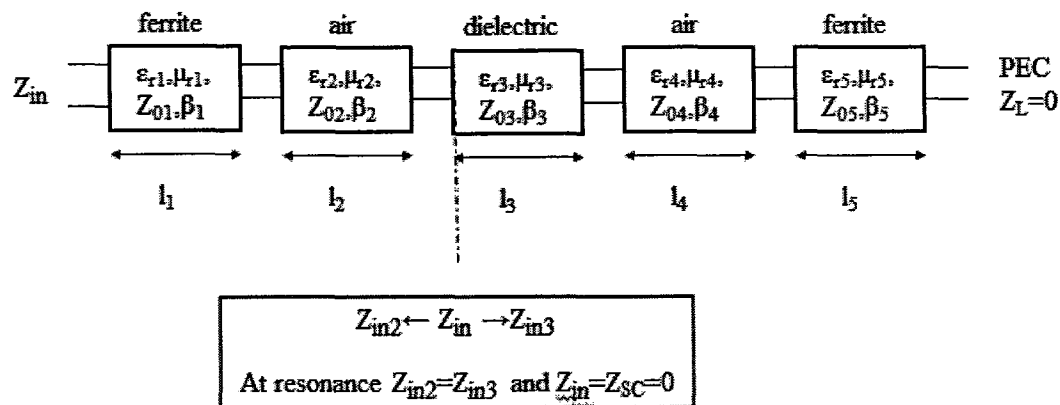


Figure 3.9 The equivalent transmission line model of Simple Five-Layer Model.

Choosing the interface as located between layer 2 and layer 3, the input impedance looking towards layer 1 is equal to the input impedance looking towards layer 5 at resonance. The defining equations starting with layer 1 and looking towards the shorted end are

$$Z_{in1} = Z_{01} \cdot \frac{Z_{L1} \cos(\beta_1 l_1) + Z_{01} \sin(\beta_1 l_1)}{Z_{01} \cos(\beta_1 l_1) + Z_{L1} \sin(\beta_1 l_1)} \quad (3.24)$$

the load impedance for layer 1 (short circuit) is defined as

$$Z_{L1} = jZ_{01} \tan(\beta_1 l_1) \quad (3.25)$$

The propagation constant for layer 1 is

$$\beta_1^2 = \omega^2 \mu_{r1} \mu_0 \epsilon_{r1} \epsilon_0 \quad (3.26)$$

Z_{in1} is the load impedance when calculating the input impedance of layer 2 looking towards the shorted end of layer 1. Equations are representative of all the layers. The final equation relating the input impedance for layers 1 and 2 with the input impedance for layers 3, 4 and 5 is the governing dispersion equation. A MATLAB

program has been developed to solve this transcendental impedance equation. The lowest order mode solution represents the resonant frequency of the composite structure. The resonant frequency of the experimental model at zero bias is 2.8 GHz.

Tuning of the resonator is a function of the change in the composite resonator permeability driven by change in the ferrite permeability with an applied magnetic bias. This approach to tuning differentiates from earlier work dependent on RF interaction with ferrite resonance.

For each EAVSMF bias applied to the ferrite, the transcendental equation of the structure must be recalculated as the bias affects the permeability value and hence the impedances as defined above. Each solution then represents a different resonant frequency of the structure.

The Simple Five-Layer Model near the calculated resonant frequency can be approximated by a parallel LC circuit. The resonant frequency, f_0 of the Simple Five-Layer Model is found graphically in the TLM Program as in Figure 3.8. The values for the equivalent shunt LC circuit of Figure 3.10 is calculated by taking the derivative of the equivalent Y admittance of the LC shunt pair with respect to frequencies about this resonant frequency.

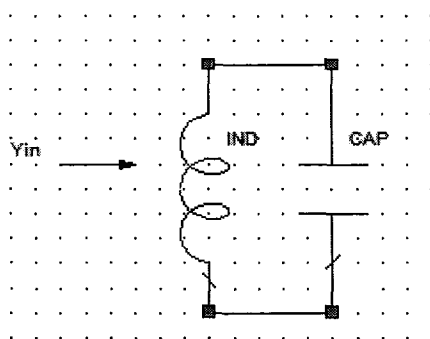


Figure 3.10 Equivalent Circuit of Simple Five-Layer Model - single pole filter.

$$Y_{in2} = \frac{1}{Z_{in2}} \quad (3.27)$$

$$Y_{in3} = \frac{1}{Z_{in3}} \quad (3.28)$$

$$Y_{in2} = Y_{in3} = Y_{in} = Y_L + Y_C = \frac{1}{j\omega L} + j\omega C \quad (3.29)$$

$$\frac{dY_{in}}{d\omega} = \frac{j}{\omega^2 L} + jC \quad (3.30)$$

This is line 682 in TLM program.

At resonance the equivalent LC circuit relationship is

$$\omega_0^2 = \frac{1}{LC} = (2\pi f_0)^2 \quad (3.31)$$

where f_0 is found graphically in Figure 3.8. The TLM program calculates the network response of a single pole resonator and a two pole resonator. The initial step of validating the frequency range of interest is performed by calculating the f_0 for the single pole Simple Five-Layer Model with no bias.

As depicted in Figure 1.7, if the direction of the top and bottom bias is in the same direction it will be referred to as “same “ bias. If the direction of the top bias and bottom ferrite are in opposite direction, it will be referred to as “opposite” bias. The permeability of the ferrite material changes with external bias. Increasing the bias decreases the permeability changing the impedance of the composite resonator structure that results in an increase of the center frequency of the bandpass filter. Figure 3.11 shows the increasing shift of center frequency with increasing applied “opposite” bias of

a single pole filter. This validates proposed approach of using an applied bias to tune filter frequency.

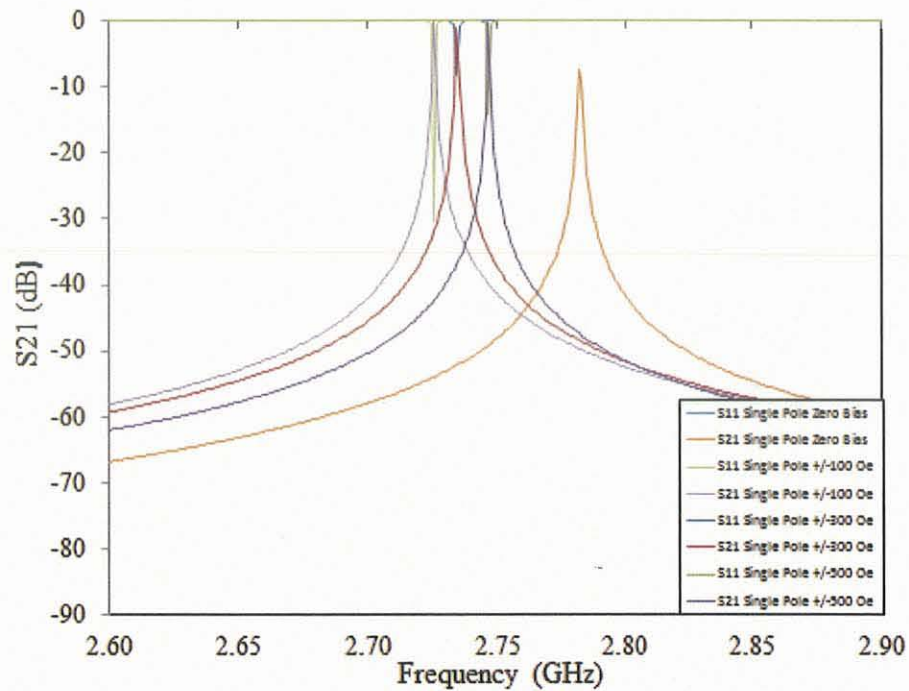


Figure 3.11 TLM Program – S Parameter curves for Simple Five-Layer Model single pole with “opposite” bias.

3.3.1 AGILENT EMPRO Simple Five-Layer Model Single Pole Filter

The MATLAB TLM result is validated with the electromagnetic simulation software AGILENT EMPRO. Figure 3.12 shows the AGILENT EMPRO structure depicting the one pole Simple Five-Layer Model.

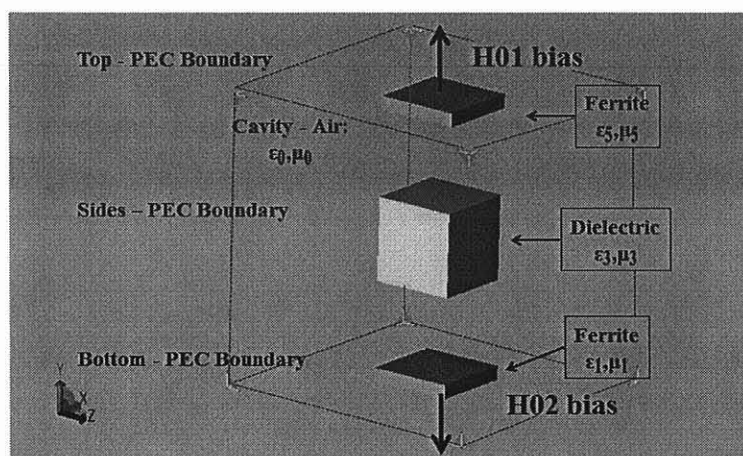


Figure 3.12 Agilent EMPro Single Mode Filter Structure.

3.4 Dual Mode Analysis and Coupling

A dual mode resonant structure is created from the Simple Five-Layer Model by coupling each mode together through some mechanism. As stated previously, the square cross-section dielectric resonator produces degenerate modes. Within the structure, various orientations of these modes can exist depending upon how the cavity is excited. Two of these modes which are orthogonal to each other can be coupled using a perturbation in cavity such as a diagonal or square cut in the corner of the cavity or the dielectric. In the experimental model, the coupling is realized with a diagonal cut in the corner of the cavity wall. The bandwidth of the resultant response is related to this coupling. In the equivalent circuit model, the two modes are modeled as two shunt parallel resonant

circuits. The coupling is modeled as a J inverter represented as a pi capacitor network for this analysis. In the EM simulated structure the coupling is realized with a diagonal cut in the corner of the dielectric resonator.

3.4.1 Experimental Model

Testing of the dual mode bandpass filter was performed at RS Microwave in Butler, NJ. The experimental model consisted of two square cross-section G113 ferrite tiles and a .5" side square cross-section dielectric puck with $\epsilon_r=20$ mounted on a Teflon mount. Each piece was placed and centered into a metal housing with an outside dimension of 1.6" x 1.7" x 1.6". The bias to the ferrite tiles was applied with two magnets placed above and below the housing. This will be referred to as the "Experimental Model".

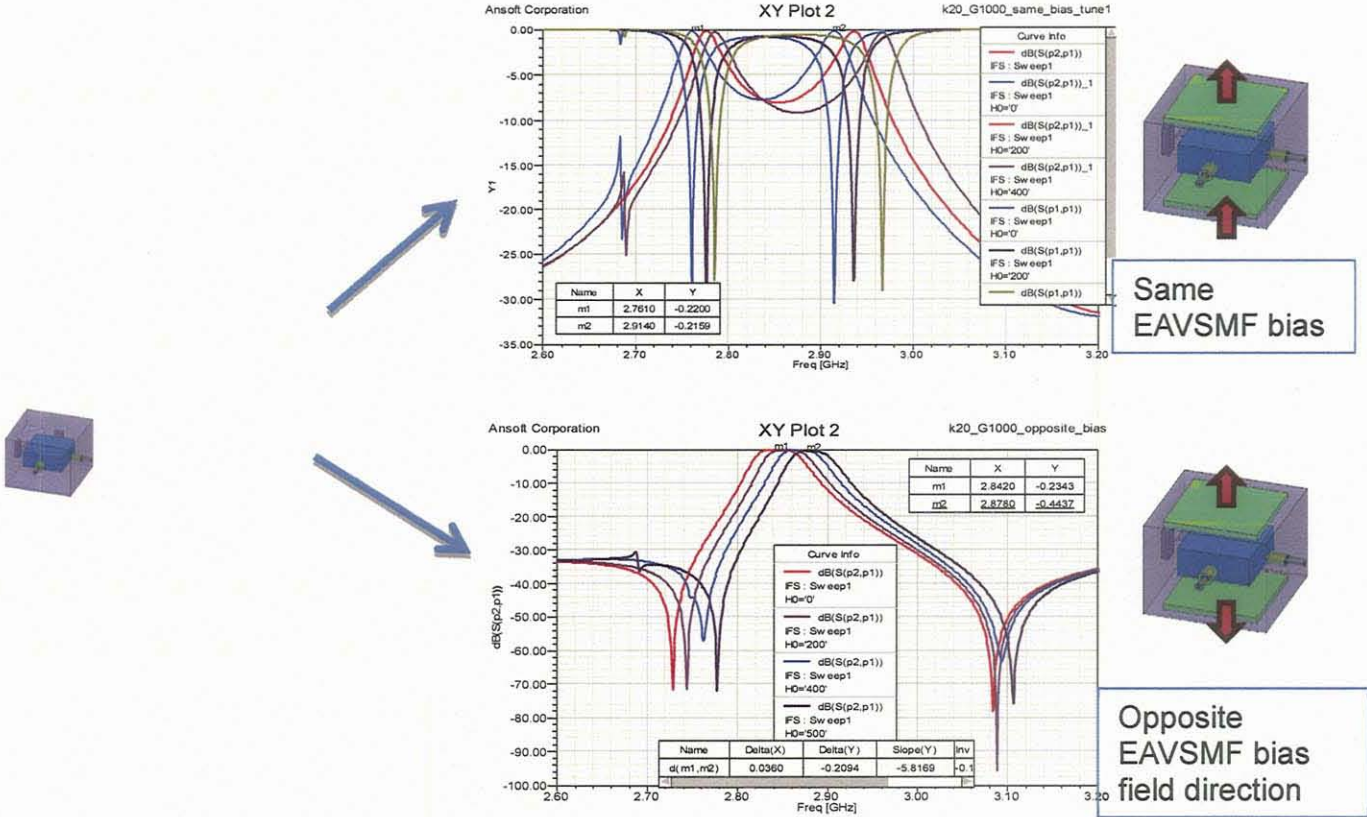


Figure 3.13 Tunable Dual Mode Bandpass Filter.

3.4.2 TLM Based Program Simple Five-Layer Model Dual Mode Bandpass Filter

The developed MATLAB program finds the resonant frequency of the one dimensional section of the physical resonator structure using the TLM method then calculates the circuit equivalent of the resulting frequency as well as the circuit equivalent of the coupling mechanism that splits this degenerate mode. Figure 3.14 depicts the circuit approximation of the dual mode bandpass filter used in the TLM based program.

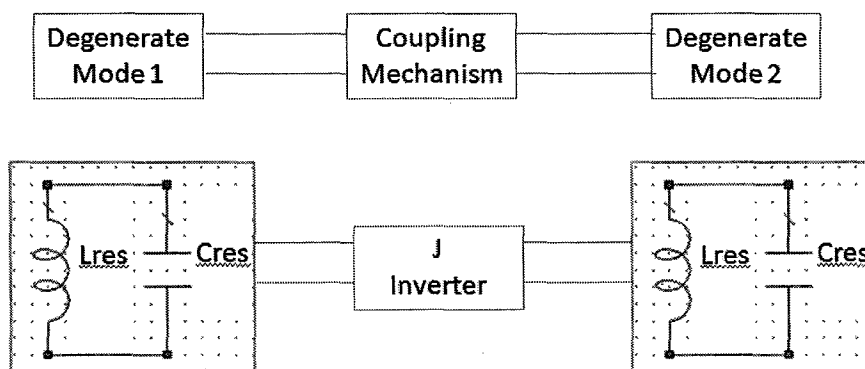


Figure 3.14 Circuit model of Dual Mode Filter.

Each of the modes of the composite structure is represented by a shunt parallel LC circuit resonating at the graphically found frequency in the MATLAB program defined as X_{fzero} . Mode frequency 1 and mode frequency 2 of the degenerate mode are equal. The inductor L and capacitor C values are the same for each mode frequency.

$$X_{fzero} = \frac{1}{2\pi\sqrt{L_{res}C_{res}}} \quad (3.32)$$

where L_{res} and C_{res} define the inductor value and the capacitor value respectively at the resonant frequency. L_{res} and C_{res} values are directly calculated in the TLM program by taking the derivative (δ) of the transcendental equation about some small range, +/-

.01Xfzero, around the resonant frequency. With C_{res} held constant, the applied bias is assumed to change the permeability of the ferrite therefore a change in the inductance. The shunt LC circuit representation of the resonant frequency of the structure is valid since a shunt LC circuit has a voltage maximum at resonance and the lowest order mode of the experimental filter structure has an electric field peak at the center of the structure where the dielectric puck is located. The ends of the filter cavity represent a short circuit as does the equivalent waveguide ends in the transmission line model.

The coupling coefficient is modeled as a pi network of capacitance as shown in Figure 3.15. This coupling mechanism splits the degenerate mode frequency 1 and 2.

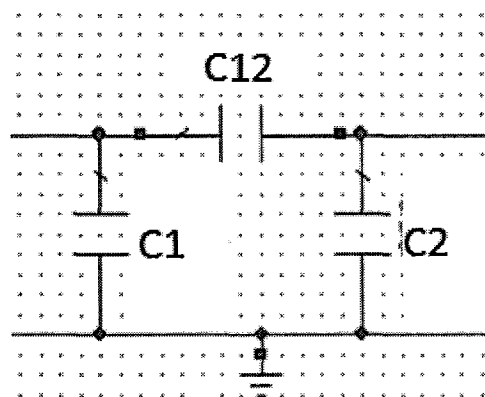


Figure 3.15 Equivalent circuit for corner cut coupling used to design a Dual Mode Filter.

The implementation of a circuit equivalent for the inter resonator coupling follows the procedure in Chapter 8 of Matthaei, Young and Jones [20]. Input/output load is assumed to be matched at 50 ohms. A fractional bandwidth, w , of 50 MHz will be assumed. The L and C designations are indicated in Figure 3.16.

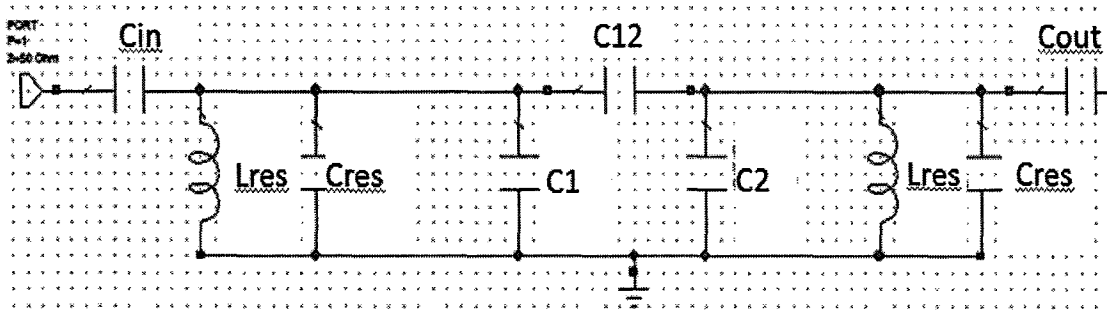


Figure 3.16 Equivalent circuit for Dual Mode Bandpass Filter including corner cut coupling.

The equations used to calculate these values are as follows

$$Z_a = 50, G_a = .02 \quad (3.33)$$

$$Z_b = 50, G_b = .02 \quad (3.34)$$

$$\omega_{\text{prime}} = 1 \quad (3.35)$$

$$\omega_0 = 2\pi f_0 = \sqrt{\frac{1}{L_{\text{res}} * C_{\text{res}}}} \quad (3.36)$$

$$\text{fracBW} = \frac{\text{BW}}{f_0} \quad (3.37)$$

$$J_{01} = \sqrt{\frac{G_a \omega_0 C_{\text{res}} \text{fracBW}}{g_0 g_1 \omega_{\text{prime}}}} \quad (3.38)$$

$$C_{\text{in}} = \frac{J_{01}}{\sqrt{J_{01,2}}} \quad (3.39)$$

$$J_{12} = \frac{C_{\text{res}} C_{\text{res}}}{g_1 g_2} \quad (3.40)$$

$$C_{12} = \frac{J_{12}}{\omega_0} \quad (3.41)$$

$$C_1 = C_{\text{res}} - C_{\text{ine}} - C_{12} \quad (3.42)$$

$$C_2 = C_1 \quad (3.43)$$

$$J_{23} = g_2 g_3 \quad (3.44)$$

$$C_{\text{out}} = \frac{J_{23}}{\omega_0 \sqrt{1 - \left(\frac{J_{23}^2}{G_b}\right)}} \quad (3.45)$$

Equations 3.33 through 3.45 are TLM program lines 742 to 814. Equation 3.42 indicates that the shunt capacitors, C_1 and C_2 absorb the series capacitance of the circuit. C_1 and C_2 can be negative. This procedure does not work when the calculated shunt capacitance values near the terminal ends yields a complex C_{in} or C_{out} value. A negative capacitance value is not physically realizable. This is not the case for the Experimental Model as the calculated values are positive real numbers. C_{in} or C_{out} becomes complex when the denominator term $\frac{J_{01}}{G_a}$ is greater than one. Figure 3.17 is a curve of the fractional bandwidth as a function of the ratio of the resonant L and C values calculated from the Experimental Model with zero applied bias. Values below the curve will keep the value of C_{in} real and positive.

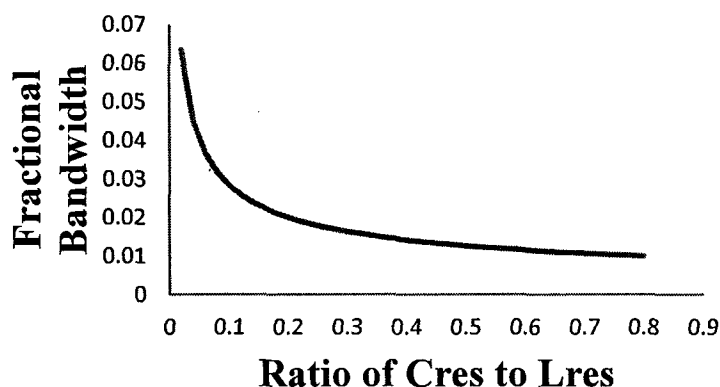


Figure 3.17 Fractional bandwidth as a function of the ratio of equivalent resonant L and C of Experimental Model at zero bias.

For the dual mode, Simple Five-Layer Model with zero bias the equivalent circuit is shown in Figure 3.18.

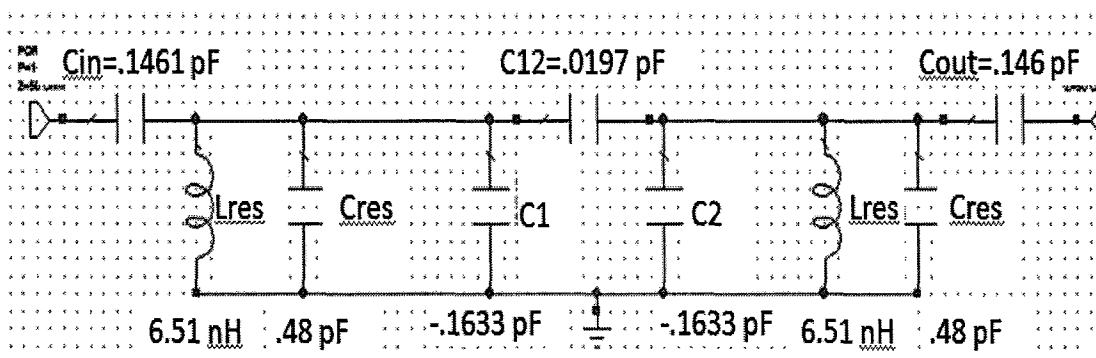


Figure 3.18 Equivalent Circuit with values calculated from TLM Program for Dual Mode Bandpass Filter including corner cut coupling.

Figure 3.19 shows the TLM calculated results for various values of applied “same” bias. The baseline structure indicated in red consists of the Simple Five-Layer Model with G113 ferrite with zero applied bias. The calculated results in Figure 3.19 show a consistent shift to higher frequencies of the filter passband as the applied “same” bias is increased.

The passband can be defined by the zeroes seen in the return loss. The lowest frequency defined as f_1 and the next frequency defined as f_2 . These frequencies are indicated for the zero biased curve in Figure 3.19. The center frequency, f_0 is defined as the midpoint of f_1 and f_2 . Note that the S parameter results of the TLM program are saved as a text file and imported into Excel for plotting.

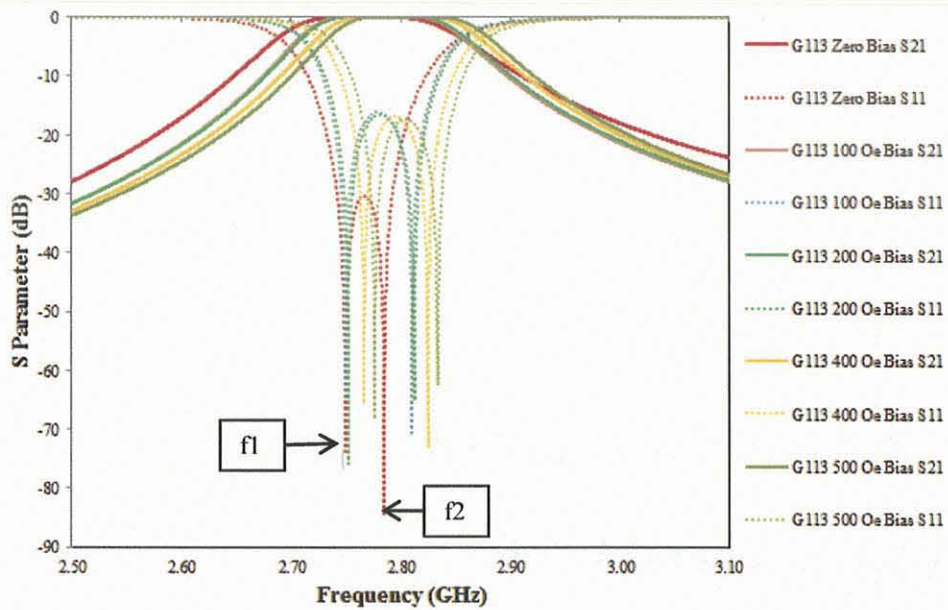


Figure 3.19 TLM Program S Parameter results for dual mode five-layer filter model with various values of “same” bias.

Figure 3.20 shows the TLM calculated results for the same structure as in Figure 3.19 with values of “opposite” bias.

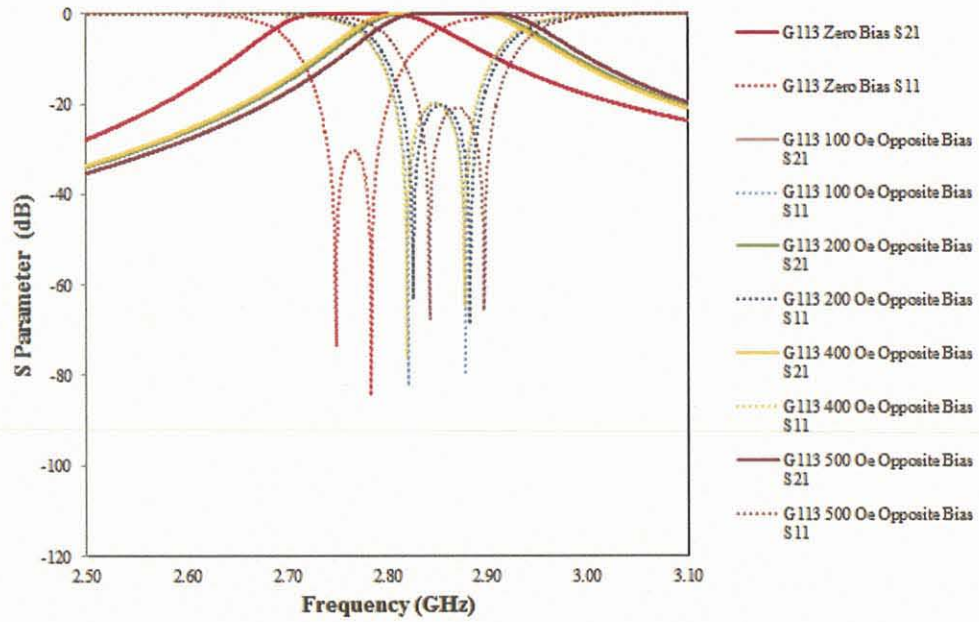


Figure 3.20 TLM Program S Parameter results for dual mode five-layer filter model with various values of “opposite” bias.

Figure 3.21 directly compares the S parameter results of the zero biased dual mode bandpass filter with the 200 Oe applied bias curves of Figures 3.19 and 3.20.

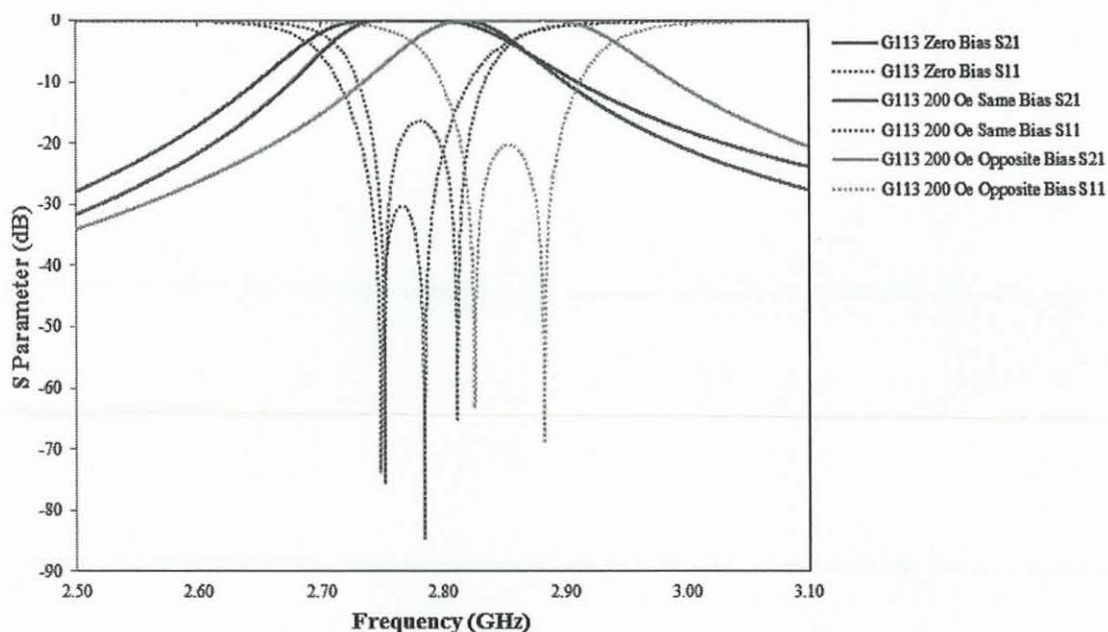


Figure 3.21 TLM Program S Parameter results comparing zero biased G113 ferrite with 200 Oe external bias applied in “same” and “opposite” directions.

A comparison of the response curves for the various bias as shown in Figure 3.21 verifies the experimental results as shown in Figure 3.13. For 200 Oe of “same” bias the frequency shift, from zero bias, of the upper frequency is greater than the lower frequency effectively changing the bandwidth. With 200 Oe of “opposite” bias, both upper and lower frequencies change similar amounts.

Table 3.3 summarizes the results as shown in Figure 3.21.

Table 3.3 Frequency Shift of f_1 , f_2 and Center Frequency f_0 with 200 Oe Applied Bias

Bias (Oe)	Direction	f_1 (MHz)	f_2 (MHz)	shift f_1 (MHz)	shift f_2 (MHz)	f_0 (MHz)	shift f_0
0		2750	2780			2765	
200	"Same"	2750	2810	0	30	2780	15
200	"Opposite"	2830	2880	80	100	2855	90

Figure 3.22 shows the response of the Experimental Model. The Experimental Model exhibits a shift of 15 MHz when an opposite external bias is applied. The TLM results match the results of the Experimental Model.

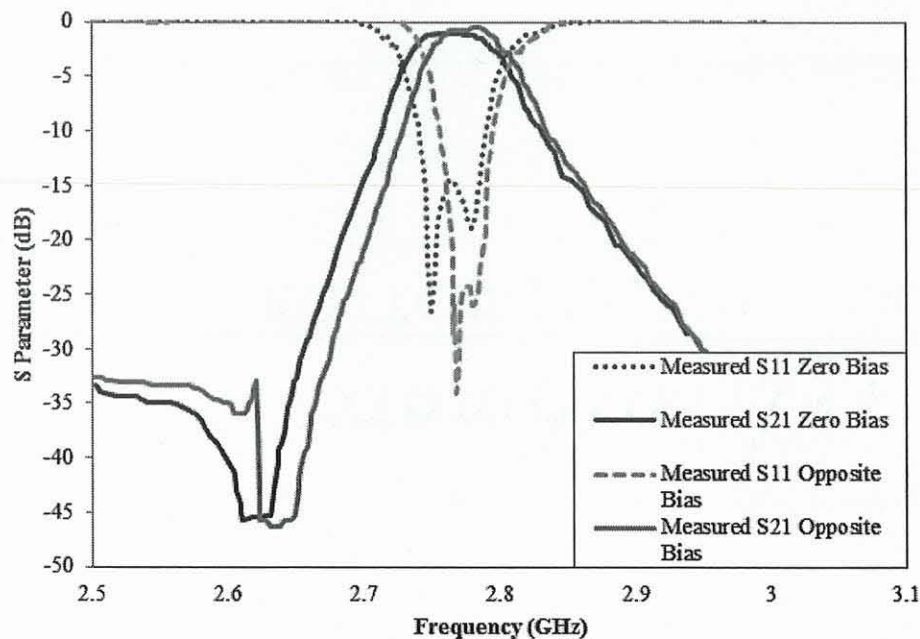


Figure 3.22 Experimental S Parameter results for dual mode five-layer filter model with “opposite” bias.

3.4.3 EM Simulated Simple Five-Layer Model Dual Mode Bandpass Filter

The AGILENT EMPRO structure for the dual mode bandpass filter using a square cross-section dielectric resonator with a .5 inches side dimension is shown below. Two input probes, a mode tuner and a corner cut was necessary to realize this design. Several tuning sessions were needed in order to match the input output coupling to realize the mode split – a time consuming process. Two wall tuners were used to further separate the modes.

This structure will be referred to as the EM simulated dual mode experimental filter structure as shown in Figure 3.24.

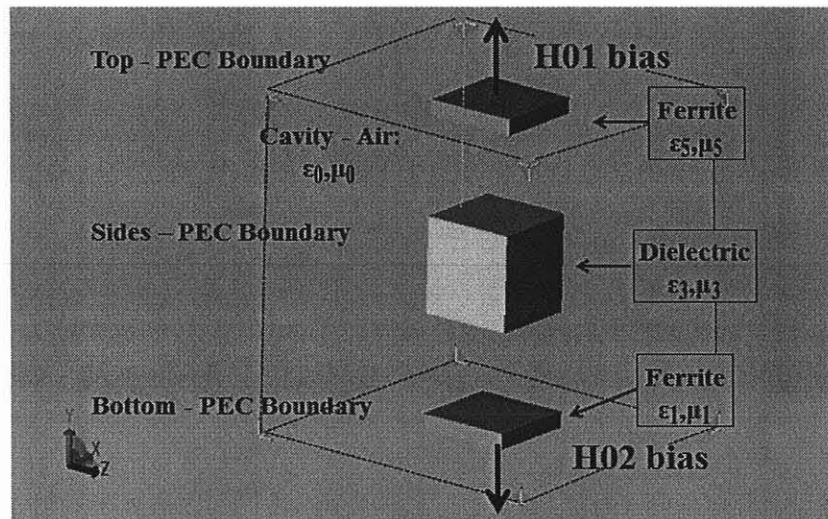


Figure 3.23 EM simulated single mode experimental filter structure.

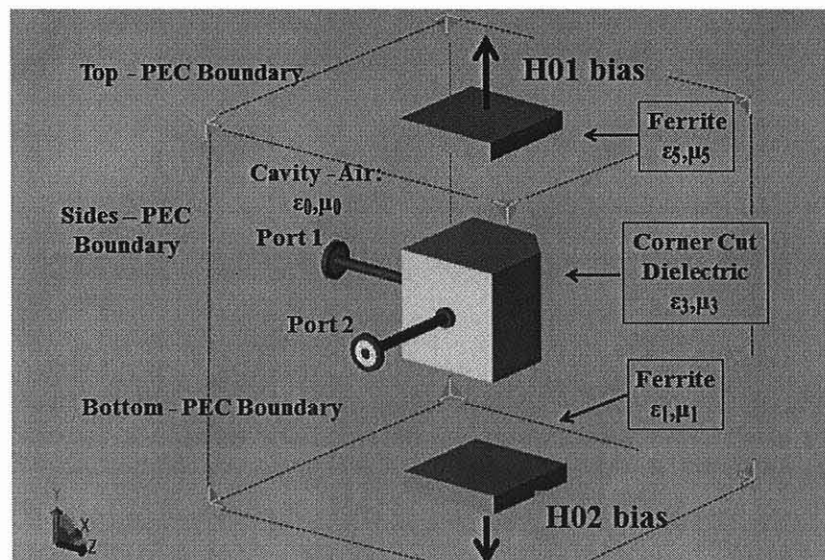


Figure 3.24 EM simulated dual mode experimental filter structure.

For the EM Simulated dual mode model, a coupling bandwidth curve versus chamfer is shown in Figure 3.25 for dual mode experimental filter structure. A dielectric

material with a relative permittivity of 15 was used to approximate a zero biased ferrite.

High losses are present when simulating G113 material with bias below 100 Oe.

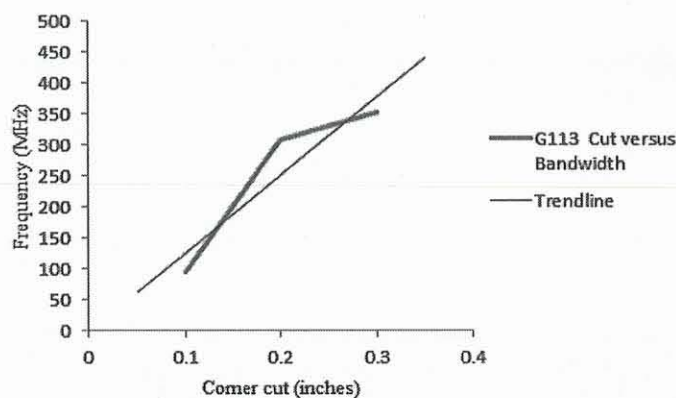


Figure 3.25 EM simulated shift of lowest order mode frequency with cavity chamfer of a sample dual mode bandpass filter.

As the perturbation is increased the modes are increasingly separated apart. As in the experimental model the coupling network is kept constant as corner cut is fixed.

3.4.4 Next Higher Order Mode

For completeness, the composite dual mode bandpass filter is analyzed over a wide band to predict the next higher order mode. Note that for this structure the next higher order mode is far from the operating frequency range. Although the TLM program developed here is not intended for wideband frequency analysis, an approximation can be made for the next higher mode of a single waveguide by considering the analysis for TE_{208} , the next eigenmode solution. Using this approach, with an applied “opposite” bias of 950 Oe the next spurious mode is predicted at 3.869 GHz as shown in Figure 3.26. The measured data for the experimental dual mode structure and a bias of 950 Oe shows a

second mode at 3.612 GHz as shown in Figure 3.27. The EM simulated data for the experimental dual mode structure with 950 Oe opposite bias shows a second mode at 3.9102 GHz as shown in Figure 3.28. The TLM prediction is off by more than 200 MHz of experimental result. The EM simulated result is more than 80 MHz greater than the experimental result. The TLM program approximates a single mode of the experimental structure in a narrow band about the resonant frequency by analyzing the impedance characteristics of the material cross sections without considering the input/output or mode coupling effects. For instance the Experimental Model shows evidence of input/output cross coupling via the rejection notches close to the pass band. These are clearly not modeled or evident in the TLM simulations. The above differences contribute to the difference in the data points. Further refinement of the TLM tool may allow closer results to be predicted in the future.

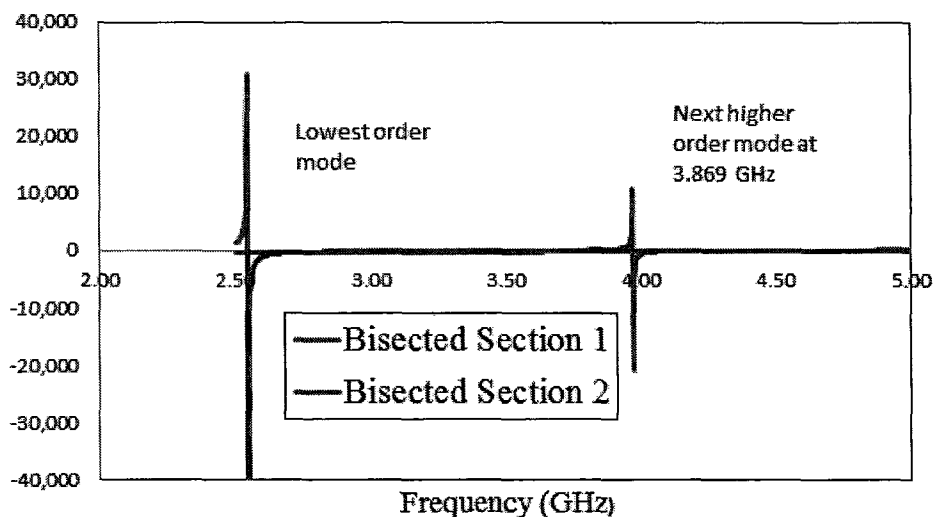


Figure 3.26 TLM Results for 950 Oe “opposite” bias showing crossover for next higher mode.

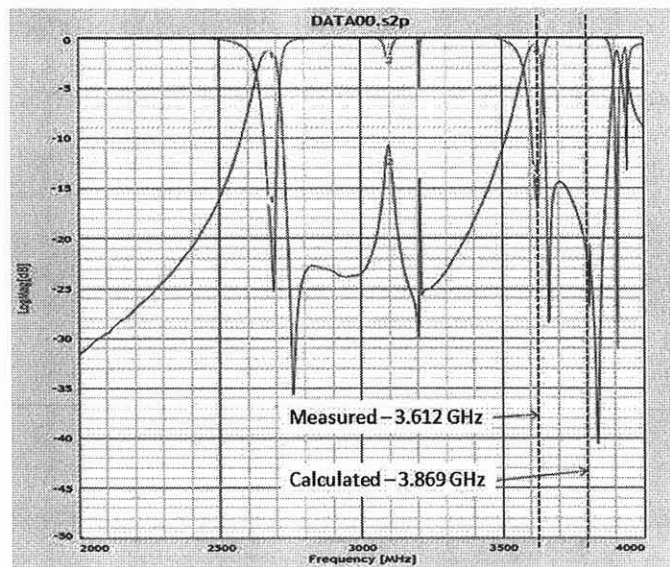


Figure 3.27 Experimental results for 950 Oe “opposite” bias showing next higher mode.

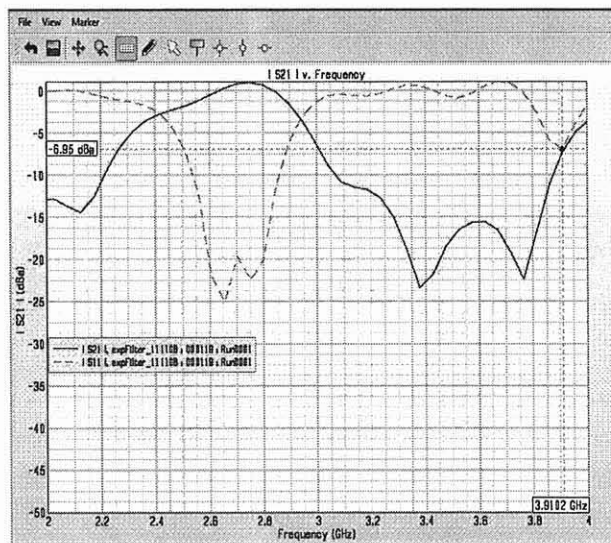


Figure 3.28 EM simulated results for 950 Oe “opposite” bias dual mode bandpass filter showing next higher mode

3.4.5 Ferrite Materials for Simple Five-Layer Dual Mode Bandpass Filter Model

Uses of different narrow line width ferrite materials are also analyzed. Transtech G510 [14] and TTVG1950 [15] ferrite material replaces G113 ferrite tiles used in the Experimental Model. The physical dimensions of the Experimental Model remain unchanged. The operating frequency is 2800 MHz. The TLM based analysis of a dual mode bandpass filter using G113 material with “opposite” bias is provided in Figure 3.20. Figure 3.29 replaces G113 ferrite material with G510 material. Figure 3.30 replaces G113 material with TTVG-1950 material. Appendix B further details how the curves were generated.

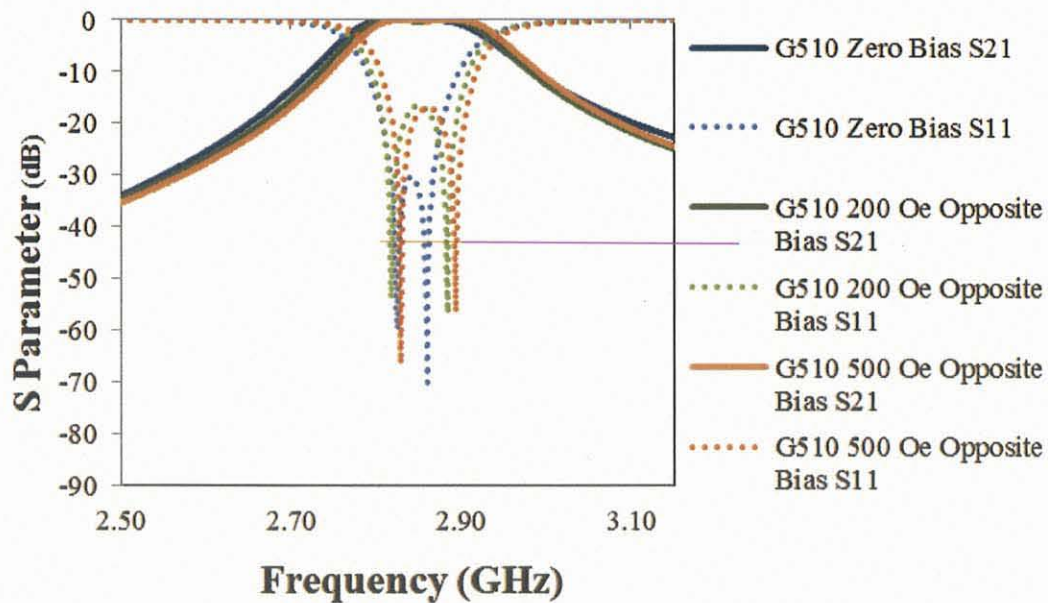


Figure 3.29 TLM calculated S Parameter curves for a Dual Mode Bandpass filter using G510 ferrite with “opposite” external bias.

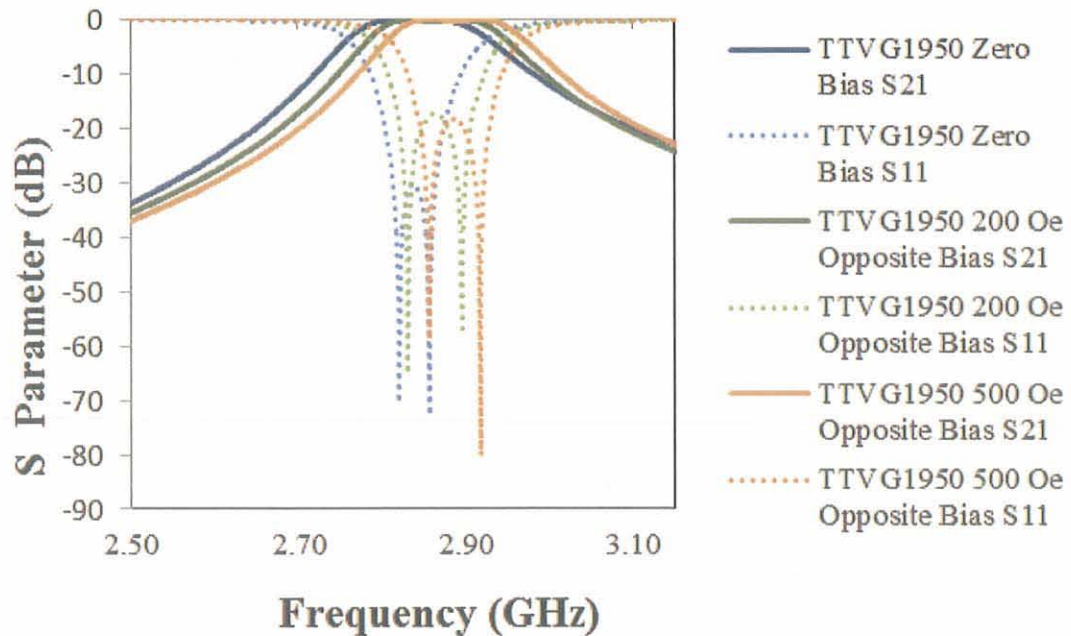


Figure 3.30 TLM calculated S Parameter curves for a Dual Mode Bandpass filter using TTVG1950 ferrite with “opposite” external bias.

At 200 Oe “opposite” applied bias all three dual mode bandpass types exhibit a small shift in frequency. At 500 Oe “opposite” applied bias G113 ferrite material shows a larger shift in frequency as compared to G510 and TTVG1950. The reason for the larger frequency shift is explained by the permeability versus frequency curves. Note that both poles move with applied bias ferrite materials.

Figure 3.31 is a plot of the different ferrites considered in this dissertation at an applied bias of 500 Oe. The operating frequency of 2800 MHz is indicated and clearly shows operation far from ferrite resonance hence all three materials have a low relative permeability value.

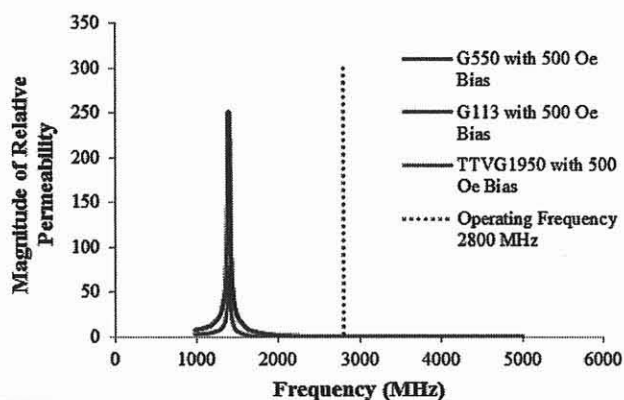


Figure 3.31 Calculated relative permeability of G113, G510 and TTVG1950 with 500 Oe applied bias.

Figure 3.32 is a plot of the different ferrites considered in this dissertation at an applied bias of 900 Oe. The operating frequency of 2800 MHz is indicated and clearly shows operation near ferrite resonance hence a greater change in relative permeability. The G113 and TTVG-1950 curves overlay with G113 curve slightly higher than TTVG1950 curve at 2800 MHz. This change in permeability is seen as a shift in the center frequency of the Simple Five-Layer Model.

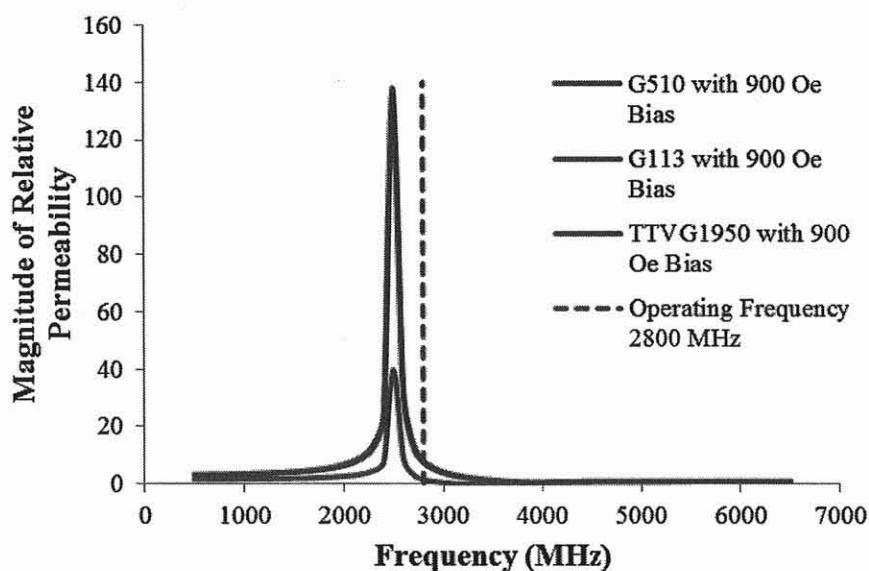


Figure 3.32 Calculated relative permeability of G113, G510 and TTVG1950 with 900 Oe applied bias.

TTVG-1950 has a higher saturation level than G113 so if the application includes high power signals TTVG-1950 would be preferred. TTVG-1950 is a newer ferrite material and further investigation to its power handling and temperature stability will need to be investigated in a future research.

3.4.6 Summary of Dual Mode Bandpass Filter Analysis

The center frequency is used as the figure of merit to compare the Experimental Model results with the TLM based calculated results and the FDTD EM simulated results. Figure 3.33 shows there is a good match between the 3 different analysis approaches. The resonant frequency of each mode is shifted with applied bias and the amount of frequency shift is dependent on the magnitude and direction of the biasing field. A summary of the shift of center frequency at “opposite” applied bias for G113 is shown in Figure 3.34.

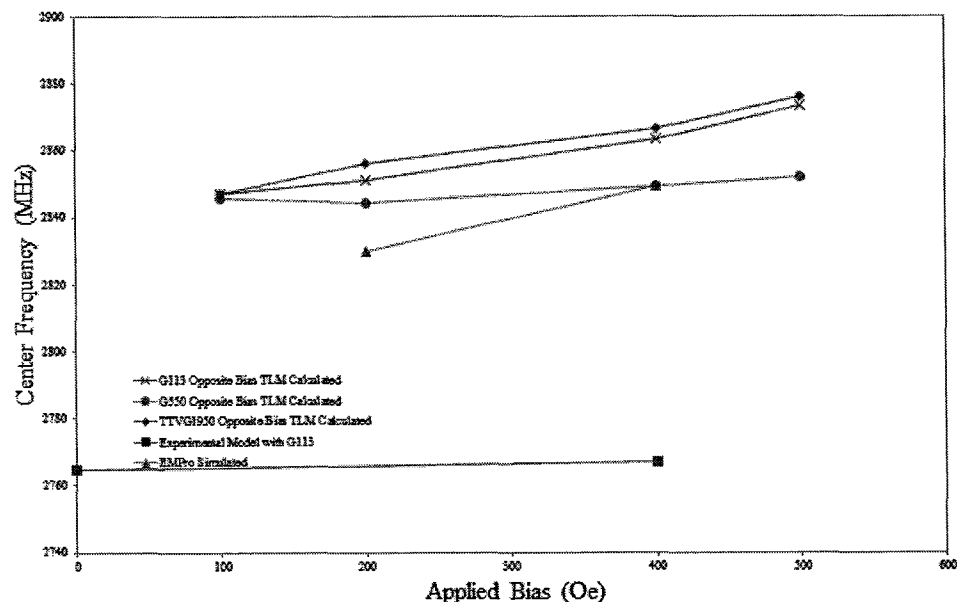


Figure 3.33 Comparison of EM simulated dual mode experimental bandpass filter and TLM Simple Five-Layer Model dual mode bandpass filter at different applied biases.

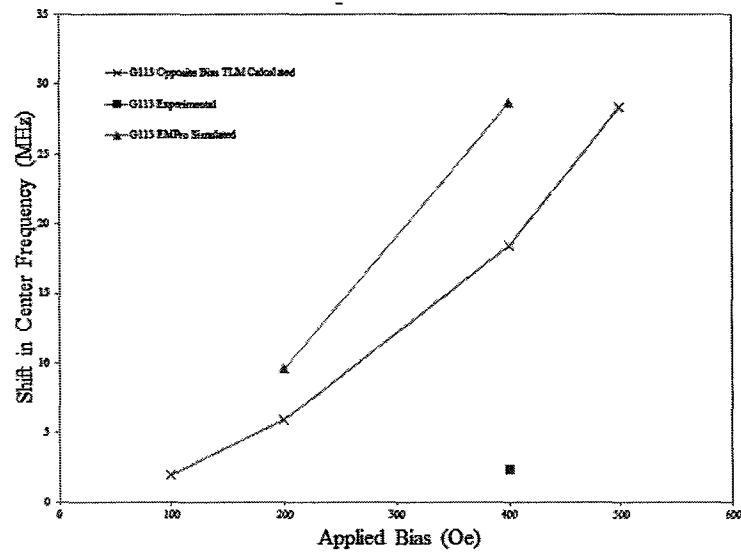


Figure 3.34 Comparison of shift in center frequency of EM simulated model, experimental bandpass filter and TLM Simple Five-Layer Model dual mode bandpass filter with “opposite” applied bias.

CHAPTER 4

TLM/SIMPLE FIVE-LAYER MODEL ANALYSIS APPLIED TO A NEW DESIGN REQUIREMENT

A new bandpass filter application is analyzed using the same Simple Five-Layer Model with G113 ferrite material as in Section 3.3. Again, the results are compared to an EM simulation tool as before. The design specifications for the new filter structure are listed in Table 4.1:

Table 4.1 Specifications of New Filter Structure

Parameter	Value
Center Frequency	3.3 GHz
Passband	3.1 – 3.5 GHz
Bandwidth	20 MHz
Number of Poles	2

4.1 TLM Program New Dual Mode Bandpass Filter Application

Figure 4.1 is a design curve of dielectric layer thickness L_3 vs. lowest order mode generated from the TLM program. This curve uses the single pole version of the Simple Five-Layer Model.

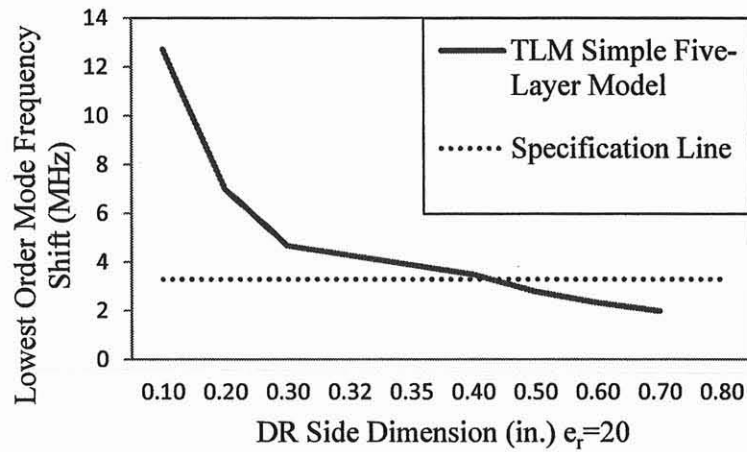


Figure 4.1 TLM design curve for square cross-section dielectric resonator size vs. center frequency in Simple Five-Layer Model.

The dielectric puck size for the desired center frequency of 3.3 GHz is determined from the TLM program. From the curve a dimension of .4 inches should be used as a first pass. Figure 4.2 details the first input screen which prompts the user to input a dielectric layer thickness in inches.

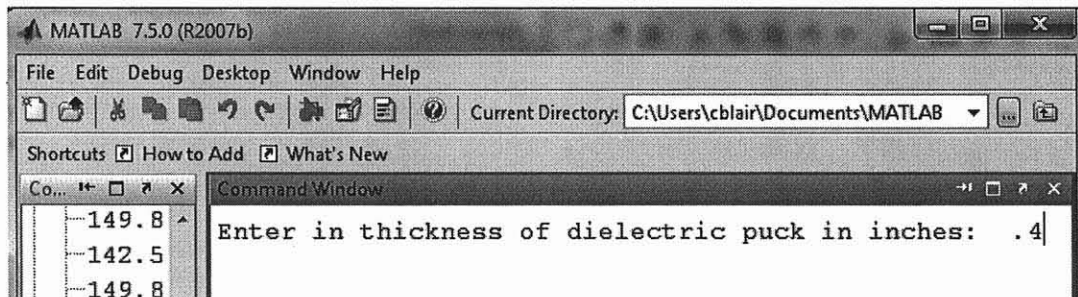


Figure 4.2 TLM Program – Input Dielectric Resonator side dimension in inches.

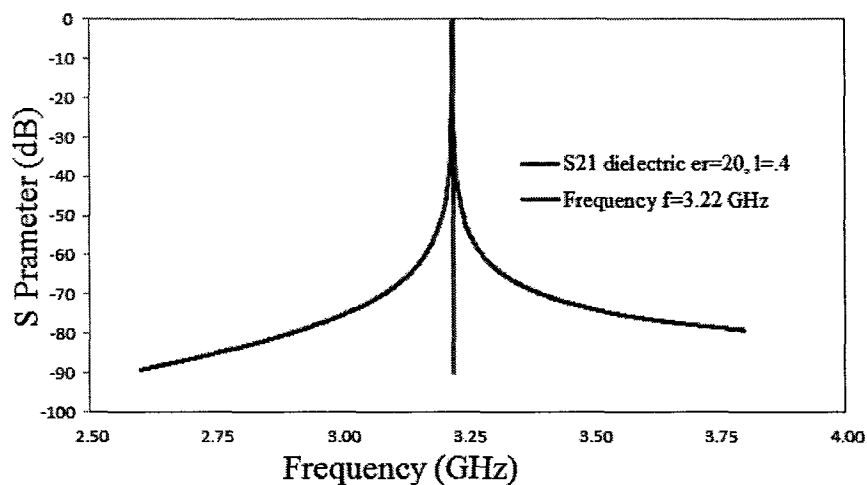


Figure 4.3 TLM Program – Single Pole Bandpass filter with G113 ferrite and .4 in. dielectric layer with zero applied bias.

The initial guess of a resonator of .4 inches square cross-section results in a composite structure whose center frequency is a bit lower than the specified design frequency of 3.3 GHz. Figure 4.4 shows that a second iteration for L3 of .425 inches yields a resonant frequency of 3.12 GHz.

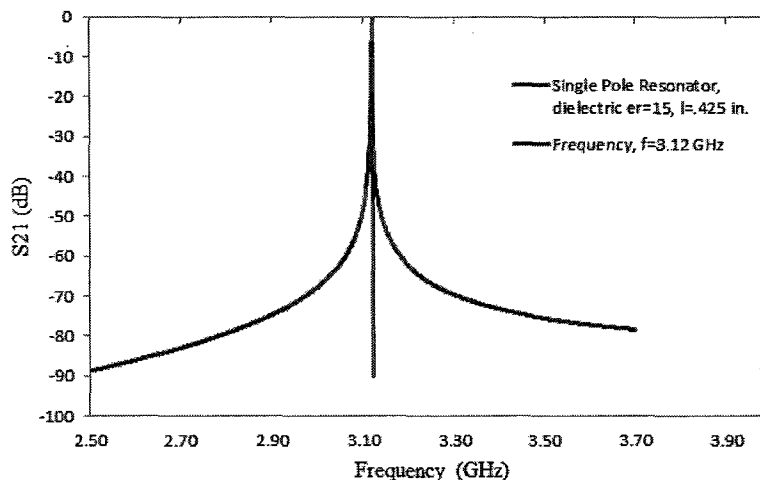


Figure 4.4 TLM Program – Single Pole Bandpass filter with G113 ferrite and .425 in. dielectric layer with zero applied bias.

The physical model of the New Filter Structure is similar in form and shape to the Experimental Model. Only the dimensions of the dielectric puck and the ferrite tiles are altered as shown in Figure 4.5. The bias is applied in the same manner with magnets above and below the ferrite. When the applied bias is of the same value and in the same direction, this is referred to as “same” bias and when the applied bias is of the same value but in opposite directions this is referred to as “opposite” bias. This conceptual model will be referred to as “New Dual Mode Bandpass Filter”.

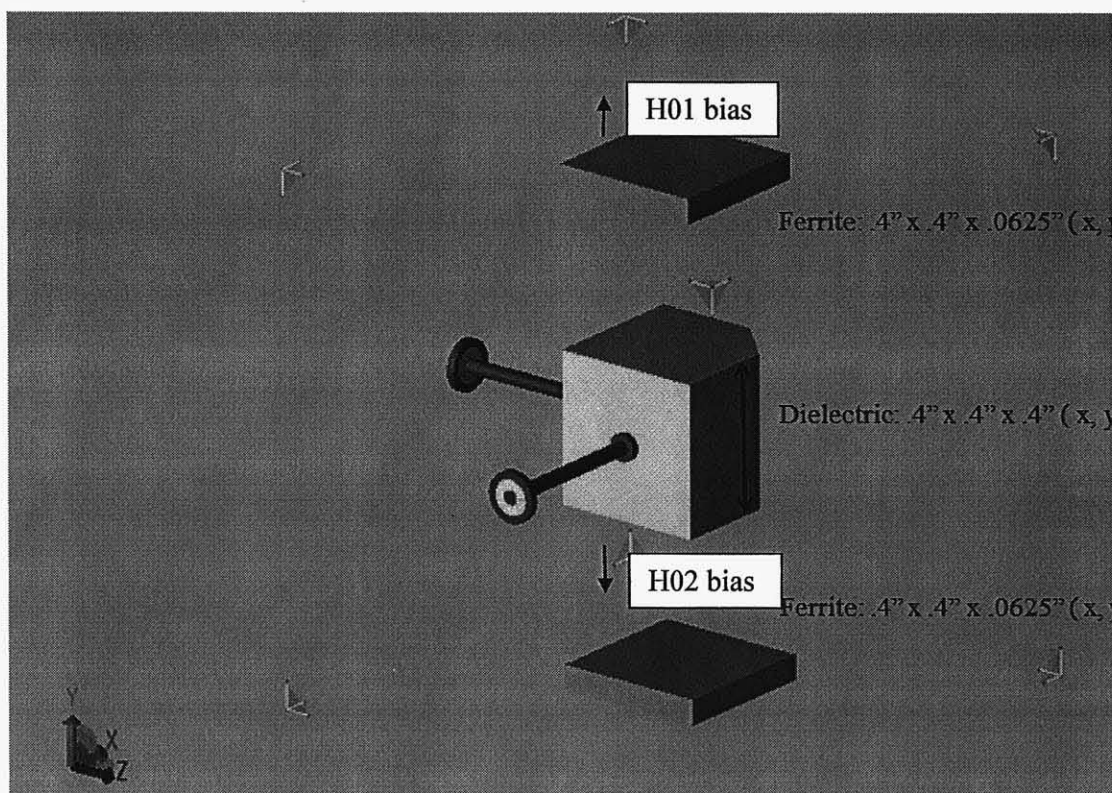


Figure 4.5 Conceptual View of New Dual Mode Bandpass filter structure with G113 ferrite and .4 in. dielectric puck.

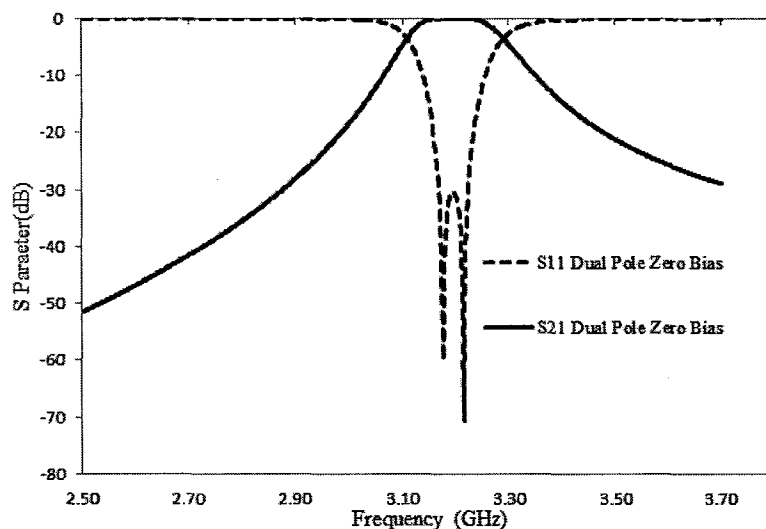


Figure 4.6 TLM Program – New Dual Mode Bandpass filter with G113 ferrite and .4 in. dielectric layer with zero applied bias.

S_{11} and S_{21} plots of this new structure at different applied bias are given below.

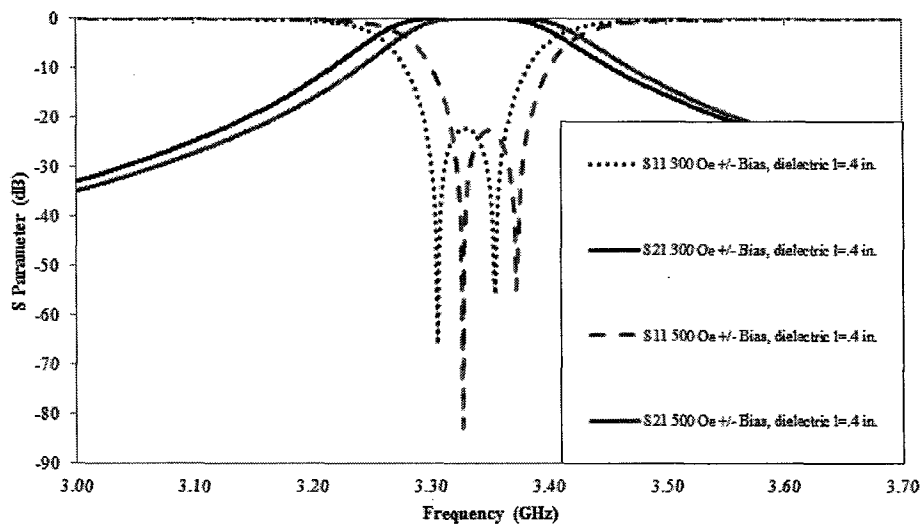


Figure 4.7 TLM Program – New Dual Mode BandPass filter with G113 ferrite and .4 in. dielectric layer with “opposite” applied bias.

4.2 EMPro Simulated Analysis New Dual Mode Bandpass Filter Application

An analysis of the new Dual Mode Bandpass filter structure using EMPro will be made at the different bias levels and compared to the results of the TLM analysis of the Simple Five-Layer Model.

Following the same procedure as with the TLM Program a design curve of the dielectric resonator side dimension versus lowest order resonant frequency is shown in Figure 4.8.

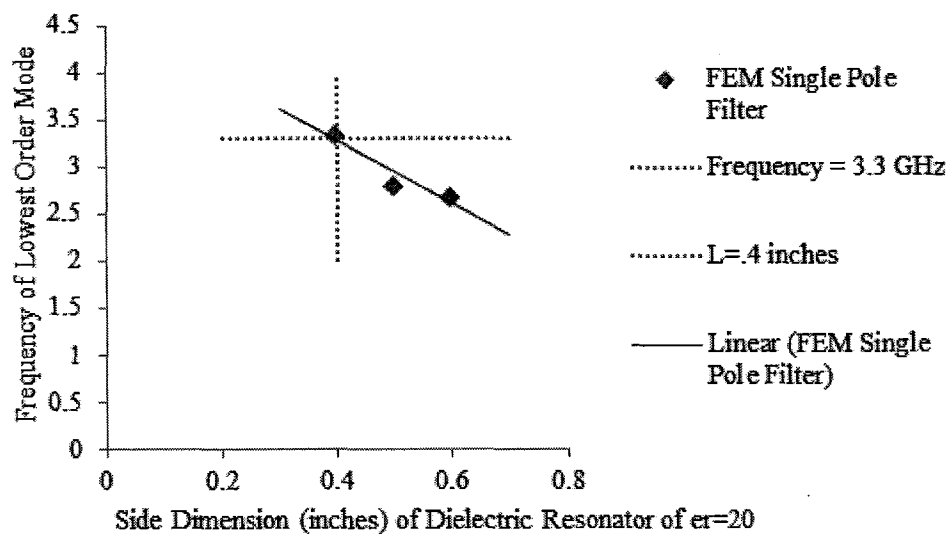


Figure 4.8 EMPro Design Curve – corner cut vs. lowest order mode frequency shift.

The discrete values, .1 inches above and below .5 inches for the Experimental Model are used in the EM simulations. From the design curve the dielectric resonator needs to be a square with .4 inches per side. This matches the TLM initial guess. S parameter plots resulting from the EMPro simulation for the Single Pole structure with different side dimensions are provided in Figure 4.9.

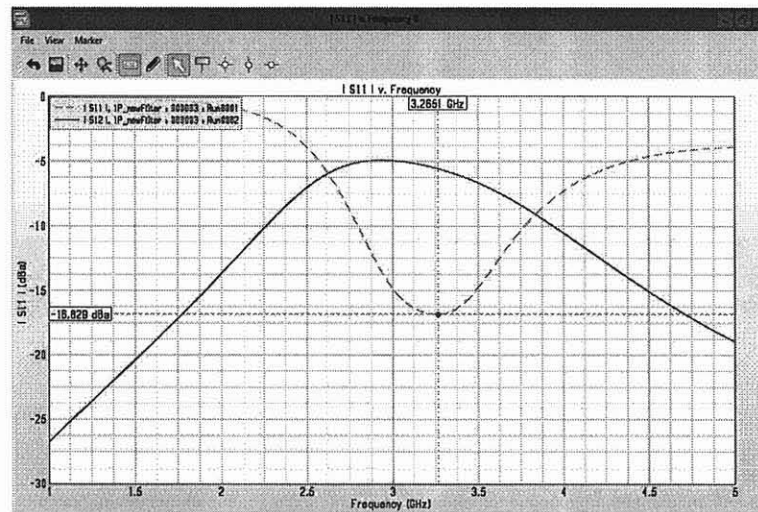


Figure 4.9 EMPro simulation – S Parameter Curve for New Bandpass - Single Pole Filter with zero applied bias (Oe).

A cavity corner cut with a side length = .1 inches is used as the perturbation.

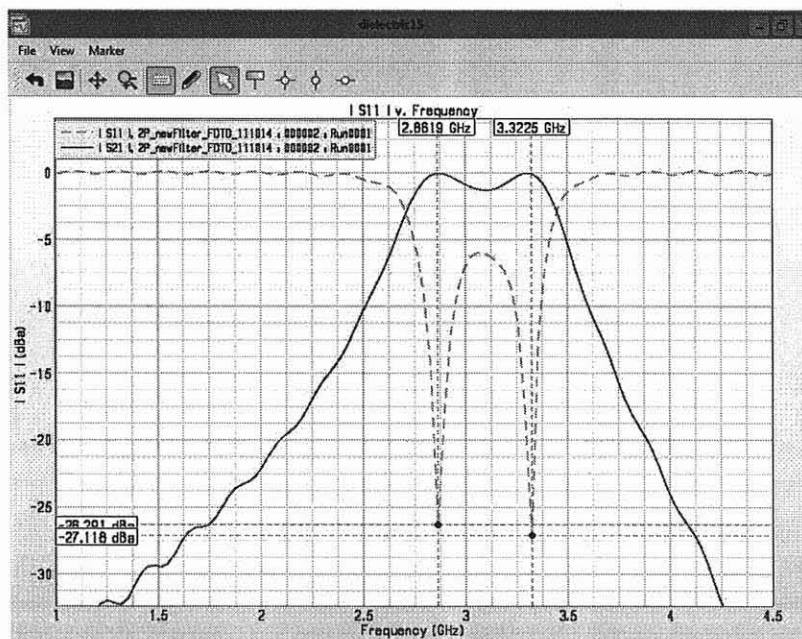


Figure 4.10 EMPro simulated S Parameter Results for New Dual Mode Filter Structure with 0 applied bias and .1 inch corner cut.

The center frequency of this structure is 3.28135 GHz. Figure 4.11 shows the S parameters results for the New Dual Mode Filter at zero and 400 Oe “opposite” bias.

Both frequency 1 and frequency 2 shifts in the same direction with “opposite” bias. The very fact that the TLM program predicts the dimension of the dielectric layer and validated by em simulation counts in favor of the model construction and the initial assumptions and approximations.

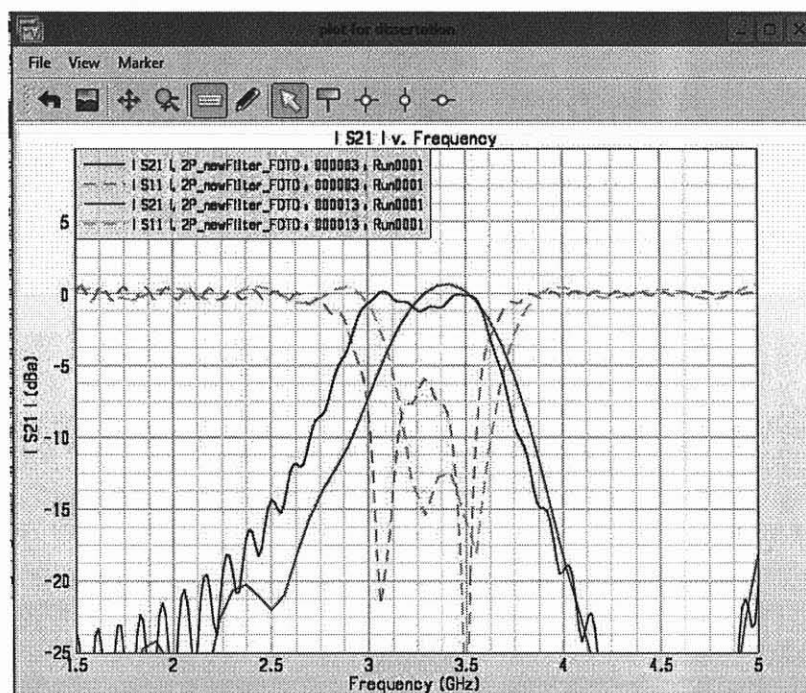


Figure 4.11 EMPro simulated S Parameter Results for New Dual Mode Filter Structure with zero applied bias and 400 Oe “opposite” applied bias.

4.3 Summary of New Dual Mode Bandpass Filter Application

A new Dual Mode Bandpass Filter structure was created for the TLM Program that is based on the Simple Five-Layer Model with a dielectric puck of $\epsilon_r=20$ material with a side dimension of .4”. The EM simulated model is based on the Experimental Model with a dielectric puck of $\epsilon_r=20$ material with a side dimension of .4” and a corner cut of .3”.

The resonant frequency of each mode is shifted with applied bias and the amount of frequency shift is dependent on the direction of the biasing field.

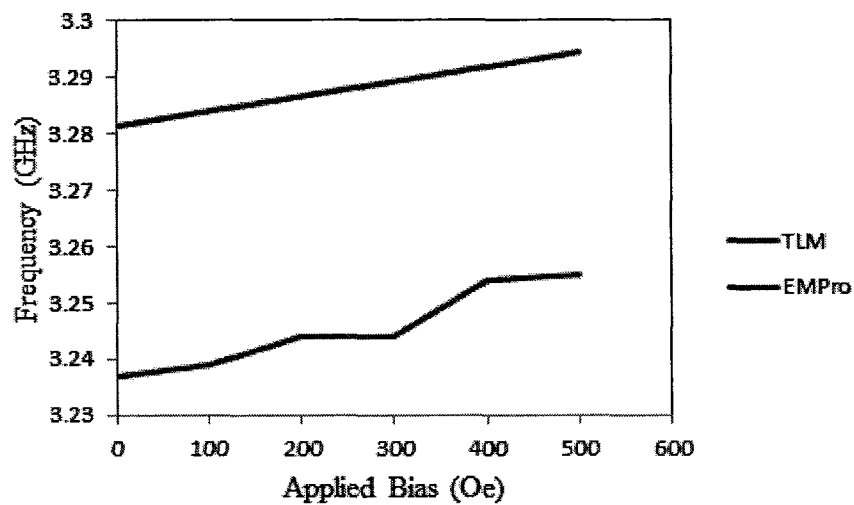


Figure 4.12 Comparison of EM simulated and TLM results of New Structure's center frequency shift with "opposite" applied bias.

CHAPTER 5

CONCLUSION

5.1 Summary of Work

This dissertation presents an analysis of a tunable bandpass filter resonator structure composed of a dielectric resonator surrounded by thin ferrite layers placed above and below the dielectric.

One objective of this dissertation is to develop a software program based on the Transmission Line Method (TLM) to quickly analyze the specific dual mode bandpass filter structure called the “Experimental Model” and implemented at RS Microwave in Butler, NJ. The Experimental Model consists of a square cross-section metal cavity with the square cross-section dielectric resonator supported by a dielectric support mechanism. The ferrite tiles are placed on top of these supports and a EAVSMF bias is applied directly to these tiles. The software program divides the ferrite and dielectric structure of the Experimental Model into two sections and uses the TLM program to equate the impedances. The frequencies at which the two impedances are equal are the resonant frequencies of the structure. This dissertation defines the lowest resonant frequency found as the lowest order mode frequency. A simple LC shunt circuit describes this lowest order mode resonant frequency. The Experimental Model is a dual mode filter where the modes are coupled by a corner cut in the cavity wall. There are several tuning elements in the Experimental Model. The TLM uses a simple capacitive pi network to describe the coupling and tuning mechanisms.

A full wave full 3D EM simulations tool, AGILENT EMPRO is used to validate the TLM program. AGILENT EMPRO simulations of many different variations of the

Experimental Model were constructed to optimize input/output coupling which involved lengthy preparation and simulation time.

To further test the TLM program a new design requirement, a dual mode bandpass filter operating between 3.3-3.5 GHz, is designed and compared with AGILENT EMPRO.

In summary the concept of using an EAVSMF applied bias to a ferrite material to implement a change in impedance is completed. To validate this concept a filter which is sensitive to frequency is used. The results of this investigation include the following:

- The EAVSMF bias field direction is the key design factor to control one of the frequencies of a dual mode filter.
- The EAVSMF bias field changes the permeability of the ferrite layers. Therefore, the impedance of the composite structure changes with applied bias. The change in impedance affects a change in the resonant frequency of the structure.
- Tunability comes from the dielectric mode resonance, not from the ferrite mode resonance. Therefore, the use of partially magnetized permeability values according to Schlöemann's equations [18] instead of Polder's permeability values has a small impact on overall analysis of composite structure.
- The dual mode dielectric resonator is tuned using permeability change of ferrite material with an external bias field change.
- From experimental observation with an equal magnitude and "same" direction bias field primarily the higher order mode of the dual mode bandpass filter was tuned. Through analysis and simulation a small shift in the lower order mode and a larger shift in the higher order mode is seen.
- From experimental observation with an equal magnitude and "opposite" external bias both frequency modes shifted simultaneously. Through analysis and simulation a frequency shift in the same direction is seen.
- Increased center frequency shift can be realized using a new ferrite material with a higher initial permeability value.

The TLM program shows good agreement with experimental results. Biasing of the ferrite tiles with and same bias magnitude and direction field shifts mainly one of the dual modes while biasing of the ferrites with a same magnitude but opposite direction field shows an equal shift of both modes. The TLM not only predicts the frequency shift with bias but is also faster in its setup and simulation time as compared to a full 3D EM software program.

5.2 Future Work

An experimental unit of the new bandpass structure with a square cross-section dielectric resonator dimension of .4 inches should be constructed to validate the design center frequency at 3.2 GHz.

In the initial research of this investigation, ferrite theory was reviewed and several different ferrite materials were investigated. It was found that the larger the slope in permeability vs. applied external bias, the greater the shift is in resonant frequency. A greater shift in frequency means a greater tunability range which is of great interest to commercial filter designers. Therefore, new materials with high permeability vs. bias slope should be investigated.

The main limitation of implementing ferrites devices in a filter topology is the need for more ferrite characterization in the partially magnetized state. When biased to an unsaturated state, the magnetic effects of the ferrite material are undefined. Previous work by Schlöemann et al. [18] has shown for specific materials the unsaturated value is a direct relationship to the saturate permeability value, the Polder value. Hence, for this investigation the Polder values are used. Also, the ferrite material height is small as

compared to wavelength validating this approximation. Future work should include an investigation of the unsaturated permeability values for the materials used. Since the magnetic field is affected by any boundary condition, future investigations will need to look at physical geometry- shape and thickness of the ferrite material tiles and its distance to the dielectric resonator. In addition, the effect of unequal and opposite bias should also be investigated.

APPENDIX A

PROGRAM FILES

A.1 Ferrite Analysis

The curves used in Chapter 3 and Appendix A are the results from the MATLAB program named ferriteCurves.m

```
% Filename - ferriteCurves.m
% Date 4/4/2011 By Charlotte Blair
%
%H0 is the magnitude of the applied bias in Oe. The maximum value happens
%to coincide with the resonance frequency and the linewidth is the 3dB
%point. This file calculates HO for some Transtech datasheets
%
clc; % Clear screen
clear; % clear all values
close all; % Close all existing figures
clear;
e0=8.854*10^-12;
m0=pi*4*10^-7;
freqRF=2800; %input ('Enter in RF frequency in MHz: ');
gamma=2.8; %Landé factor MHz/Oe
wRF=2*pi*freqRF; %
biasRF=freqRF/gamma;
ferrite='G113';
lw=25;%in MHz
lw1=200; %Oe
lw2=500; %Oe
w1loss=gamma*2*lw1; %loss calculation
w2loss=gamma*2*lw2;
f1loss=w1loss/(2*pi);
f2loss=w2loss/(2*pi);
T1=1/f1loss;
T2=1/f2loss;
npts=2000;
Msat_G113=1780;
Msat_G510=550;
Msat_TTVG1950=1950;
Msat_newFerrite=4000;
fm_G113=gamma*Msat_G113;%
```

```

wm_G113=2*pi*fm_G113;
fm_G510=gamma*Msat_G510;
wm_G510=2*pi*fm_G510;
fm_TTVG1950=gamma*Msat_TTVG1950;
wm_TTVG1950=2*pi*fm_TTVG1950;
fm_newFerrite=gamma*Msat_newFerrite;
wm_newFerrite=2*pi*fm_newFerrite;
Msat=[1780 550 1950 3000 1800]; % Msat(5) is to test Pozar example
Msat_select=Msat(1);
fm_select=gamma*Msat_select;
wm_select=2*pi*fm_select;
m0_G113=134; % Initial permeability for low freq domain wall
m0_G510=130;
m0_TTVG1950=130;
m0_Select=m0_G113;
%Ferrite susceptbility (permeability and susceptbility with applied bias)
biasMax=2000;
biasMin=0;
biasStep=(biasMax-biasMin)/npts;
for n=1:npts+1
    bias(n)=biasMin+(n-1)*biasStep;
    f0(n)=gamma*bias(n); % resonant frequency MHz
    w0(n)=2*pi*f0(n);
    x_xx(n)=(w0(n)*wm_select)/(w0(n)^2-wRF^2); %wm changes with direction
    x_xy(n)=(1i*wRF*wm_select)/(w0(n)^2-wRF^2);
    xxreal(n)=real(x_xx(n));
    xximag(n)=imag(x_xx(n));
    xyreal(n)=real(x_xy(n));
    xyimag(n)=imag(x_xy(n));
    w01(n)=w0(n)+1i/T1; % now calculate with loss
    w02(n)=w0(n)+1i/T2; % now calculate with loss
    x1_xx(n)=(w01(n)*wm_select)/(w01(n)^2-wRF^2);
    x2_xx(n)=(w02(n)*wm_select)/(w02(n)^2-wRF^2);
    xx1real(n)=real(x1_xx(n));
    xx2real(n)=real(x2_xx(n));
    xx1imag(n)=imag(x1_xx(n));
    xx2imag(n)=imag(x2_xx(n));
    x1_xy(n)=1i*wRF*wm_select/(w01(n)^2-wRF^2);
    x2_xy(n)=1i*wRF*wm_select/(w02(n)^2-wRF^2);
    xy1real(n)=real(x1_xy(n));
    xy2real(n)=real(x2_xy(n));
    xy1imag(n)=imag(x1_xy(n));
    xy2imag(n)=imag(x2_xy(n));
    mr(n)=(1+x_xx(n));
    mrSq(n)=mr(n)*mr(n);
    kappa(n)=-1*imag(x_xy(n));

```

```

    kappaSq(n)=kappa(n)*kappa(n);
    meff(n)=(mrSq(n)-kappaSq(n))/mr(n);
end;
figure;
subplot(2,1,1);
plot(bias,xxreal);
titlestr=[ferrite,' - Lossless Susceptibility coefficients (real Xxx) vs bias with RF
frequency=', num2str(freqRF),' MHz, Ms=',num2str(Msat_select),...
' G, Saturation frequency=',num2str(fm_select),' MHz'];
title(titlestr);
legend('LF real x\ _xx');
xlabel('Bias (Oe)');
ylabel('Susceptibility');
subplot(2,1,2);
plot(bias,xximag);
titlestr=[ferrite,' - Lossless Susceptibility coefficients (imag Xxx) vs bias with RF
frequency=', num2str(freqRF),' MHz, Ms=',num2str(Msat_select),...
' G, Saturation frequency=',num2str(fm_select),' MHz'];
title(titlestr);
legend('LF imag x\ _xx');
xlabel('Bias (Oe)');
ylabel('Susceptibility');
figure;
subplot(2,1,1);
plot(bias,xyreal);
titlestr=[ferrite,' - Lossless Susceptibility coefficients (real Xxy) vs bias with RF
frequency=', num2str(freqRF),' MHz, Ms=',num2str(Msat_select),...
' G, Saturation frequency=',num2str(fm_select),' MHz'];
title(titlestr);
legend('LF real x\ _xy');
xlabel('Bias (Oe)');
ylabel('Susceptibility');
subplot(2,1,2);
plot(bias,xyimag);
titlestr=[ferrite,' - Lossless Susceptibility coefficients (imag Xxy) vs bias with RF
frequency=', num2str(freqRF),' MHz, Msat=',num2str(Msat_select),...
' G and saturation frequency=',num2str(fm_select),' MHz'];
title(titlestr);
legend('LF imag x\ _xy');
xlabel('Bias (Oe)');
ylabel('Susceptibility');
%now permeability and Kappa
subplot(2,2,1);
plot(bias,mr);
titlestr=[ferrite,' - Lossless Relative permeability vs bias with RF frequency=',
num2str(freqRF),' MHz, Msat=',num2str(Msat_select),...

```

```

    ' G and saturation frequency=',num2str(fm_select),' MHz'];
title(titlestr);
legend('mue');
xlabel('Bias (Oe)');
ylabel('Susceptibility');
subplot(2,2,2);
plot(bias,kappa);
titlestr=[ferrite,' - Lossless Susceptibility vs bias with RF frequency=', num2str(freqRF),'
MHz, Msat=',num2str(Msat_select),...
    ' G and saturation frequency=',num2str(fm_select),' MHz'];
title(titlestr);
legend('susceptibility');
xlabel('Bias (Oe)');
ylabel('Susceptibility');
subplot(2,2,3);
plot(bias,meff);
titlestr=[ferrite,' - Lossless Effective permeability vs bias with RF frequency=',
num2str(freqRF),' MHz, Msat=',num2str(Msat_select),...
    ' G and saturation frequency=',num2str(fm_select),' MHz'];
title(titlestr);
legend('Effective permeability');
xlabel('Bias (Oe)');
ylabel('Susceptibility');
%separate graphs for dissertation need font size at least 24
%Figures 3.6 to 3.10 Comparing linewidths used to validate with Lax and Button
figure4.3
separatePlots=1;
max_realxx1=max(abs(xx1real(n)));
max_imagxx1=max(abs(xx1imag(n)));
max_realxx2=max(abs(xx2real(n)));
max_imagxx2=max(abs(xx2imag(n)));
max_realxy1=max(abs(xy1real(n)));
max_imagxy1=max(abs(xy1imag(n)));
max_realxy2=max(abs(xy2real(n)));
max_imagxy2=max(abs(xy2imag(n)));
if separatePlots ==1
figure;
plot(bias,xx1real,bias,xx2real);
set(gca,'FontSize',36,'FontName','Times')
titlestr=[ferrite,'- Lossy susceptibility-permeability coefficient (mue) with RF
frequency=', num2str(freqRF),' MHz, Ms=4pi', num2str(Msat_select),...
    ' G, Saturation frequency=',num2str(fm_select),' MHz'];
title(titlestr);
set(gca,'FontSize',24,'FontName','Times')
legStr1=['linewidth= ',num2str(lw1),' Oe - real x1\ _xx'];
legStr2=['linewidth= ',num2str(lw2),' Oe - real x2\ _xx'];

```

```

legend(legStr1,legStr2);
xlabel('Bias (Oe)');
ylabel('Susceptibility - real');
figure;
plot(bias,abs(xx1 imag),bias,abs(xx2 imag));
set(gca,'FontSize',36,'FontName','Times')
titlestr=[ferrite,' - Lossy susceptibility-permeability coefficient (mue) with RF
frequency=', num2str(freqRF),' MHz, Ms=4pi', num2str(Msat_select),...
' G, Saturation frequency=',num2str(fm_select),' MHz'];
title(titlestr);
set(gca,'FontSize',24,'FontName','Times')
legStr1=['LW= ',num2str(lw1),' Oe - imag x1\ _xx'];
legStr2=['LW= ',num2str(lw2),' Oe - imag x2\ _xx'];
legend(legStr1,legStr2);
xlabel('Bias (Oe)');
ylabel('Susceptibility - imag');
figure;
set(gca,'FontSize',36,'FontName','Times')
plot(bias,xy1 real,bias,xy2 real);
titlestr=[ferrite,' -Lossy susceptibility-susceptibility coefficient (kappa) with RF
frequency=', num2str(freqRF),' MHz, Ms=4pi', num2str(Msat_select),...
' G, Saturation frequency=',num2str(fm_select),' MHz'];
title(titlestr);
set(gca,'FontSize',24,'FontName','Times')
legStr1=['linewidth= ',num2str(lw1),' Oe - real x1\ _xy'];
legStr2=['linewidth= ',num2str(lw2),' Oe - real x2\ _xy'];
legend(legStr1,legStr2);
xlabel('Bias (Oe)');
ylabel('Susceptibility-real');
figure;
set(gca,'FontSize',36,'FontName','Times')
plot(bias,xy1 imag,bias,xy2 imag);
titlestr=[ferrite,' - Lossy susceptibility-susceptibility coefficient (kappa) with RF
frequency=', num2str(freqRF),'MHz, Ms=4pi', num2str(Msat_select),...
' G, Saturation frequency=',num2str(fm_select),' MHz'];
title(titlestr);
set(gca,'FontSize',24,'FontName','Times')
legStr1=['linewidth= ',num2str(lw1),' Oe - imag x1\ _xy'];
legStr2=['linewidth= ',num2str(lw2),' Oe - imag x2\ _xy'];
legend(legStr1,legStr2);
xlabel('Bias (Oe)');
ylabel('Susceptibility-imag');
end; separatePlots;
abs_sepPlots=1;
if abs_sepPlots == 1
figure;

```

```

plot(bias,abs(xx1real),bias,abs(xx2real));
set(gca,'FontSize',20,'FontName','Times')
titlestr=[ferrite,'- Lossy susceptibility-permeability coefficient (mue) with RF
frequency=', num2str(freqRF),' MHz, Ms=4pi', num2str(Msat_select),...
' G, Saturation frequency=',num2str(fm_select),' MHz'];

title(titlestr);
set(gca,'FontSize',16,'FontName','Times')
legStr1=['linewidth= ',num2str(lw1),' Oe - real x1\ _xx'];
legStr2=['linewidth= ',num2str(lw2),' Oe - real x2\ _xx'];
legend(legStr1,legStr2);
xlabel('Bias (Oe)');
ylabel('Magnitude of Susceptibility - real');
figure;
plot(bias,abs(xx1imag),bias,abs(xx2imag));
set(gca,'FontSize',20,'FontName','Times')
titlestr=[ferrite,' - Lossy susceptibility-permeability coefficient (mue) with RF
frequency=', num2str(freqRF),' MHz, Ms=4pi', num2str(Msat_select),...
' G, Saturation frequency=',num2str(fm_select),' MHz'];
title(titlestr);
set(gca,'FontSize',16,'FontName','Times')
legStr1=['LW= ',num2str(lw1),' Oe - imag x1\ _xx'];
legStr2=['LW= ',num2str(lw2),' Oe - imag x2\ _xx'];
legend(legStr1,legStr2);
xlabel('Bias (Oe)');
ylabel('Magnitude of Susceptibility - imag');
figure;
set(gca,'FontSize',20,'FontName','Times')
plot(bias,abs(xy1real),bias,abs(xy2real));
titlestr=[ferrite,'-Lossy susceptibility-susceptibility coefficient (kappa) with RF
frequency=', num2str(freqRF),' MHz, Ms=4pi', num2str(Msat_select),...
' G, Saturation frequency=',num2str(fm_select),' MHz'];
title(titlestr);
set(gca,'FontSize',16,'FontName','Times')
legStr1=['linewidth= ',num2str(lw1),' Oe - real x1\ _xy'];
legStr2=['linewidth= ',num2str(lw2),' Oe - real x2\ _xy'];
legend(legStr1,legStr2);
xlabel('Bias (Oe)');
ylabel('Magnitude of Susceptibility-real');
figure;
set(gca,'FontSize',20,'FontName','Times')
plot(bias,abs(xy1imag),bias,abs(xy2imag));
titlestr=[ferrite,' - Lossy susceptibility-susceptibility coefficient (kappa) with RF
frequency=', num2str(freqRF),' MHz, Ms=4pi', num2str(Msat_select),...
' G, Saturation frequency=',num2str(fm_select),' MHz'];
title(titlestr);

```

```

set(gca,'FontSize',16,'FontName','Times')
legStr1=['linewidth= ',num2str(lw1),' Oe - imag x1\_xy'];
legStr2=['linewidth= ',num2str(lw2),' Oe - imag x2\_xy'];
legend(legStr1,legStr2);
xlabel('Bias (Oe)');
ylabel('Magnitude of Susceptibility-imag');
end; separatePlots;
saveLW=0;
%pwd
%cd C:\Users\cblair\njit\matlab\ferritePlots
if saveLW==1
save bias.txt bias -ASCII
save xx1real.txt xx1real -ASCII
save xx2real.txt xx2real -ASCII
save xx1imag.txt xx1imag -ASCII
save xx2imag.txt xx2imag -ASCII
save xy1real.txt xy1real -ASCII
save xy2real.txt xy2real -ASCII
save xy1imag.txt xy1imag -ASCII
save xy2imag.txt xy2imag -ASCII
end;

%%%%%%%%%%%%%%%%%%%%%%%%%%%%%%%%%%%%%%%%%%%%%%%%%%%%%%%%%%
%%%%%%%%%%%%%%%%%%%%%%%%%%%%%%%%%%%%%%%%%%%%%%%%%%%%%%%%%%
%%%%%%%%%%%%%%%%%%%%%%%%%%%%%%%%%%%%%%%%%%%%%%%%%%%%%%%%%%
%Figure 3.11 Resonant Frequency Graph
figure;
plot(bias,f0,bias,freqRF,'r--');
grid on;

set(gca,'FontSize',30,'FontName','Times'); % changes the size and font
of the axis number
title('Resonant Frequency as a Function of Applied DC Bias, Landé
factor=2');
set(gca,'FontSize',24,'FontName','Times');
legend('resonant frequency','RF frequency');
xlabel('Applied DC Bias H0(Oe)');
ylabel('Resonant Frequency - MHz');

%%%%%%%%%%%%%%%%%%%%%%%%%%%%%%%%%%%%%%%%%%%%%%%%%%%%%%%%%%
%%%%%%%%%%%%%%%%%%%%%%%%%%%%%%%%%%%%%%%%%%%%%%%%%%%%%%%%%%
%%%%%%%%%%%%%%%%%%%%%%%%%%%%%%%%%%%%%%%%%%%%%%%%%%%%%%%%%%
%Figure 3.12 - Calculate Saturation Frequencies wm vs Msat

mStart=100; mStop=4000;mStep=(mStop-mStart)/npts;

```

```

for n=1:npts+1
    someMsat(n)=mStart+(n-1)*mStep;
    fm(n)=gamma*someMsat(n);
end;

figure;
plot(someMsat,fm,Msat_G113,fm_G113,'rx-
',Msat_G510,fm_G510,'gx-',Msat_TTVG1950,fm_TTVG1950,'bx-
','MarkerSize',20);
grid off;
set(gca,'FontSize',30,'FontName','Times')
%title('S');
set(gca,'FontSize',24,'FontName','Times');
leg1=('Saturation Frequency gamma*Ms');
leg2=['G113 ',num2str(fm_G113),' MHz'];
leg3=['G510 ',num2str(fm_G510),' MHz'];
leg4=['TTVG1950 ',num2str(fm_TTVG1950),' MHz'];
legend(leg1,leg2,leg3,leg4);
xlabel('Saturation Magnetization');
ylabel('Saturation Frequency - MHz');

%%%%%%%%%%%%%%%%%%%%%%%%%%%%%%%%%%%%%%%%%%%%%%%%%%%%%%%%
%%%%%%%%%%%%%%%%%%%%%%%%%%%%%%%%%%%%%%%%%%%%%%%%%%%%%%%%
%%%%%%%%%%%%%%%%%%%%%%%%%%%%%%%%%%%%%%%%%%%%%%%%%%%%%%%%
%%%%%%%%%%%%%%%%%%%%%%%%%%%%%%%%%%%%%%%%%%%%%%%%%%%%%%%%
%Figure 3.13 - G113 Ferrite Permeability Curve vs Frequency at some
bias use
%3000 for LB figure 4-3 page 155
ferrite='G113';
bias_Select=3000; %Oe
f0_Select=gamma*bias_Select; % resonant frequency
w0=m0*gamma*H0
w0_Select=2*pi*f0_Select;
w0Loss=w0_Select+1i/T1;
freqStart=1; freqStop=5000; freqStep=(freqStop-freqStart)/npts;
for n=1:npts+1
    freq(n)=freqStart+(n-1)*freqStep;
    w(n)=2*pi*freq(n);
    xxx(n)=w0Loss*wm_G113*sign(bias(n))/(w0Loss^2-w(n)^2);%wm
changes with direction
    xxy(n)=1i*w(n)*wm_G113*sign(bias(n))/(w0Loss^2-w(n)^2);
    xxreal=abs(xxx(n));
    xximag=imag(xxx(n));
    mue_G113(n)=1+xxx(n);
    %kappa_G113(n)=xxy(n);

```



```

mue_real(n)=abs(mue_G113(n));
mue_imag(n)=imag(mue_G113(n));
kappa_real(n)=abs(xxy(n));
kappa_imag(n)=imag(xxy(n));
end;
figure;
%plot(freq,xxreal,freq,xximag,fm_G113,0,'rX-',f0_Select,0,'mo-
','MarkerSize',10);
plot(freq,mue_real,freq,mue_imag,fm_G113,0,'rX-',f0_Select,0,'mo-
','MarkerSize',20);
grid off;
set(gca,'FontSize',30,'FontName','Times');
titlestr=[ferrite, ' - Susceptibility with an Applied Bias=',
num2str(bias_Select),...
' Oe, Linewidth=',num2str(lw),' Oe'];
title(titlestr);
set(gca,'FontSize',24,'FontName','Times')
leg1=['Real part of lossy mue'];
leg2=['Imag part of lossy mue'];
leg3=['Saturation Frequency:gamma*Ms =',num2str(fm_G113),'
MHz'];
leg4=['Resonance frequency:gamma H0 =',num2str(f0_Select),'
MHz'];
legend(leg1,leg2,leg3,leg4);
xlabel('Frequency - MHz');
ylabel('mue');

figure;
plot(freq,kappa_real,freq,kappa_imag,fm_G113,0,'rX-
',f0_Select,0,'mo-', 'MarkerSize',20);
grid off;
set(gca,'FontSize',30,'FontName','Times');
titlestr=[ferrite, ' - Susceptibility with an Applied Bias=',
num2str(bias_Select),...
' Oe, Linewidth=',num2str(lw),' Oe'];
title(titlestr);
set(gca,'FontSize',24,'FontName','Times')
leg1=['Real part of lossy susceptibility'];
leg2=['Imag part of lossy susceptibility'];
leg3=['Saturation Frequency:gamma*Ms =',num2str(fm_G113),'
MHz'];
leg4=['Resonance frequency:gamma H0 =',num2str(f0_Select),'
MHz'];
legend(leg1,leg2,leg3,leg4);
xlabel('Frequency - MHz');
ylabel('susceptibility');

```

A.2 TRANSMISSION LINE METHOD – IMPEDANCE CALCULATIONS

```

% Don't forget to change SaveFile flag!!!!!!
% 11/1/11 added line 145 direction variable that changes all places
here
% bias direction needs to be done. Three manually changes eliminated

% 10/28/2011 line 451 change kzmin and max to include 950 Oe

%Filename - TLM Program - Five-Layer Model.m
% Date 9/15/2011 By Charlotte Blair
%
%Structure
%L1-ferrite L2-air L3-DR L4-air L5-ferrite
clc; % Clear screen
clear; % clear all values
close all; % Close all existing figures
clear;

% Variable
% a inches, b inches    guide dimension in inches
% a, b                  guide dimensions in meters
% f                     frequency (Hz)

% Constants
e0=8.854*10^-12;
m0=pi*4*10^-7;
c0=1/sqrt(e0*m0);%speed of light
n0=sqrt(m0/e0);
Z0=120*pi; Y0=1/Z0;

%Inputs
%Cavity Dimensions
%ainches= input ('x axis - long side in inches: ');
ainches = 1.6;
%binches= input ('y axis - input short side in inches: ');
binches=1.7;
%binches= input ('z axis - input propagation depth in inches: ');
d inches=1.6;
% convert to metric
a=ainches*0.0254; b=binches*0.0254; d=d inches*0.0254;

defaultValues=1;
    l3in=.5;
    l1in=1/16;

if defaultValues==0
l3in=input ('Enter in thickness of dielectric puck in inches: ');
l1in=input ('Enter in thickness of ferrite in inches: ');

```

```

end

l3max=binches-2*llin;
if l3in>l3max
    stop;
end

npts=2500;

%%%%%%%%%%%%%%%%%%%%%%%%%%%%%%%%%%%%%%%%%%%%%%%%%%%%%%%%%%%%%%%%%%%%%%%%
%Inputs for ferrite
ferrite='G113';
lw=15;%in MHz
lw1=25; %Oe
lw2=100; %Oe
gamma=2.8;%lande factor in MHz
w1loss=gamma*2*lw1; %loss calculation
w2loss=gamma*2*lw2;
f1loss=w1loss/(2*pi);
f2loss=w2loss/(2*pi);
T1=1/f1loss;
T2=1/f2loss;

% For this program to work we need to know the RF frequency but
original
% TLM program calculates the cavity resonances exactly through TL
method so
% we will put input in a RF freq so we can get some permeability
values.
% These should not change much with a small change in RF freq

freqRF=2800; %input ('Enter in RF frequency in MHz: ');
gammaFactor=2.8; %lande factor MHz/Oe
wRF=2*pi*freqRF; %*10^6;

biasMax=4000;
biasMin=-500;
biasStep=(biasMax-biasMin)/npts;
%negative sign indicates change of direction of applied bias - same
value

%Plot f0 vs bias

%%%%%%%%%%%%%%%%%%%%%%%%%%%%%%%%%%%%%%%%%%%%%%%%%%%%%%%%%%%%%%%%%%%%%%%%
%%%%%%%%%%%%%%%%%%%%%%%%%%%%%%%%%%%%%%%%%%%%%%%%%%%%%%%%%%%%%%%%%%%%%%%%
%Figure 3.11 Resonant Frequency Graph

for n=1:npts+1
    bias(n)=biasMin+(n-1)*biasStep;
    f0(n)=gammaFactor*bias(n); % resonant frequency
    w0(n)=2*pi*f0(n);
end;

```



```

direction=-1; % direction=1 same direction direction=-1 opposite
direction

f0MHz_bias1=gammaFactor*bias1
f0_bias1=f0MHz_bias1/10^3;
f0_bias1_lo=f0_bias1-lw;
f0_bias1_hi=f0_bias1+lw;

f0_select=gammaFactor*bias1;
w0_select=2*pi*f0_select;
w0Loss=w0_select+1i/T1;

if w0_select == wRF %at resonance
    mr1=m0_Select;
else
    mr1=1+f0_select*fm_select/(f0_select^2-freqRF^2);
end;

%Input mr5
mr1=1+mr1
mr5=1+mr1 % magnitude of bias is the same just change of direction

%Figure 3.13 - G113 Ferrite Permeabilty Curve vs Frequency at some bias

freqTemp=[f0_select fm_select];
freqStart=floor(min(freqTemp))-500;
freqStop=ceil(max(freqTemp));
freqStart=round(freqStart);
freqStop=round(freqStop/100)*100;
freqStep=(freqStop-freqStart)/npts;
for n=1:npts
    freq(n)=freqStart+(n-1)*freqStep;
    temp=freq(n);
    if round(temp) == freqRF
        freq(n)=.99*freq(n);
    end;
    w(n)=2*pi*freq(n);
    xxx(n)=w0Loss*wm_select/(w0Loss^2-w(n)^2);%wm changes with
direction
    xxy(n)=1i*w(n)*wm_select/(w0Loss^2-w(n)^2);
    xxreal=real(xxx(n)); %if w > wres than susceptibility can be
negative
    xximag=imag(xxx(n));
    mue_G113(n)=1+xxx(n);
    %kappa_G113(n)=xxy(n);
    mue_real(n)=real(mue_G113(n));
    mue_imag(n)=imag(mue_G113(n));
    kappa_real(n)=real(xxy(n));
    kappa_imag(n)=imag(xxy(n));
end;

max1=max(mue_real);
max2=max(mue_imag);

```

```

%Magnitude
figure;
plot(freq, (mue_real), freq, (mue_imag), fm_select, 0, 'rX-', f0_select, 0, 'mo-',
'MarkerSize', 20);
grid off;
set(gca, 'FontSize', 30, 'FontName', 'Times');
titlestr=[ferrite, ' - Permeability with an Applied Bias=',
num2str(bias_Select), ...
'Oe, Linewidth=', num2str(lw), ' Oe'];
title(titlestr);
set(gca, 'FontSize', 24, 'FontName', 'Times')
leg1=['Real part of lossy mue'];
leg2=['Imag part of lossy mue'];
leg3=['Saturation Frequency:gamma*Ms =', num2str(fm_select), ' MHz'];
leg4=['Resonance Frequency:gamma H0 =', num2str(f0_select), ' MHz'];
legend(leg1, leg2, leg3, leg4);
xlabel('Frequency - MHz');
ylabel('Susceptibility');

```

```

%Figure 3.13, 3.15
figure;
plot(freq, abs(mue_real), freq, abs(mue_imag), fm_select, 0, 'rX-',
f0_select, 0, 'mo-', 'MarkerSize', 20);
grid off;
set(gca, 'FontSize', 30, 'FontName', 'Times');
titlestr=[ferrite, ' - Magnitude of Permeability with an Applied
Bias=', num2str(bias_Select), ...
'Oe, Linewidth=', num2str(lw), ' Oe'];
title(titlestr);
set(gca, 'FontSize', 24, 'FontName', 'Times')
leg1=['Real part of lossy mue'];
leg2=['Imag part of lossy mue'];
leg3=['Saturation Frequency:gamma*Ms =', num2str(fm_select), ' MHz'];
leg4=['Resonance Frequency:gamma H0 =', num2str(f0_select), ' MHz'];
legend(leg1, leg2, leg3, leg4);
xlabel('Frequency - MHz');
ylabel('Susceptibility');

```

```

%Figure 3.14
figure;
plot(freq, abs(kappa_real), freq, abs(kappa_imag), fm_select, 0, 'rX-',
f0_select, 0, 'mo-', 'MarkerSize', 20);
grid off;
set(gca, 'FontSize', 30, 'FontName', 'Times');
titlestr=[ferrite, ' - Magnitude of Susceptibility with an Applied
Bias=', num2str(bias_Select), ...
'Oe, Linewidth=', num2str(lw), ' Oe'];
title(titlestr);
set(gca, 'FontSize', 24, 'FontName', 'Times')
leg1=['Real part of lossy kappa'];
leg2=['Imag part of lossy kappa'];
leg3=['Saturation Frequency:gamma*Ms =', num2str(fm_select), ' MHz'];
leg4=['Resonance Frequency:gamma H0 =', num2str(f0_select), ' MHz'];
legend(leg1, leg2, leg3, leg4);
xlabel('Frequency - MHz');

```

```

ylabel('Susceptibility');

%%%%%%%%%%%%%%%%%%%%%%%%%%%%%%%%%%%%%%%%%%%%%%%%%%%%%%%%%%%%%%%%%%%%%%%%
% Set L1 & L5 Ferrite properties
m1=mr1*m0;
m5=mr5*m0;

%%%%%%%%%%%%%%%%%%%%%%%%%%%%%%%%%%%%%%%%%%%%%%%%%%%%%%%%%%%%%%%%%%%%%%%%
% Initialize Cavity Layers with L1 at top
l3=(l3in*.0254);er3=20; e3=er3*e0;mr3=1;m3=mr3*m0;

% L1=L5 ferrite layers
l1=l1in*.0254;er1=15;e1=er1*e0;
l5=l1in*.0254;er5=15;e5=er5*e0;

%L2=L4 air layers
l2=(b-l3-2*l1)/2;er2=1; e2=er2*e0;mr2=1;m2=mr2*m0;
l4=l2;er4=1;e4=er4*e0;mr4=1;m4=mr4*m0;
cavY=(l1+l2+l3+l4+l5);
cavYin=(l1+l2+l3+l4+l5)/.0254;
er=[er1 er2 er3 er4 er5];mr=[mr1 mr2 mr3 mr4 mr5];
ermax=max(er);mrmx=max(mr);
ermin=min(er);mrmin=min(mr);
ermean=mean(er);mrmean=mean(abs(mr));
erwtmean=(sqrt(l1*er1/b)^2+(l2*er2/b)^2+(l3*er3/b)^2+(l4*er4/b)^2+(l5*er5/b)^2)/5;
mrwtmean=(sqrt(l1*mr1/b)^2+(l2*mr2/b)^2+(l3*mr3/b)^2+(l4*mr4/b)^2+(l5*mr5/b)^2)/5;
n=1;m=0;l=1; %xyz mode

%Cutoff Frequency for homogenous cavities
c1=c0/sqrt(er1*mr1); c2=c0/sqrt(er2*mr2);
c3=c0/sqrt(er3*mr3); c4=c0/sqrt(er4*mr4);c5=c0/sqrt(er5*mr5);
fres0=(c0/(2*pi))*(((n*pi/a)^2 +(m*pi/b)^2+(l*pi/d)^2 )^.5)/10^9;
fc1=(c1/(2*pi))*(((n*pi/a)^2 +(m*pi/b)^2+(l*pi/d)^2 )^.5)/10^9;
fc2=(c2/(2*pi))*(((n*pi/a)^2 +(m*pi/b)^2+(l*pi/d)^2 )^.5)/10^9;
fc3=(c3/(2*pi))*(((n*pi/a)^2 +(m*pi/b)^2+(l*pi/d)^2 )^.5)/10^9;
fc4=(c4/(2*pi))*(((n*pi/a)^2 +(m*pi/b)^2+(l*pi/d)^2 )^.5)/10^9;
fc5=(c5/(2*pi))*(((n*pi/a)^2 +(m*pi/b)^2+(l*pi/d)^2 )^.5)/10^9;
fc=[fc1 fc2 fc3 fc4 fc5];
fcstart=round(min(fc));
fcstop=ceil(max(fc));
%find max and min of fcutoff since er2>er1 fc2<fc1 kgoes as sqrt of er
%fstop=fc3;fstart=fc1;

% Frequency Range
% calculate at cutoff
%lambda=c0/f;w=2*pi*f;
kx1=m*pi/a;kx2=m*pi/a;kx3=m*pi/a;
wc1=2*pi*fc1*10^9;wc2=2*pi*fc2*10^9;wc3=2*pi*fc3*10^9;
wc4=2*pi*fc4*10^9;wc5=2*pi*fc5*10^9;
wres0=2*pi*fres0*10^9; % make in base units

%Propagation Constants
%k1^2=kx1^2+ky1^2+kz^2=(m*pi/cx)^2+ky1^2+kz^2=w^2*m1*e1

```

```

%Plot K1,k2,k3 and find kzmin and kzmax
kz=0; % Find cutoff freq of composite

fcstart=2.5; fcstop=5;
fstep=(fcstop-fcstart)/npts;
f=fcstart:fstep:fcstop;
w=2*pi*f*10^9;
k1= sqrt(w.^2*m1*e1); %kz=0 and kx=0
k2= sqrt(w.^2*m2*e2);
k3= sqrt(w.^2*m3*e3);
k4= sqrt(w.^2*m4*e4);
k5= sqrt(w.^2*m5*e5);

kcy1=sqrt(k1.^2-kz^2);
kcy2=sqrt(k2.^2-kz^2);
kcy3=sqrt(k3.^2-kz^2);
kcy4=sqrt(k4.^2-kz^2);
if direction == 1
    kcy5=sqrt(k5.^2-kz^2);
else
    kcy5=sqrt(-k5.^2+kz^2);
end
kcy=[kcy1 kcy2 kcy3 kcy4 kcy5];
kcymin=round(min(kcy));
kcymin=round(min(kcy));

TE=1;
%for TE modes
if TE==1
    mode='TE';
    Z01=2*pi.*f*10^9*m1./kcy1;Z01zero=2*pi.*f*10^9*m0./kcy1;
    Z02=2*pi.*f*10^9*m2./kcy2;
    Z03=2*pi.*f*10^9*m3./kcy3;
    Z04=2*pi.*f*10^9*m4./kcy4;Z05=(2*pi.*f*10^9*m5./kcy5);

    Z01mean=mean(Z01);Z02mean=mean(Z02);Z03mean=mean(Z03);Z04mean=mean(Z04)
    ;Z05mean=mean(Z05);

    Z0=[Z01 Z02 Z03 Z04 Z05];
    Z0zero=[Z01zero Z02 Z03 Z04 Z01zero];
    Z0mean2=[Z01mean Z02mean Z03mean Z04mean Z05mean];
    meanZ02=mean(Z0mean2);
    Z0mean=mean(Z0);
    Z0zeromean=mean(Z0zero);
    Y0mean=1./Z0mean;

else
%for TM modes
mode='TM';
Z01=kcy1./(2*pi.*f*10^9*e1);Z02=kcy2./(2*pi.*f*10^9*e2);
Z03=kcy3./(2*pi.*f*10^9*e3);Z04=kcy4./(2*pi.*f*10^9*e4);Z05=kcy5./(2*pi
.*f*10^9*e5);
Z0=[Z01 Z02 Z03 Z04 Z05];
Z0mean=mean(Z0);

```



```

Y0mean=1./Z0mean;
end

showPlot=0;
if showPlot==1
figure;
plot(f,kcy1,'m--',f,kcy2,'b--',f,kcy3,'cx-',f,kcy4,'b--',f,kcy5,'m--
');
titlestr=('Propagation constant of each layer at kz=0 cutoff ');
title(titlestr);
legend('kcy1-ferrite','kcy2-air','kcy3-dielectric','kcy4-air','kcy5-
ferrite');
xlabel('Frequency GHz'); ylabel('kcy');
ylabel('Propagation');
grid on;

figure;
plot(f,Z01,f,Z02,f,Z03,f,Z04,f,Z05);
grid on;
title('TE Characteristic Impedance of Layers ');
legend('Z01-ferrite','Z02-air','Z03-dielectric','Z04-air','Z05-
ferrite');
xlabel('Frequency - GHz');
ylabel('Impedance');
end

%TLM Program
%Zero Bias
%Zin=Z0*(ZL+j*Z0*tan(k*l))/(Z0+j*ZL*tan(k*l));
%Zin=Z0*(ZL*cot(k*l)+j*Z0)/(Z0*cot(k*l)+j*ZL);
%Yin=Y0*(YL+j*Y0*tan(k*l))/(Y0
%+j*YL*tan(k*l))
%ZSCin=j*Z0*tan(k*l); YSCin=-j*Y0/tan(k*l)
%For our stucture ZLoad3 and ZLoad1 is a SC

%ZL3a=1i*Z03*tan(2*pi.*f*10^9*sqrt(m3*e3)*l3); %Z3SC
%ZL3=-1i*Z03.*cot(2*pi.*f*10^9*sqrt(m3*e3)*l3);%Z3OC
%LHSre=real(LHS);LHSimag=imag(LHS);LHSabs=abs(LHS);

Zin1=1i*Z01.*tan(2*pi.*f*10^9*sqrt(m0*e1*l1)); %Z1SC as long as Z0 is
real and positive
Zin5=1i*Z05.*tan(2*pi.*f*10^9*sqrt(m0*e5*l5)); %Z5SC

ZL2=Zin1;
num2=ZL2+1i.*Z02.*tan(k2.*l2);
denom2=Z02+(1i.*ZL2.*tan(k2.*l2));
Zin2temp=num2./denom2;
Zin2=Z02.*Zin2temp;

ZL4=Zin5;
num4=ZL4+1i.*Z04.*tan(k4.*l4);
denom4=Z04+1i.*ZL4.*tan(k4.*l4);
Zin4temp=num4./denom4;
Zin4=Z04.*Zin4temp;

```

```

ZL3=Zin4;
num3=ZL3+1i.*Z03.*tan(k3.*l3);
denom3=Z03+1i.*ZL3.*tan(k3.*l3);
Zin3temp=num3./denom3;
Zin3=Z03.*Zin3temp;

imagZin2=imag(Zin2);
imagZin3=imag(Zin3);
max2=max(imagZin2(:));
max3=max(imagZin3(:));
cross2=find(imagZin2==max2);
cross3=find(imagZin3==max3);
lowestOrder=min(cross2,cross3);
XfzeroDC=fcstart+lowestOrder*fstep

tempResDC=strcat('Resonance Frequency is :',num2str(f0_select/10^3),'
GHz at Bias= 0 Oe');
tempRes=strcat('Resonance Frequency is :',num2str(f0_select/10^3),' GHz
at Bias= ', num2str(bias1), 'Oe');
tempSat=strcat('Saturation Frequency is :',num2str(fm_select/10^3),'
GHz');
%keepOut=(f0_select/10^3+fm_select/10^3)
keepOut1=(f0_select-lw)/10^3;
keepOut2=(f0_select+lw)/10^3;
tempKeepOut=strcat('Suggested range is : ',num2str(keepOut2),' to :
',num2str(fm_select/10^3));
textLegDC={tempResDC,tempSat,tempKeepOut};
textLeg={tempRes,tempSat,tempKeepOut};
if temp <2

figure;
plot(f,imagZin2,f,imagZin3,XfzeroDC,0,'rx-');
set(gca,'FontSize',26,'FontName','Times');
titlestr=['Zero Bias Transcendental Equation for a Square Cavity with
Dielectric Permittivity= ',num2str(er3),' and side
dimension=',num2str(l3in),' in.'];
title(titlestr);
set(gca,'FontSize',20,'FontName','Times');
legend('Zin2-ferrite/air','Zin3-dielectric/air/ferrite');
xlabel('Frequency GHz');
grid on;

figure;
plot(f,imagZin2,f,imagZin3,XfzeroDC,0,'go-',abs(f0_bias1_hi),0,'rx-
','MarkerSize',20);
titlestr=['Saturation: Zero Bias Transcendental Equation for a Square
Cavity with Dielectric Permittivity= ',num2str(er3),' and side
dimension=',num2str(l3in),' in.'];
title(titlestr);
legend('Zin2-ferrite/air','Zin3-dielectric/air/ferrite');
xlabel('Frequency GHz');
grid on;
else

```

```

figure;
plot(f, imagZin2, f, imagZin3, XfzeroDC, 0, XfzeroDC, 0, 'ro-
', 'MarkerSize', 20); % first XfzeroDC is placeholder for Legend title
set(gca, 'FontSize', 26, 'FontName', 'Times');
titlestr=['Zero Bias Transcendental Equation for a Square Cavity with
Dielectric Permittivity= ', num2str(er3)]; % and side
dimension=', num2str(l3in), ' in.'];
title(titlestr);
set(gca, 'FontSize', 20, 'FontName', 'Times');
legend('Zin2-ferrite/air', 'Zin3-dielectric/air/ferrite');
xlabel('Frequency GHz');
hleg1=legend(textLegDC);
set(hleg1, 'Location', 'SouthWest');
grid on;
end;

```

```

XfzeroDC=input ('Zero Bias - Enter in X component (GHz) of 1st
crossover point: ');

```

```

% for interative kz we know kz composite must lie between kzair and
kzdiel .
% so setup this matrix
% fcutoff of air is higher than composite so kzair is zero until this
freq
% so use kzmin as 0 and use kcymax as max - just need a value here
kzstart=abs(.9*kcymn); kzstop=abs(kcymax); kzstep=(kzstop-
kzstart)/npts;
%kz=kzstart:kzstep:kzstop;

%ky1sq=k1.^2-kz.^2; ky1=(sqrt(ky1sq));
%ky2sq=k2.^2-kz.^2; ky2=(sqrt(ky2sq));
%ky3sq=k3.^2-kz.^2; ky3=(sqrt(ky3sq));
%ky4sq=k4.^2-kz.^2; ky4=abs(sqrt(ky4sq));
%ky5sq=k5.^2-kz.^2; ky5=(sqrt(ky5sq));
y3L=l3/cavY;

for n=1:npts
    kz(n)=kzstart+n*kzstep;
    fz(n)=(fcstart+n*fstep)*10^9;
    k1(n)= sqrt((2*pi*fz(n))^2*m1*e1);
    ky1sq(n)=k1(n)^2 -kz(n)^2;
    ky1(n)=sqrt(ky1sq(n));
    k2(n)= sqrt((2*pi*fz(n))^2*m2*e2);
    ky2sq(n)=k2(n)^2 -kz(n)^2;
    ky2(n)=sqrt(ky2sq(n));
    k3(n)= sqrt((2*pi*fz(n))^2*m3*e3);
    ky3sq(n)=k3(n)^2 -kz(n)^2;
    ky3(n)=sqrt(ky3sq(n));
    k4(n)= sqrt((2*pi*fz(n))^2*m4*e4);
    ky4sq(n)=k4(n)^2 -kz(n)^2;
    ky4(n)=sqrt(ky4sq(n));

```

```

k5(n)=sqrt((2*pi*fz(n))^2*(m5*e5));
if direction == -1
    ky5sq(n)=k5(n)^2 -kz(n)^2;
else
    ky5sq(n)=-k5(n)^2 +kz(n)^2;
end
ky5(n)=sqrt(ky5sq(n));

end;

showKplots=0;

if showKplots==1
figure;
plot(kz,real(ky1),'m--',kz,imag(ky1),'mx-',kz,real(ky2),'b--',
kz,imag(ky2),'bx-',kz,real(ky3),'co-',...
kz,imag(ky3),'cx-',kz,real(ky4),'b--',kz,imag(ky4),'bx-',
kz,real(ky5),'m--',kz,imag(ky5),'mx-');
legend('Zero Bias: beta1-ferrite real','beta1-ferrite imag','beta2-air
real','beta2-air imag','betay3-dielectric real','betay3-dielectric
imag',...
'beta4-air real','beta4-air imag','beta5-ferrite real','beta5-
ferrite imag');
xlabel('betaZ'); ylabel('betaY per layer');
grid on;
end;

% Now with an Applied Bias

%Zin1=1i*Z01.*tan(2*pi.*f*10^9*sqrt(m1*e1)*l1); %Z1SC
%Zin5=1i*Z05.*tan(2*pi.*f*10^9*sqrt(m5*e5)*l5); %Z5SC
Zin1=1i*Z01.*tan(k1.*l1); %Z1SC
Zin5=1i*Z05.*tan(k5.*l5); %Z5SC

ZL2=Zin1;
num2=ZL2+1i.*Z02.*tan(k2.*l2);
denom2=Z02+(1i.*ZL2.*tan(k2.*l2));
Zin2temp=num2./denom2;
Zin2=Z02.*Zin2temp;

ZL4=Zin5;
num4=ZL4+1i.*Z04.*tan(k4.*l4);
denom4=Z04+1i.*ZL4.*tan(k4.*l4);
Zin4temp=num4./denom4;
Zin4=Z04.*Zin4temp;

ZL3=Zin4;
num3=ZL3+1i.*Z03.*tan(k3.*l3);
denom3=Z03+1i.*ZL3.*tan(k3.*l3);
Zin3temp=num3./denom3;
Zin3=Z03.*Zin3temp;
%XFzero=Zin2-Zin3;% transental equation.
imagZin2=imag(Zin2);
imagZin3=imag(Zin3);
absZin3=abs(Zin3);

```

```

max2=max(imagZin2(:));
max3=max(imagZin3(:));
max4=max(absZin3(:));
cross2=find(imagZin2==max2);
cross3=find(imagZin3==max3);
cross4=find(absZin3==max4);
lowestOrder=min(cross2,cross3);
lowestOrder2=min(cross2,cross4);
Xfzero1=fcstart+lowestOrder*fstep
Xfzero2=fcstart+lowestOrder2*fstep
figure;
plot(f,imagZin2,f,imagZin3,XfzeroDC,0,Xfzero1,0,Xfzero2,0,'go-
','MarkerSize',20);
titlestr=['Transcendental Equation for a Square Cavity with Dielectric
Permittivity= ',num2str(er3),' and side dimension=',num2str(l3in),' in.
with an Applied Bias'];
title(titlestr);
legend('Zin2-ferrite/air','Zin3-dielectric/air/ferrite');
xlabel('Frequency GHz'); ylabel('Bz');
hleg1=legend(textLeg);
set(hleg1,'Location','SouthWest');
grid on;

savePlot=0;
if savePlot ==1
    save 950pt5TransEqnFreq_11015.txt f -ASCII
    save 950pt5imagZin2_11015.txt imagZin2 -ASCII
    save 950pt5imagZin_11015.txt imagZin3 -ASCII
end;

Xfzero=input('Applied Bias: Enter in frequency of lowest zero beta
crossover point in GHz: ');

% now need some kz based on bias plot
%knowing e2>e1>e3 we can say kyl and ky3 are below cutoff - evanescent
%waves so really kyl=-j *alpha1 and ky3=-j*alpha3
% exp(-j*kyl*y)=exp(-j*(-j*alpha1)*y)=exp(-alpha1*y)
% using Y admittance value YSC=-Y0/tan(kl)
%YL3=1i*Y03/tan(2*pi.*f*10^9*sqrt(m3*e3)*l3);

for n=1:npts
    kz(n)=kzstart+n*kzstep;
    fz(n)=(fcstart+n*fstep)*10^9;
    k1(n)=sqrt((2*pi*fz(n))^2*m1*e1);
    kylsq(n)=k1(n)^2 -kz(n)^2;
    kyl(n)=sqrt(kylsq(n));
    k2(n)=sqrt((2*pi*fz(n))^2*m2*e2);
    ky2sq(n)=k2(n)^2 -kz(n)^2;
    ky2(n)=sqrt(ky2sq(n));
    k3(n)=sqrt((2*pi*fz(n))^2*m3*e3);
    ky3sq(n)=k3(n)^2 -kz(n)^2;
    ky3(n)=sqrt(ky3sq(n));
    k4(n)=sqrt((2*pi*fz(n))^2*m4*e4);
    ky4sq(n)=k4(n)^2 -kz(n)^2;

```

```

    ky4(n)=sqrt(ky4sq(n));
    k5(n)=sqrt((2*pi*fz(n))^2*m5*e5);
    if direction ==1
    ky5sq(n)=k5(n)^2 -kz(n)^2;
    else
        ky5sq(n)=-k5(n)^2 +kz(n)^2;
    end
    ky5(n)=sqrt(ky5sq(n));
end;

ksubplots=0;
if ksubplots ==1;
figure;
subplot(3,3,1);
plot(kz,real(ky1),kz,imag(ky1));
xlabel('some betaz'); ylabel('betaY1');

subplot(3,3,2);
plot(kz,real(ky2),kz,imag(ky2));
xlabel('some betaz'); ylabel('betaY2');

subplot(3,3,3);
plot(kz,real(ky3),kz,imag(ky3));
xlabel('some betaz'); ylabel('betaY3');

subplot(3,3,4);
plot(kz,real(ky4),kz,imag(ky4));
xlabel('some betaz'); ylabel('betaY4');

subplot(3,3,5);
plot(kz,real(ky5),kz,imag(ky5));
xlabel('some betaz'); ylabel('betaY5');
end;

showAllKPlot =0;
if showAllKPlot == 1
figure;
plot(kz,real(ky1),'m--',kz,imag(ky1),'m-',kz,real(ky2),'b--',
kz,imag(ky2),'b-',kz,real(ky3),'c-',...
kz,imag(ky3),'c-',kz,real(ky4),'b--',kz,imag(ky4),'b-',
kz,real(ky5),'m--',kz,imag(ky5),'m-');
legend('beta1-ferrite real','beta1-ferrite imag','beta2-air
real','beta2-air imag','betay3-dielectric real','betay3-dielectric
imag',...
'beta4-air real','beta4-air imag','beta5-ferrite real','beta5-
ferrite imag');
xlabel('betaZ'); ylabel('betaY per layer');
grid on;
else
figure;
%plot(kz,imag(ky2),kz,real(ky3));
plot(kz,abs(ky2),kz,abs(ky3));
titlestr=('Propagation Curves - Select lowest crossover point');
title(titlestr);
legend('beta2-air imag','betay3-dielectric real');
xlabel('betaZ'); ylabel('betaY per layer');

```

```

grid on;
end;

%Use this betaZ which varies with frequency to find the resonant
frequency
%Use layer3 of dielectric

if defaultValues ==1
    kzPlot=109;
    kylPlot=238;
end;
%%%%%%%%%%%%%%%%%%%%%%%%%%%%%%%%%%%%%%%%%%%%%%%%%%%%%%%%%%%%%%%%%%%%%%%%

kzPlot=input ('Enter in X component (kz) of dr at 1st crossover point:
');
kylPlot=input ('Enter in Y component (kyl) of dr at crossover point:
');
%kzPlot=109;
%kylPlot=238;

%kydiff=ky2Plot-kylPlot;
%kylPlot=kylPlot+kydiff/2;
%kx1=m*pi/a=kx2=kx3 %kx is constant dependent on m mode
%k3^2=kx3^2+ky3^2+kz^2=w^2*m3*e3 %layer 1
%(2*pi*f)^2*m3*e3=(m*pi/a)+ky3^2 +kzPlot^2
temp=(m*pi/a)^2+kylPlot^2+kzPlot^2;
kDC=((m*pi/a)^2+(kylPlot/mrmean)^2+(kzPlot/mrmean)^2);
temp_zero=kDC/(m0*ermean*e0); % at DC all mr=1 so no need to add mean
which will include biased mr
temp_bias=temp/(mrmean*m0*ermean*e0); %this adds effect of mr
tempdr=temp/(mr3*m0*er3*e0);
%fresCalc=sqrt(temp2)/(2*pi);
temp_air=temp/(m0*e0);
fresCalc0=sqrt(temp_air)/(2*pi);%for air filled cavity correct
%tempmean=temp/(m0*ermean*e0);%to get an equiv mr
%fresCalcmean=sqrt(tempmean)/(2*pi);
tempwtmean=temp/(m0*erwtmean*mrwtmean*e0);
fresml=sqrt(tempwtmean)/(2*pi);
fresml_air=sqrt(temp_air)/(2*pi);
fresml_zero=XfzeroDC*10^9

fresml_dr=sqrt(tempdr)/(2*pi);
fresml_bias=Xfzero*10^9;

%Show Sparameter plot for single pole
wres_ml_air=2*pi*fresml_zero; %LC=1/wres^2;
wres_ml_bias=2*pi*fresml_bias;
wres_ratio=wres_ml_air/wres0; %assuming eps is constant and only mue
changed this is prop to sqrt of mue
mueepsreleff=sqrt(wres_ratio);
mueepsmean=mrmean*m0*ermean*e0;

% find Lzero and Czero
% need to find a delta w so assume some very small diff
deltaLo=.95;

```

```

deltaHi=1.1;
%fres_m1_minus=deltaLo*fresm1;
%fres_m1_plus=deltaHi*fresm1;
fres_m1_minus=deltaLo*fresm1_zero;
fres_m1_plus=deltaHi*fresm1_zero;
wres_m1_air_minus=2*pi*fres_m1_minus;
wres_m1_air_plus=2*pi*fres_m1_plus;
beta_m1_fresminus=wres_m1_air_minus*sqrt(e0*m0*ermean);
beta_m1_fresplus=wres_m1_air_plus*sqrt(e0*m0*ermean);

% Using same observation point as above
l_LHS=l1+l2;
l_RHS=l3+l4+l5;

arg1res_m1_plus=(-beta_m1_fresplus.*l_RHS);% must be <90 degrees to be
a resonant circuit
arg2res_m1_plus=(beta_m1_fresplus.*l_LHS);
arg1res_m1_minus=(-beta_m1_fresminus.*l_RHS);
arg2res_m1_minus=(beta_m1_fresminus.*l_LHS);

tan1_m1_plus=tan(arg1res_m1_plus);%tan in quadI and III same
tan2_m1_plus=tan(arg2res_m1_plus);%tan in Quad II and IV same - neg of
QI and QIII
tan1_m1_minus=tan(arg1res_m1_minus);
tan2_m1_minus=tan(arg2res_m1_minus);

Y0mleff=1/Z0zeromean; % assume TE is lowest order mode but for a sq
caviti ZOTE=ZOTM
Ylin_minus_m1=-li*Y0mleff*tan1_m1_minus;
Y2in_minus_m1=-li*Y0mleff*tan2_m1_minus;
RHS_minus_m1=(Ylin_minus_m1);
LHS_minus_m1=(Y2in_minus_m1);

Ylin_plus_m1=-li*Y0mleff*tan1_m1_plus;
Y2in_plus_m1=-li*Y0mleff*tan2_m1_plus;
RHS_plus_m1=(Ylin_plus_m1);
LHS_plus_m1=(Y2in_plus_m1);

deltaYin_m1=RHS_plus_m1-RHS_minus_m1;
deltaw_m1=2*pi*fresm1*(deltaHi-deltaLo);
deltaYinw_m1=deltaYin_m1/deltaw_m1;

LC=1/wres_m1_air^2;
Lnum=(1/wres_m1_air^2)+LC;

L_zero=abs(Lnum/(deltaYinw_m1));
LnH_zero=L_zero*10^9
%C_zero=LC/L_zero;
w0zero=2*pi*fresm1_zero;
temp=L_zero*w0zero^2;
C_zero=1/temp;
CpF_zero=C_zero*10^12
f0GHzzero=(w0zero/(2*pi*10^9)); %this is a check and should be same as
fres_m1 from above
diff=fresm1_zero-(f0GHzzero*10^9);

```



```

if diff > 100
    stop;
end;

if bias1 > 0;
% find Lbias and Cbias
fres_mlbias_minus=deltaLo*fresml_bias;
fres_mlbias_plus=deltaHi*fresml_bias;
wres_mlbias_air_minus=2*pi*fres_mlbias_minus;
wres_mlbias_air_plus=2*pi*fres_mlbias_plus;
beta_mlbias_fresminus=wres_mlbias_air_minus*sqrt(e0*m0*mueepsreleff);
beta_mlbias_fresplus=wres_mlbias_air_plus*sqrt(e0*m0*mueepsreleff);

arg1res_mlbias_plus=(-beta_mlbias_fresplus.*l_RHS);% must be <90
degrees to be a resonant circuit
arg2res_mlbias_plus=(beta_mlbias_fresplus.*l_LHS);
arg1res_mlbias_minus=(-beta_mlbias_fresminus.*l_RHS);
arg2res_mlbias_minus=(beta_mlbias_fresminus.*l_LHS);

tan1_mlbias_plus=tan(arg1res_mlbias_plus);
tan2_mlbias_plus=tan(arg2res_mlbias_plus);
tan1_mlbias_minus=tan(arg1res_mlbias_minus);
tan2_mlbias_minus=tan(arg2res_mlbias_minus);

Ylin_minus_mlbias=-li*Y0mleff*tan1_mlbias_minus;
Y2in_minus_mlbias=-li*Y0mleff*tan2_mlbias_minus;
RHS_minus_mlbias=(Ylin_minus_mlbias);
LHS_minus_mlbias=(Y2in_minus_mlbias);

Ylin_plus_mlbias=-li*Y0mleff*tan1_mlbias_plus;
Y2in_plus_mlbias=-li*Y0mleff*tan2_mlbias_plus;
RHS_plus_mlbias=(Ylin_plus_mlbias);
LHS_plus_mlbias=(Y2in_plus_mlbias);

deltaYin_mlbias=RHS_plus_mlbias-RHS_minus_mlbias;
deltaw_mlbias=2*pi*fresml_bias*(deltaHi-deltaLo);
deltaYinw_mlbias=deltaYin_mlbias/deltaw_mlbias;

% Change is in L not C with bias
w0bias=2*pi*fresml_bias;
f0bias_MHz=w0bias/(2*pi*10^6)
C_bias=C_zero;
temp=wres_mlbias^2*C_bias;
L_bias=1/temp;
LnH_bias=L_bias/10^-9

end;

%Now that we have LC for resonator calculate coupling pi matrix from J
%inverters
% first calculate g values for 2 pole Chebyshev with .01db ripple

n=2; %order of filter
rippledB=.01;
beta=log(coth(rippledB/17.37));

```

```

gamma=sinh(beta/(2^n));
a1=sin(pi/(2^n));
a2=sin(((2*2-1)*pi)/2^n);
b1=gamma^2 +(sin(pi/n))^2;
g0=1;
g1=2*a1/gamma;
g2=4*a1*a2/(b1*g1);
g3=(coth(beta/4))^2;

%now calculate J values
Zl=50;Zs=50;
GA=1/Zl;GB=1/Zs;
wprime=1;
BW=50*10^6;
fracWzero=BW/fresml_zero;
fracWbias=BW/fresml_bias;

%C1=C_zero=Cres-Cin-Cseries;
%C01=J01/w0zero;

J011Pzero_num=GA*w0zero*C_zero;
J011P_denom=g0*wprime;
J011Pzero=J011Pzero_num/J011P_denom;
Cin1P_zero_denom=w0zero*sqrt(1-(J011Pzero/GA)^2);
Cin1P_zero=J011Pzero/Cin1P_zero_denom;
Cin1P_zeropF=Cin1P_zero/10^-12;

J01zero_num=GA*w0zero*C_zero*fracWzero;
J01_denom=g0*g1*wprime;
J01zero_num=GA*w0zero*C_zero*fracWzero;
temp=J01zero_num/J01_denom;
temp2=sqrt(temp);
J01zero=sqrt(J01zero_num/J01_denom);
Cin_zero_denom=w0zero*sqrt(1-(J01zero/GA)^2);
Cin_zero=J01zero/Cin_zero_denom;
Cin_zeropF=Cin_zero/10^-12
CinE_zero_denom=1+(w0zero*Cin_zero/GA)^2;
CinE_zero=Cin_zero/CinE_zero_denom;
CinE_zeropF=CinE_zero/10^-12

J12_denom=g1*g2;
J12zero_num=C_zero*C_zero;
J12zero=fracWzero*w0zero*sqrt(J12zero_num/J12_denom);
Cseries_zero=J12zero/w0zero;
Cseries_zeropF=Cseries_zero/10^-12
C1_zero=C_zero-CinE_zero-Cseries_zero;
C1_zeropF=C1_zero/10^-12

C1Total_zero=C_zero-CinE_zero-Cseries_zero;
C1shunt_zero=-CinE_zero-Cseries_zero;
C1shunt_zeropF=C1shunt_zero/10^-12
Cshunt_zero=C1shunt_zero;
Cshunt_zeropF=Cshunt_zero/10^-12

%For Zs != Zl

```

```

J23_denom=g2*g3;
J23zero_num=GB*w0zero*C_zero*fracWzero;
J23zero=sqrt(J23zero_num/J23_denom);
Cout_zero_denom=w0zero*sqrt(1-(J23zero/GB)^2);
Cout_zero=J23zero/Cout_zero_denom;
Cout_zeropF=Cout_zero/10^-12;
CoutE_zero_denom=1+(w0zero*Cout_zero/GB)^2;
CoutE_zero=Cout_zero/CoutE_zero_denom;
CoutE_zero_pF=CoutE_zero/10^-12

C2zero=C_zero-Cseries_zero-CoutE_zero;
C2shunt_zero=-Cseries_zero-CoutE_zero;
C2shunt_zeropF=C2shunt_zero/10^-12

fstart=floor(.8*fresml_zero/10^8);fstart=fstart/10;
fstop=ceil(1.15*fresml_zero/10^8);fstop=fstop/10;
fstep=(fstop-fstart)/npts;

%no bias

for n=1:npts

    freq=n*fstep;
    freq1=freq+fstart;
    nf(n)=(freq+fstart)*10^9;

    %single mode no bias
    ZC1series1P=1/(1i*2*pi*nf(n)*Cin1P_zero);
    ZC1series=1/(1i*2*pi*nf(n)*Cin_zero);
    ZL1shunt=1i*2*pi*nf(n)*L_zero;
    YL1shunt=1/ZL1shunt;
    ZC2shunt=1/(1i*2*pi*nf(n)*C_zero);
    YC2shunt=1/ZC2shunt;
    ZC3series=1/(1i*2*pi*nf(n)*Cout_zero);

    A11P=[1 ZC1series1P; 0 1];%Cin one Pole
    A1=[1 ZC1series; 0 1];%Cin
    A2=[1 0; YL1shunt 1]; %shunt
    A3=[1 0; YC2shunt 1]; %shunt
    A1out=[1 ZC3series; 0 1];

    tank=A2*A3;
    ABCD=A11P*tank*A11P;

    A=ABCD(1);
    B=ABCD(3);
    C=ABCD(2);
    D=ABCD(4);

    denom=(A+B/Z1+C*Zs+D);
    S11num=A+B/Z1-C*Z1-D;
    S22num=-A+B/Z1-C*Z1+D;
    S12num=2*(A*D-B*C);

    S11=((S11num/denom));

```

```

S12=( (S12num/denom) );
S21=(2/denom);
S22=(S22num/denom);

S11ABCDdB(n)=(10*log(S11));
S12ABCDdB(n)=(10*log(S12));
S22ABCDdB(n)=(10*log(S22));
S21ABCDdB(n)=(10*log(S21));

%coupling network
ZC3shunt=1/(li*2*pi*nf(n)*C1shunt_zero);
YC3shunt=1/ZC3shunt;
ZC4series=1/(li*2*pi*nf(n)*Cseries_zero);
ZC5shunt=1/(li*2*pi*nf(n)*C2shunt_zero);
YC5shunt=YC3shunt;

%coupling ABCD
A4=[1 0; YC3shunt 1]; %shunt
A5=[1 ZC4series; 0 1];%series
A6=[1 0; YC5shunt 1]; %shunt
ABCDcpl=A4*A5*A6;

ABCDdual=A1*tank*ABCDcpl*tank*Alout;

Adual=ABCDdual(1);
Bdual=ABCDdual(3);
Cdual=ABCDdual(2);
Ddual=ABCDdual(4);

denomdual=(Adual+Bdual/Zl+Cdual*Zs+Ddual);
S11numdual=Adual+Bdual/Zl-Cdual*Zl-Ddual;
S22numdual=-Adual+Bdual/Zl-Cdual*Zl+Ddual;
S12numdual=2*(Adual*Ddual-Bdual*Cdual);

S11dual=( (S11numdual/denomdual) );
S12dual=( (S12numdual/denomdual) );
S21dual=(2/denomdual);
S22dual=(S22numdual/denomdual);

S11dualABCDdB(n)=(10*log(S11dual));
S12dualABCDdB(n)=(10*log(S12dual));
S22dualABCDdB(n)=(10*log(S22dual));
S21dualABCDdB(n)=(10*log(S21dual));

end;

%calculating resonant circuit with a bias

if bias1>10
for n=1:npts

freq=n*fstep;

```

```

freq1=freq+fstart;
nf(n)=(freq+fstart)*10^9;
%single mode
% use same zero bias Cin and out
ZC1series1Pbias=1/(1i*2*pi*nf(n)*Cin1P_zero);
ZC1series=1/(1i*2*pi*nf(n)*Cin_zero);
ZC3series=1/(1i*2*pi*nf(n)*Cout_zero);

ZL1shuntbias=1i*2*pi*nf(n)*L_bias;
YL1shuntbias=1/ZL1shuntbias;
ZC2shuntbias=1/(1i*2*pi*nf(n)*C_bias);
YC2shuntbias=1/ZC2shuntbias;

AllPbias=[1 ZC1series1P; 0 1];%series
Albias=[1 ZC1series; 0 1];%series
A2bias=[1 0; YL1shuntbias 1]; %shunt
A3bias=[1 0; YC2shuntbias 1]; %shunt
A4bias=[1 ZC3series; 0 1];%series

tank_bias=A2bias*A3bias;

ABCDbiaspl=AllPbias*tank_bias*AllPbias; %A3*A1*A2*A4;

    Abias=ABCDbiaspl(1);
    Bbias=ABCDbiaspl(3);
    Cbias=ABCDbiaspl(2);
    Dbias=ABCDbiaspl(4);

denombias=(Abias+Bbias/Zl+Cbias*Zs+Dbias);
S11numbias=Abias+Bbias/Zl-Cbias*Zl-Dbias;
S22numbias=-Abias+Bbias/Zl-Cbias*Zl+Dbias;
S12numbias=2*(Abias*Dbias-Bbias*Cbias);

S11bias=(S11numbias/denombias);
S12bias=(S12numbias/denombias);
S21bias=(2/denombias);
S22bias=(S22numbias/denombias);

S11ABCDbiasdB(n)=(10*log(S11bias));
S12ABCDbiasdB(n)=(10*log(S12bias));
S22ABCDbiasdB(n)=(10*log(S22bias));
S21ABCDbiasdB(n)=(10*log(S21bias));

%coupling network
ZC3shunt=1/(1i*2*pi*nf(n)*Cshunt_zero);
YC3shunt=1/ZC3shunt;
ZC4series=1/(1i*2*pi*nf(n)*Cseries_zero);
ZC5shunt=ZC3shunt;
YC5shunt=YC3shunt;

ABCDdualbias=Albias*tank_bias*ABCDcpl*tank_bias*Albias;

    Adualbias=ABCDdualbias(1);
    Bdualbias=ABCDdualbias(3);
    Cdualbias=ABCDdualbias(2);

```

```

Ddualbias=ABCDdualbias(4);

denomdualbias=(Aduabias+Bdualbias/Z1+Cdualbias*Zs+Ddualbias);
S11numdualbias=Aduabias+Bdualbias/Z1-Cdualbias*Z1-Ddualbias;
S22numdualbias=-Aduabias+Bdualbias/Z1-Cdualbias*Z1+Ddualbias;
S12numdualbias=2*(Aduabias*Ddualbias-Bdualbias*Cdualbias);

S11dualbias=(S11numdualbias/denomdualbias);
S12dualbias=(S12numdualbias/denomdualbias);
S21dualbias=(2/denomdualbias);
S22dualbias=(S22numdualbias/denomdualbias);

S11biasdualABCDdB(n)=(10*log(S11dualbias));
S12biasdualABCDdB(n)=(10*log(S12dualbias));
S22biasdualABCDdB(n)=(10*log(S22dualbias));
S21biasdualABCDdB(n)=(10*log(S21dualbias));

end;
end;

nf=nf/10^9; % back to MHz for plotting
bias5=direction*bias5;
figure;
plot(nf,real(S22ABCDdB),nf,real(S21ABCDdB),nf,real(S11ABCDbiasdB),nf,real(S21ABCDbiasdB));
grid on;
xlabel('Frequency (GHz)');
ylabel('S(dB)');
legend('S11 Single no bias','S21 Single no bias','S11 Single with bias','S21 Single with bias');
titlestr=['Single Mode Filter with ', ferrite, ' of er=',num2str(er3),', side dimension=',num2str(l3in),' in., bias1= 0 and ',num2str(bias1),' Oe and bias5= 0 and ',num2str(bias5),' Oe'];
title(titlestr);

plot2 =1;
if plot2 ==1
figure;
plot(nf,real(S11dualABCDdB),nf,real(S21dualABCDdB),nf,real(S11biasdualABCDdB),nf,real(S21biasdualABCDdB));
%plot(nf,real(S21dualABCDdB),nf,real(S21biasdualABCDdB));
grid on;
xlabel('Frequency (GHz)');
ylabel('S(dB)');
legend('S11 Dual Mode with no bias','S21 Dual mode with no bias','S11 Dual Mode with bias','S21 Dual mode with bias');
titlestr=['Dual Mode Filter with ', ferrite, ' of er=',num2str(er3),', side dimension=',num2str(l3in),' in., bias1=',num2str(bias1),' Oe and bias5=',num2str(bias5),' Oe'];
title(titlestr);
else
figure;
plot(nf,real(S11biasdualABCDdB),nf,real(S21biasdualABCDdB));

```

```

grid on;
xlabel('Frequency (GHz)') ;
ylabel('S(dB)') ;
legend('S11 Dual Mode with bias','S21 Dual mode with bias');
titlestr=['Dual Mode Filter with ', ferrite,' of er=',num2str(er3),' ,
side dimension=',num2str(l3in),' in., bias1= ',num2str(bias1),' Oe and
bias5= ',num2str(bias5Value),' Oe'];
title(titlestr);
end

saveFile=1;% Change directory Change FILENAME
if saveFile ==1
    %pwd
    %cd C:\Users\cblair\njit\matlab\TTVG1950TLMdatafiles
    %cd pt425

save freq_111101.txt    nf -ASCII
%save 100pt5singleS11_same.txt    S11ABCDbiasdB -ASCII
%save 100pt5singleS21_same.txt    S21ABCDbiasdB -ASCII
save 100pt5S11dual_opposite111102.txt S11biasdualABCDdB -ASCII
save 100pt5S21dual_opposite111102.txt S21biasdualABCDdB -ASCII
end;

saveZero=1;
%only need to do zerobias once at 100 Oe opp for consistency
if saveZero==1
%save 0pt5singleS11same.txt    S22ABCDdB -ASCII
%save 0pt5singleS21same.txt    S21ABCDdB -ASCII
save 0pt5dualS11_111102.txt    S11dualABCDdB -ASCII
save 0pt5dualS21_111102.txt    S21dualABCDdB -ASCII
end;

```

APPENDIX B

DETAILS FOR TLM BASED FIGURE 3.29

This appendix details the creation of Figures 3.29, 3.30 and 3.31. The datapoints are generated from the TLM based MATLAB program in Appendix A. This program is used to calculate the modes in a stratified waveguide. The layers' length and width are in the X and Y direction and depth is in the Z direction. The cavity and layer dimensions are manually declared in lines 27-40 as shown in Appendix A. The top and bottom layers represent the ferrite tiles. The ferrite layer thicknesses are automatically calculated and are of equal thicknesses. The user selects the external biases from an array of values in lines 135-141.

The TLM program plots the zero biased transcendental impedance equations of each of the two bisected sections with frequency as shown in Figure B.1. The user is required to input the crossover frequency point of these two line graphs as seen in Figure B.2. This input parameter is named $X_{fzeroDC}$ in the MATLAB program. The MATLAB data cursor is dependent on the zoom level. Use of a high zoom level is preferred. This input value is used to calculate the overall resonant frequency of the unbiased composite structure which is the initial guess for the biased structure. The TLM program recalculates the impedance equations of the two bisected sections at the applied bias and plots the line curves as in Figure B.3. The user is required to input the frequency crossover point as shown in Figure B.4. This input is named X_{fzero1} . Figure B.5 is the line curve for the propagation constant of the bisected sections. The user is required to input both the x and y coordinates of the crossover point.

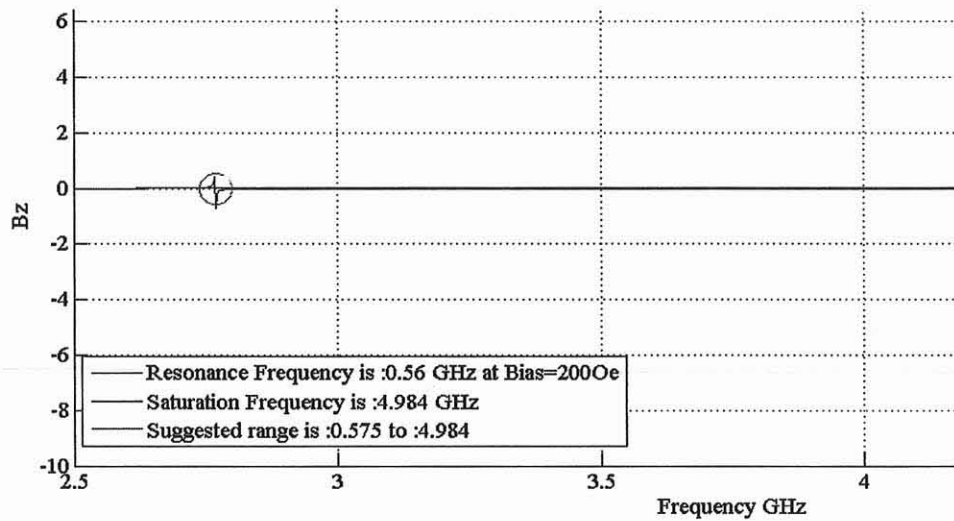


Figure B.1 Screenshot of line curves for transcendental impedance equations with zero applied bias plotted against frequency.

```

Command Window
New to MATLAB? Watch this Video, see Demos, or read Getting Started.

bias1 =
    100

f0MHz_bias1 =
    280

mr1 =
    1.8202

mr5 =
   -1.8202

XfzeroDC =
    2.8450

fx Zero Bias - Enter in X component (GHz) of 1st crossover point: 2.844|
  
```

Figure B.2 Screenshot of required user input for first crossover point for zero bias.

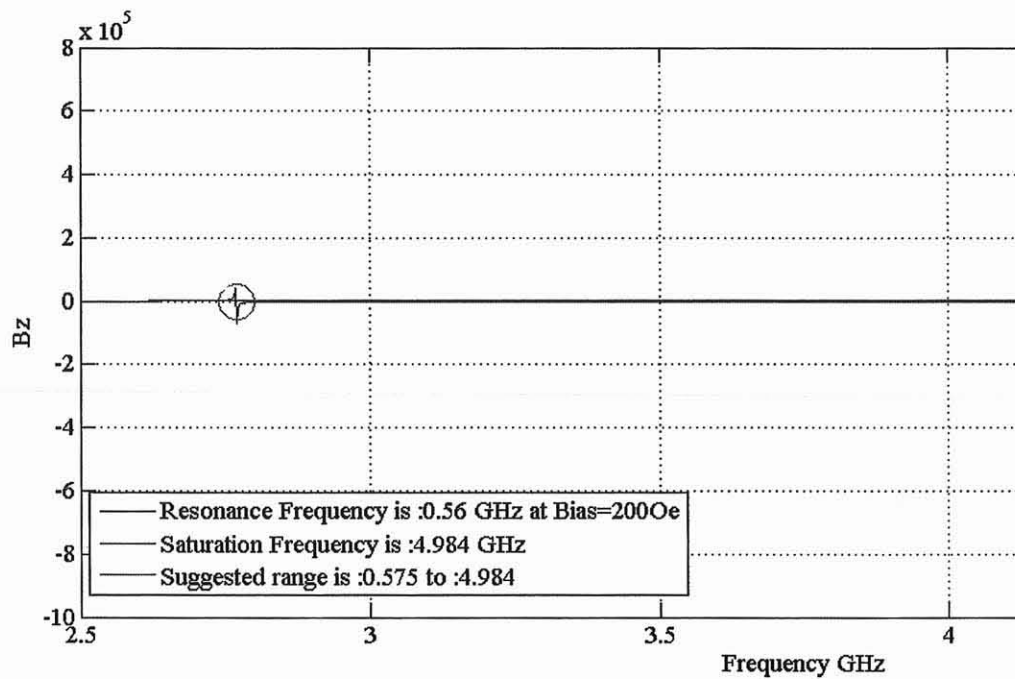


Figure B.3 Screenshot of line curves for transcendental impedance equations with an applied bias plotted against frequency.

```

Command Window
New to MATLAB? Watch this Video, see Demos, or read Getting Started.

f0MHz_bias1 =
    280

mr1 =
    1.8202

mr5 =
   -1.8202

XfzeroDC =
    2.8450

Zero Bias - Enter in X component (GHz) of 1st crossover point: 2.844

Xfzerol =
    2.7650

Applied Bias: Enter in frequency of lowest zero beta crossover point in GHz: 2.763
  
```

Figure B.4 Screenshot of required user input for first crossover point for an applied bias.

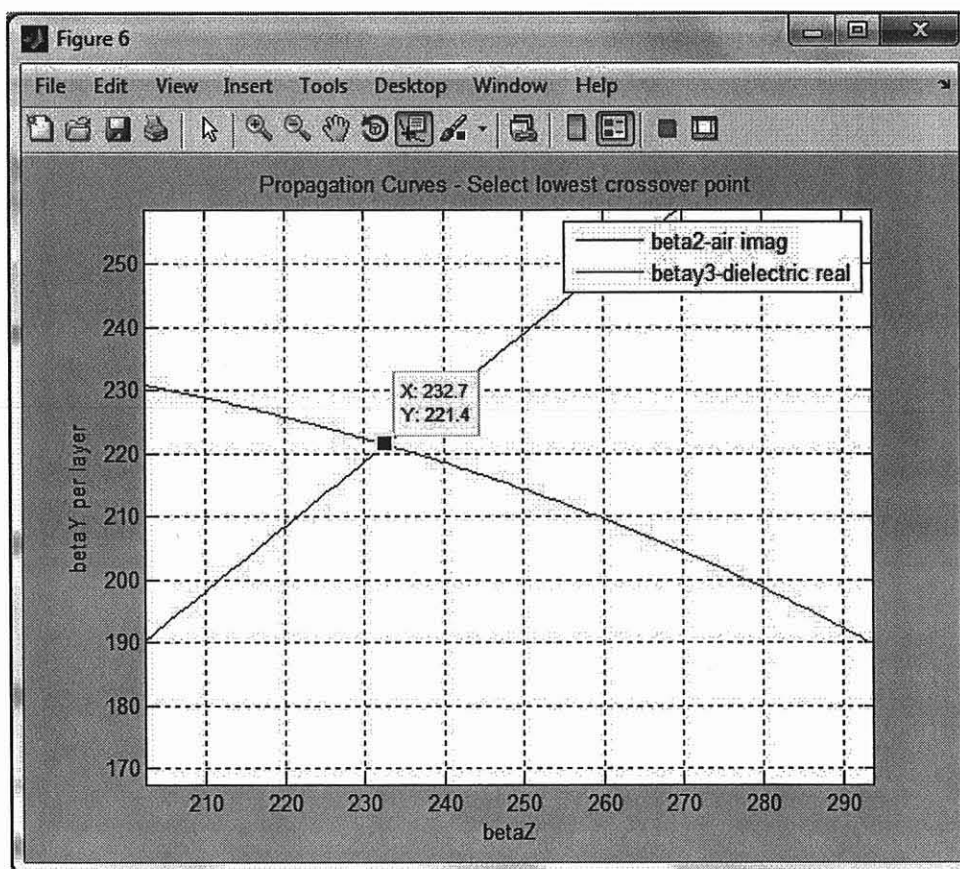


Figure B.5 Screenshot of line curves of the propagation constants of the composite structure.

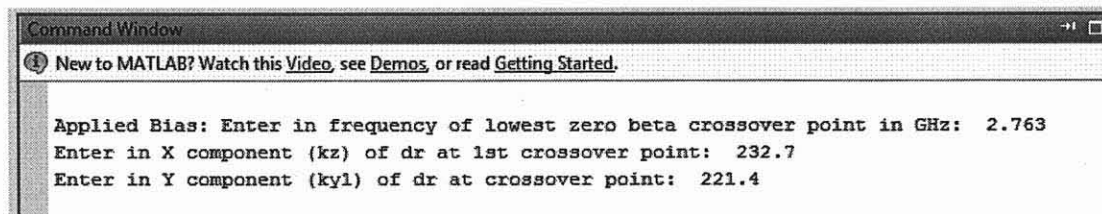


Figure B.6 Screenshot of required user input for the crossover point for propagation curves.

The S_{11} and S_{21} calculated curves of the dual mode bandpass filter with and without bias are shown in Figure B.7. MATLAB data markers for the lowest order frequency, f_1 and the next lowest order, f_2 are indicated. These values at the different bias levels for the different ferrite materials are saved in an Excel file named

dissertationData.xls and a section for G113 is shown in Figure B.8. Both “opposite” and “same” biases are shown.

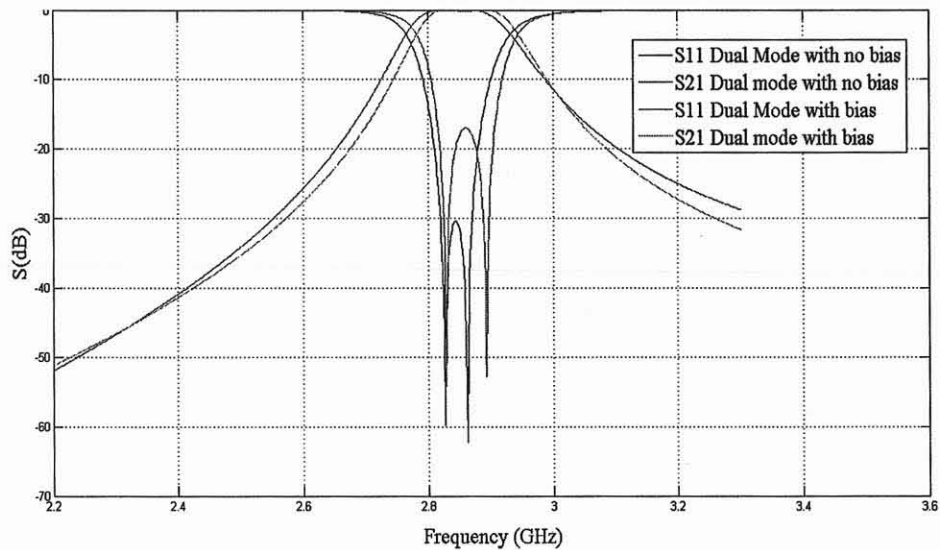


Figure B.7 Calculated S11 and S21 plots of Dual Mode Bandpass Filter with zero and applied bias.

The user manually sets the ferrite material in the MATLAB program line 130 as shown in Figure B.8. This sets the saturation value of the selected ferrite material.

```

129 - Msat=[Msat_G113 Msat_G510 Msat_ITVG1950 Msat_newFerrite Msat_Pt
130 - Msat_select=Msat(1);
131 - fm_select=gamma*Msat_select;
132 - wm_select=2*pi*fm_select;

```

Figure B.8 Screenshot of User Selected Ferrite Material.

Tabulated values for the figures are detailed in Figure B.9.

Matlab R2011a Version 7.12										Matlab R2011a Version 7.12									
Filename TLM Program FiveLayer Model_110915										Filename TLM Program FiveLayer Model_110915									
dial xyz 0.5										dial xyz 0.5									
G113										G113									
Opposite	CrossOver1	CrossOver2	kz	ky	f1	f2	f0	shiftf0		Opposite Bias	CrossOver1	CrossOver2	kz	ky	f1	f2	f0	shift f0	
0	from bias=100					2826	2861	2843.5		0	from bias=100					2826	2861	2843.50	
0	from bias=200					2826	2862	2844		0	from bias=200					2826	2862	2844.00	
0	from bias=400					2819	2854	2836.5		0	from bias=400					2819	2854	2836.50	
0	from bias=500					2817	2852	2834.5		0	from bias=500					2817	2852	2834.50	
0	from bias=950					2849	2885	2867											
0	average					2827.4	2862.8	2845.1		average						2811.00	2848.00	2829.50	
100	2844.00	2763.00	232.70	221.40	2814.00	2880.00	2847.00	1.90		100	2.844	2.763	232.8	221.4	2821.00	2886.00	2853.50	24.00	
100	2844.00	2763.00	232.70	221.40	2814.00	2880.00	2847.00	1.90		200	3	2.763	233.1	222.1	2828.00	2893.00	2860.50	31.00	
100	2844.00	2763.00	232.70	221.40	2814.00	2880.00	2847.00	1.90		500	2.844	2.763	232.8	221.4	2854.00	2915.00	2884.50	55.00	
200	2845.00	2768.00	239.00	227.40	2818.00	2884.00	2851.00	5.90											
200	2845.00	2768.00	239.00	227.40	2818.00	2884.00	2851.00	5.90											
400	2838.00	2781.00	252.50	240.20	2831.00	2896.00	2863.50	18.40											
400	2838.00	2781.00	252.50	240.20	2831.00	2896.00	2863.50	18.40											
500	2836.00	2791.00	252.50	240.20	2842.00	2905.00	2873.50	28.40											
500	2836.00	2791.00	252.50	240.20	2842.00	2905.00	2873.50	28.40											
950	2868.00	2547.00	185.00	176.00	2693.00	2764.00	2728.50	-116.60											
950	2868.00	2546.00	185.00	175.90	2693.00	2764.00	2728.50	-116.60											

Matlab R2011a Version 7.12										Matlab R2011a Version 7.12									
Filename TLM Program FiveLayer Model_110915										Filename TLM Program FiveLayer Model_110915									
dial xyz 0.5										dial xyz 0.5									
G550										TTVG1950									
Opposite	CrossOver1	CrossOver2	kz	ky	f1	f2	f0	shiftf0		Opposite Bias	CrossOver1	CrossOver2	kz	ky	f1	f2	f0	shift f0	
0	from bias=100					2825	2860	2842.50		0	from bias=100					2825	2861	2843.00	
0	from bias=200					2826	2862	2844.00		0	from bias=200					2821	2857	2839.00	
0	from bias=400					2826	2861	2843.50		0	from bias=400					2820	2856	2838.00	
0	from bias=500					2826	2862	2844.00		0	from bias=500					2818	2853	2835.50	
0	from bias=950					2834	2859	2846.50		0	from bias=950					2853	2889	2871.00	
0	average					2827.4	2860.8	2844.10		0	average					2827.40	2863.20	2845.30	
100	2.8430	2.7620	229.60	218.30	2812.00	2879.00	2845.50	1.40		100	2.8440	2.7630	233.10	222.10	2814.00	2880.00	2847.00	1.70	
200	2.8430	2.7600	231.00	219.90	2811.00	2878.00	2844.50	0.40		200	2.8400	2.7730	240.30	228.80	2823.00	2889.00	2856.00	10.70	
400	2.8440	2.7660	235.20	223.90	2816.00	2883.00	2849.50	5.40		400	2.8390	2.7840	252.40	240.20	2835.00	2898.00	2866.50	21.20	
500	2.8450	2.7690	239.00	227.10	2819.00	2885.00	2852.00	7.90		500	2.8370	2.7930	252.40	240.20	2845.00	2907.00	2876.00	30.70	
950	2.8520	2.7260	209.20	199.20	2791.00	2859.00	2825.00	-19.10		950	2.872	2.531	184.10	175.10	2694.00	2771.00	2732.50	-112.80	

Figure B.9 Tabulated TLM data for G113, G510 and TTVG-1950

REFERENCES

1. D. M. Pozar, *Microwave Engineering*. Reading, Mass.: Addison-Wesley, 1990.
2. R.F. Harrington, *Time Harmonic Electromagnetic Fields*. New York: McGraw-Hill Inc., 1962.
3. C. A. Balanis, *Antenna theory : Analysis and Design*, 3rd ed. Hoboken, NJ: John Wiley, 2005.
4. R. E. Collin, *Foundations for Microwave Engineering*, 2nd Edition, 2nd Edition ed.: Wiley-IEEE Press, 2001.
5. J. A. Kong, *Maxwell Equations*: EMW Publishing, 2002.
6. M. S. Sodha and N. C. Srivastava, *Microwave Propagation in Ferrimagnetics*. New York: Plenum Press, 1981.
7. B. Lax. and K. Button, *Microwave Ferrites and Ferrimagnetics*, New York: McGraw-Hill, 1962.
8. G. Barzilai and G. Gerosa, "Modes in Rectangular Guides Loaded with a Transversely Magnetized Slab of Ferrite Away from the Side Walls," *Microwave Theory and Techniques, IRE Transactions on*, vol. 9, pp. 403 - 408 September 1961.
9. R.J. Mongia and A. Ittipiboon.; , "Theoretical and Experimental Investigations on Rectangular Dielectric Resonator Antennas," *Antennas and Propagation, IEEE Transactions on* vol. 45, pp. 1348 - 1356 September 1997.
10. J. Krupka, "Magnetic Tuning of Cylindrical H_{01δ}- Mode Dielectric Resonators," *Microwave Theory and Techniques, IEEE Transactions on* vol. 37, pp. 743 - 747 Apr 1989.
11. J. Krupka and A. Abramowicz , "Magnetically tunable filters for cellular communication terminals," *Microwave Theory and Techniques, IEEE Transactions on* vol. 54, pp. 2329 - 2335, June 2006.
12. S.S.Iqbal and M.Dawoud., "Novel Semiconductor Phase Shifters for Phased-Array Antennas," presented at the 7th Annual IEEE Technical Exchange Meeting, King Fahd University of Petroleum and Minerals, April 2000.
13. TransTech Products,:Trans-Tech/Products Homes/Ferrites & Magnetic Materials/Narrow Linewidth/G-113: Trans-Tech, 2011.
14. TransTech Products: Matetials, Trans-Tech/Products Homes/Ferrites & Magnetic Materials/Aluminum & Aluminum Gadolinium Substituted Garnets/G-510: Trans-Tech, 2011.
15. TransTech Products: Materials, Trans-Tech/Products Homes/Ferrites & Magnetic Materials/Narrow Linewidth/TTVG-1950: Trans-Tech, 2011.

16. L.B. Felsen, and N. Marcuvitz. *Radiation and Scattering of Waves*. Hoboken, NJ: Wiley, 2003, sec 2.4.
17. G. T. Rado, "Magnetic Spectra of Ferrites," *Reviews of Modern Physics*, vol. 25, pp. 81-89, 1953.
18. E. Schlomann, "Microwave behavior of partially magnetized ferrites," *Journal of Applied Physics*, vol. 41, pp. 204 - 214, January 1970.
19. A. Nassiri. (June 2003). *Lecture 14 Ferrite Materials*. Available: <http://www.aps.anl.gov/asd/people/nassiri/USPAS2003/Lecture14.pdf>
20. G. L. Matthaei, L. Young, and E. M. T. Jones, *Microwave filters, impedance-matching networks, and coupling structures*. Dedham, MA: Artech House Books, 1980.
21. L. D. Landau and E M. Lifshitz, "ON THE THEORY OF THE DISPERSION OF MAGNETIC PERMEABILITY IN FERROMAGNETIC BODIES," *Phys. Zeitsch. der Sow.*, vol. 8, pp. 153–169, 1935.
22. G. F. Craven and R. F. Skedd, *Evanescent mode microwave components*. Boston: Artech House, 1987.